2018

UNDERSTANDING LARGE-SCALE NATURAL MINE WATER-GEOLOGIC FORMATION SYSTEMS FOR GEOTHERMAL APPLICATIONS

Ting Bao
Michigan Technological University, tbao@mtu.edu

UNDERSTANDING LARGE-SCALE NATURAL MINE WATER-GEOLOGIC FORMATION SYSTEMS FOR GEOTHERMAL APPLICATIONS

By

Ting Bao

A DISSERTATION

Submitted in partial fulfillment of the requirements for the degree of

DOCTOR OF PHILOSOPHY

In Civil Engineering

MICHIGAN TECHNOLOGICAL UNIVERSITY

2018

This dissertation has been approved in partial fulfillment of the requirements for the Degree of DOCTOR OF PHILOSOPHY in Civil Engineering.

Department of Civil and Environmental Engineering

Dissertation Advisor:	*Zhen (Leo) Liu*
Committee Member:	*Stanley J. Vitton*
Committee Member:	*Pengfei Xue*
Committee Member:	*Kazuya Tajiri*
Department Chair:	*Audra Morse*

To Yun Wang and My Little Boy

Table of Contents

List of Figures

List of Tables

Preface

The contents of this dissertation are adopted from either published conference papers, manuscripts that are under review, or paper drafts that will be summited to journals later. Details are summarized below:

The contents of Chapter 1 are adopted from a part of a manuscript to be submitted to a journal later. The author conducted the literature review and paper writing with the indispensable help from Dr. Zhen (Leo) Liu and Dr. Stanley Vitton.

The contents of Chapter 2 are adopted from a part of a manuscript to be submitted to a journal later. The author conducted economic analysis and paper writing with the indispensable help from Dr. Zhen (Leo) Liu. Kelsey Bird helped summarize site geology and the background of the Quincy mine. Dr. Stanley Vitton helped proofread site geology. Mr. Jay Meldrum and Mr. Christopher Green from the Keweenaw Research Center, who co-authored the paper, have been managing a project demonstration.

The contents of Chapter 3 are adopted partially from a conference paper published in the proceedings of Geo-Chicago 2016 and partially from a manuscript that has been submitted to "Energy Conversion and Management" and is currently in the first round of revision. The author conducted numerical modeling, model validations, data collection, data analysis, and paper writing with the indispensable help from Prof. Zhen (Leo) Liu. The field test was conducted by a crew from the Great Lakes Research Center and Mr. Jay

Meldrum and Mr. Christopher Green from the Keweenaw Research Center helped us understand and interpret the data.

The contents of Chapter 4 are adopted from a manuscript to be submitted to a journal later. The author conducted numerical analysis, model validation, data analysis and paper writing with the help from Prof. Zhen (Leo) Liu. The valuable suggestions from Prof. Pengfei Xue helped improve the quality of the study. The knowledge from Prof. Kazuya Tajiri also helped shape up the study.

The contents of Chapter 5 are from another manuscript that will be submitted to a journal later. Prof. Zhen (Leo) Liu helped design the study and highlight the novelty of the study. The numerical simulation, data analysis, and discussion were finished by the author under the instruction from Prof. Zhen (Leo) Liu. The paper draft was also proofread with the indispensable help from Dr. Zhen (Leo) Liu.

Acknowledgments

First and foremost, I would like to express my sincere appreciation to my Ph.D. advisor, Prof. Zhen (Leo) Liu, who had offered me continuous mentorship, guidance, inspiration, instruction, and financial support, which greatly helped my completion of Ph.D. research and led me towards a real Dr. finally. His support and encouragement through my doctoral research are indispensable, for which I am forever indebted. His high standard of professionalism, work ethics, and integrity is a "lighthouse" to open a new window in my career and has been shaping me into a real and independent scholar as who I am today.

I also extend my great appreciation to my committee members, Prof. Stanley J. Vitton, Prof. Pengfei Xue, and Prof. Kazuya Tajiri. Prof. Stanley J. Vitton taught me valuable knowledge of geology. Prof. Pengfei Xue taught me valued knowledge regarding hydrodynamics modeling. Prof. Kazuya Tajiri improved my in-depth understanding of heat transfer in fluid mechanics. Their guidance is very significant and helps design my research plan and resolve research changelings and difficulties. I really appreciate their help in improving the quality of this dissertation.

I also would like to acknowledge suggestions and help from the faculty, staff, and students in the Department of Civil and Environmental Engineering, especially thanks to Prof. Jacob Hiller, Prof. Ralph J. Hodek, Kiko de Melo e Silva, Rob Fritz, Angela Keranen, Shelle Sandell and Amanda Cadwell for their advice and help for both life and research throughout my Ph.D. study.

During my Ph.D. study at Michigan Technological University, I am fortunate enough to not only earn mentorship but also friendship. I am thankful to my colleagues and also great friends: Ruilong Han, Bing Han, Chao Zhang, Shuaidong Zhao, Xu Yang, Xiao Sun, Hui Yao, Siyu Chen, Fan Yang, Weilue He, Huaguang Wang, Jian Chen, Mohammadhossein Sadeghiamirshahidi and many others who are not listed here for their consistent help and support. Because of them, my life in a different country became much more rewarding and colorful.

The financial support from the Finishing Fellowship of the Graduate School of Michigan Technological University is also greatly appreciated. With this support, the final two chapters of this dissertation would be very smooth to complete. I also want to acknowledge the financial support from the National Science Foundation during my Ph.D. study.

Finally, and most importantly, I sincerely appreciate support and encouragement from my mother and my parents-in-law. I could hardly complete my doctoral study without their support and encouragement. In particular, I would like to express my great appreciation to my wife Yun Wang. Her endless support is very significant, for which I am forevermore grateful. Also, I genuinely appreciate my wife who made me a father to have my first baby, the most precious gift in my life.

List of Abbreviations

UP=Upper Peninsula

PLLS=Portage Lake Lava Series

TER=Thermal Energy Recharge

KRC=Keweenaw Research Center

DDC=Double-Diffusive Convection

2D=2-Dimensional

3D=3-Dimensional

FVM=Finite Volume Element

Abstract

Geothermal energy recovery from flooded mines has been gaining momentum worldwide. Numerous mines are flooded after their closure, either naturally or artificially, in which the water in the mines can be heated by the surrounding geologic formations due to geothermal gradients, leading to sizeable man-made reservoirs of warm water. Such mine water, therefore, can be treated as a renewable geothermal resource for heating/cooling buildings, which has the potential to benefit over millions of people in the United States and much more around the world. Though some real projects and/or installations launched worldwide for the use of flooded mines for geothermal applications, there are many uncertainties in the theoretical aspect of this application, in particular, the scientific understanding of the large-scale natural mine water-geologic formation system is still in a preliminary stage and thus far lags behind its application.

Motived by this missing scientific linkage, the current dissertation presents an investigation with multiphysics analyses to understand the large-scale natural mine water-geologic formation system. The main objective is to provide an in-depth understanding of this system for guiding and optimizing this large-scale geothermal application from a scientific perspective. For the purpose, this dissertation presents four specific investigations.

The first investigation explores a specific site with comprehensive information relevant to the natural mine water-geologic formation system for recovering geothermal energy from deep abandoned mines for heating and cooling buildings.

The second investigation presents the results of field tests and multiphysics analysis of a flooded shaft for understanding the transport of heat and mass in the natural mine water-geologic formation system.

The third investigation addresses a key scientific issue regarding the layering phenomenon observed in large bodies of mine water, which controls the temperature distribution and heat energy storage in the deep geothermal field for the proposed energy renovation.

The fourth investigation aims to provide insights into the dominant heat and mass transport mechanisms underlying thermohaline stratifications and investigate the factors influencing thermohaline stratifications.

The above four investigations presented in this dissertation provide the urgently needed scientific understanding of the natural mine water-geologic formation system for this large-scale geothermal application, which eventually offers scientific bases for the future optimal design of this unique large-scale application of recovering geothermal energy from flooded mines.

1 Motivation and Objective

1.1 Background and Motivation

Geothermal energy, defined as heat from the Earth's core (Williamson et al. 2001; Gallup 2009), is a renewable (Kagel et al. 2005), clean (Rybach 2003), abundant (Rybach and Mongillo 2006), and flexible (Mock et al. 1997) resource. Due to these advantages, geothermal energy has been considered as a renewable resource to supply humanity's energy needs in the U.S. and around the world (Kagel et al. 2005). Among the major categories of geothermal applications (Handbook 2009), geothermal heat pumps that transfer heat to or from the ground are the most energy efficient means of heating and cooling buildings in most areas of the U.S. (Lund 1990; Lienau 1997) and possibly the only one that can be used almost everywhere (Hepbasli and Akdemir 2004; Lund et al. 2004). Because of this reason, geothermal heat pumps have been receiving increasing attention (Handbook 2009; Chiasson 1999). Applications of geothermal heat pumps involve the extraction of energy from a low enthalpy (or roughly, temperature) source, i.e., water circulated in a closed loop, such as groundwater and surface water, to a high enthalpy fluid circulated in heat pumps, which will be later used for heating (cooling uses an opposite process). Although less discussed for geothermal applications, the mine water, especially that in abandoned mines (Jessop et al. 1995; Rottluff 1998), has been gaining acceptance as an economically and environmentally attractive geothermal energy resource (Raymond et al. 2008; Behrooz et al. 2008). The hypothesis of the mine water-based geothermal resource is that the mine water stored in deep mines and heated by the Earth can be used for heating buildings in winter and/or cooling buildings in summer. The conceptual model of this hypothesis is shown in Figure 1.1. The use of the mine water for geothermal purposes falls into the category of Surface Water Heat Pump (SWHP) application. Compared with conventional Geothermal Heat Pump (GHP) applications, this SWHP application offers various remarkable advantages:

1. The mine water is mostly deemed as a useless material, the recyclable use of this material as a geothermal resource is thus sustainable.
2. The mine water reaches much deeper locations in the ground, which has a higher temperature than surface water, and thus presents a geothermal energy resource of a higher quality.
3. The volume of the mine water is usually large compared to the water in pipes or soil pores, which makes its energy reserve exceed that of conventional GHP applications by many orders.
4. It offers much better heat transfer (directly between the mine water and the surrounding geologic formations) than that in Ground-Coupled Heat Pump (GCHP) systems (via heat exchangers (pipes)) and avoids the technical difficulties and environmental problems in circulating pore water in Ground-Water Heat Pump (GWHP) systems.
5. As abandoned mines and the mine water are existing facilities, no extra cost is needed for their construction, which saves a significant amount of expenditure compared to other GHP applications.

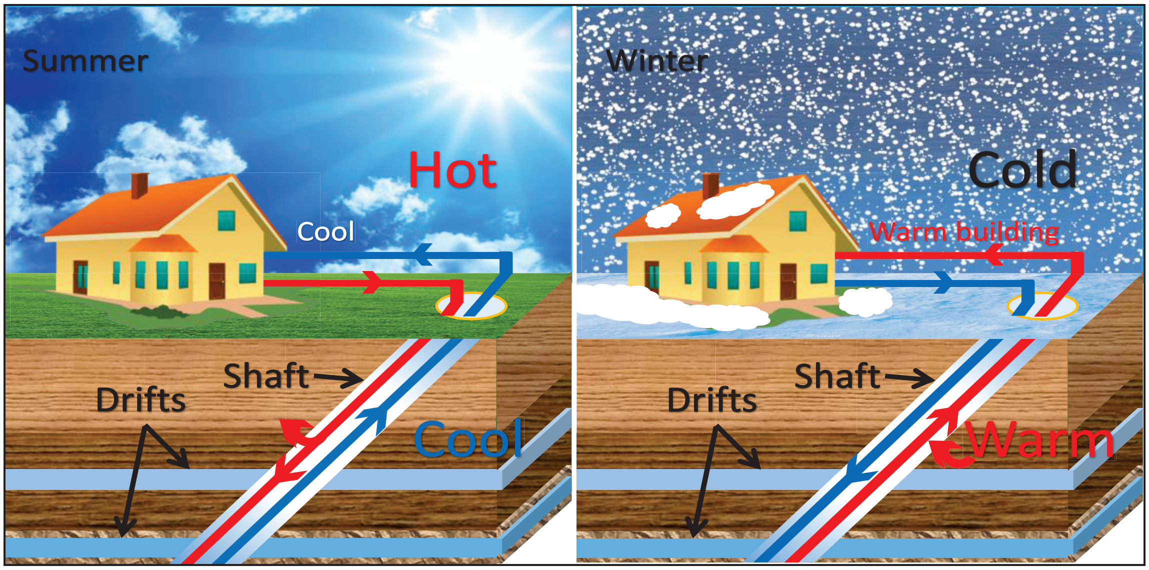

Figure 1.1. Representative graphics for the use of the mine water for geothermal applications.

While less understood from a scientific perspective, the exploitation of the mine water as a geothermal resource has been pioneered in projects around the world. The utilization of the mine water for heating and cooling of buildings and industrial processes started officially in 1989 when the Town of Springhill developed an industrial park where companies could utilize geothermal energy supply from the local abandoned coal mines. Since this pioneering work in Canada (Jessop et al. 1995; Jessop 1995), the idea of using flooded mines as heat exchangers has been gaining momentum worldwide. As a result, a number of demonstration projects are in progress, mostly in Europe and Canada (Watzlaf and Ackman 2006; Ghomshei and Eng 2007; Renz et al. 2009; Ramos and Falcone 2013; Gammons et al. 2009). In addition to Springhill (Jessop et al. 1995; Jessop 1995), two other typical demonstration projects, which were repeatedly mentioned in the literature

(Malolepszy 2003; Barsuglia and Garzonio 2005), are the installations of geothermal heat pumps in Germany (Rottluff 1998) and Scotland (Burke 2002). Behrooz et al. (2008) also introduced the geothermal use of an abandoned coal mine in Heerlen, Netherlands. Other sites include the Aachen/German coal mining area, Folldal in Norway; Shettleston in the UK, and Ochil View in the UK (Hall et al. 2011; Wolkersdorfer 2008; Banks et al. 2003).

Besides the real installations and/or demonstration projects, many assessment studies have been carried out to evaluate the potential and/or to develop preliminary plans for mine water-based geothermal applications at many sites, such as the Central Mining Institute (Kotyrba and Michalak 1987), Silesian region (Malolepszy and Ostaficzuk 1999), Yellowknife in Canada (Ghomshei and Eng 2007), Quebec and other Canadian provinces (Raymond et al. 2008), and Rhenish Massif in Germany (Wieber and Pohl 2008). In addition to these isolated investigations, trust in this opportunity also prompted international efforts across countries. One example is the European project, “Mine-water”, for reviving old and declining mining areas by producing energy from water in flooded mines (Behrooz et al. 2008), in which feasibility studies were primarily conducted. Specific site studies have shown that the geothermal energy reserves in underground mines range from a few hundreds of kilowatts to hundreds of megawatts (Behrooz et al. 2008; Malolepszy 2003; Malolepszy et al. 2005; Ordóñez et al. 2012; Tóth and Bobok 2007; Ghomshei and Meech 2005).

In addition to the technical merits, historical statistics also strongly supports the application. Figure 1.2 illustrates the potential mine sites for potential geothermal use in the U.S., which lists over 23,000 past/closed underground mines (USGS). In addition, active mines at some point will be closed so that the number of potential sites will increase. In another estimate (abandonedmines.gov), there are 500,000 abandoned mines in the U.S. Therefore, the merits of the geothermal energy recovery from the mine water provide a possibly viable high-tech solution to reuse these abandoned mines.

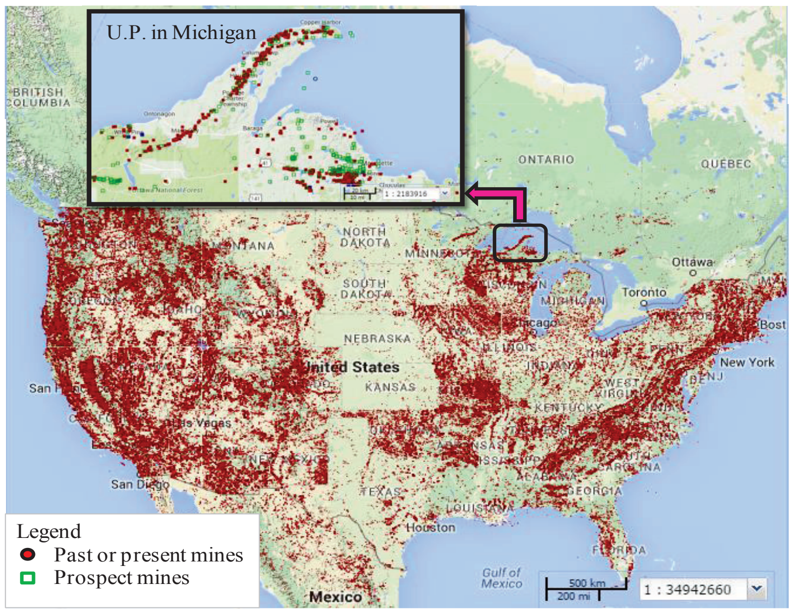

Figure 1.2. Potential sites for the use of the mine water (USGS Mineral Resources Data System).

Though some real projects and/or installations launched worldwide for the use of flooded mine for geothermal applications, there are many uncertainties in theoretical aspects of the large-scale application of geothermal energy recovery from flooded mines, in particular, the scientific understanding of the proposed large-scale geothermal energy recovery is still in a preliminary stage and thus far lags behind its application. To be more specific, the key to the efficiency and sustainability of the exploration is the distribution and variation of the temperature in the mine water (Malolepszy 2003), which highly depend on the movement of the mine water (Hamm and Sabet 2010; Hamm et al. 2008). This water movement is extremely complex and hard to predict, since it is not well understood due to the complex mechanisms of heat transfer. Interestingly enough, a unique phenomenon can be produced by this water movement. This unique phenomenon in the mine water is summarized as ‘thermohaline staircases’ caused by a thermosolutal flow (Reichart et al. 2011). More specifically, a buoyancy-driven flow, which results from the density difference due to temperature (thermal) and salinity (solute) differences, is proposed to be the major process of interest in the mine water. However, the heat and mass mechanisms of a buoyancy-driven flow have been not well understood. To advance the topic via providing the scientific understanding of the natural mine water-geologic formation system, the motivation of this dissertation stems from the following facts and considerations:

1. No comprehensive study has been reported on the large-scale application of geothermal energy recovery from flooded mines. Especially, such a comprehensive study needs to incorporate a site exploration, site geology and field conditions, an energy reserve estimation, a demonstration project, a field study, and theoretical and numerical analyses for a specific site.
2. No research has been reported on addressing the critical scientific issue about energy and mass transport in large bodies of subterranean water: the layering phenomenon observed in flooded mines, i.e., thermohaline stratifications, which govern the temperature distribution and variation in the mine water.

3. Critical insights into the heat and mass transport mechanisms of thermohaline stratifications are still lacking. In particular, no investigation has been conducted to address the following six critical issues: (1-3) influences of the key transport parameters, i.e., effective thermal diffusivity, effective kinematic viscosity, and diffusivity ratio, on thermohaline stratifications; (4) mechanisms behind the layer-merging; (5) effect of the buoyancy ratio on the structure and development of thermohaline stratifications; and (6) possibility of predicting the initial distributions of temperature and salinity for the purpose in predicting the future development of thermohaline stratifications from the current status.

1.2 Objective

The major goal of this dissertation is to scientifically understand the large-scale natural mine water-geologic formation system in providing scientific bases for the future optimal design of this large-scale geothermal application. To be more specific, the objective of this dissertation is summarized in the following.

1. Present a comprehensive investigation on the large-scale application of recovering geothermal energy from deep abandoned mines for heating and cooling buildings, including a site exploration, a collection and analysis of geologic and field conditions, energy reserve estimations, a demonstration project, a field study, and theoretical and numerical analyses for a specific site.

2. Unveil the scientific myth regarding the layering phenomenon in flooded mines (i.e., thermohaline stratifications) and reproduce such a phenomenon using multiphysics simulations with non-isothermal and non-isosolutal hydrodynamics.
3. Provide critical insights into the heat and mass transport mechanisms of thermohaline stratifications by addressing the following critical issues: influences of key transport parameters, i.e., effective thermal diffusivity, effective kinematic viscosity, and diffusivity ratio, on thermohaline stratifications; the mechanisms behind the layer-merging; the effect of the buoyancy ratio on the structure and development of thermohaline stratifications; and the possibility of predicting the initial distributions of temperature and salinity.

1.3 Organization of Dissertation

This dissertation is organized to cover all relevant and key aspects of the scientific understanding of the large-scale application of geothermal energy recovery from flooded mines, which consists of six chapters. The contents of each chapter are mostly or partially from either a published paper or a manuscript that will be submitted to a journal later. The details of the chapters are presented as below.

1) Chapter 1 provides an overview of this dissertation, including background, motivation, objective, and organization of dissertation.
2) Chapter 2 introduces the first three essential parts of a comprehensive investigation on the large-scale application of recovering geothermal energy from deep abandoned mines for heating and cooling buildings: the site geology and field

conditions, the site exploration and its energy reserve estimation, and a demonstration project and lessons learned from the demonstration project.

3) Chapter 3 presents the last three crucial part of a comprehensive investigation on the large-scale application: a field test, numerical framework development, and multiphysics numerical analyses. The field test is conducted on a flooded vertical shaft to reveal the distributions of temperature and chemical components for heat potential evaluation. The numerical analyses focus on understanding the quasi-equilibrium water movement to interpret the field test results.

4) Chapter 4 explores the formation of thermohaline stratification and reproduces thermohaline stratifications in the large-scale mine water using multiphysics simulations with unique non-isothermal and non-isosolutal hydrodynamics.

5) Chapter 5 investigates the above proposed six critical issues (see objective No.3 in Section 1.2) for providing in-depth insights into the dominant heat and mass transport mechanisms underlying thermohaline stratifications.

6) Chapter 6 presents the summary, conclusions, and recommendations for future studies for the proposed geothermal energy renovation.

2 Site Geology, Site Exploration, and Project Demonstration

This chapter presents the results of exploring a specific site for the use of flooded mines for heating and cooling buildings, including the site exploration, the geologic and field conditions, the energy reserve estimation, and a demonstration project and lessons learned from the demonstration project on the large-scale geothermal application. This study is conducted in the Upper Peninsula of Michigan, which is a historical copper mining area with enormous abandoned copper mine working spaces. These underground spaces reach deep locations with high temperatures, e.g., several kilometers, and about 95% of them are filled with water, which is available as the potential geothermal energy resource.

2.1 Introduction

Since the pioneering work for the use of flooded mines for geothermal applications in Canada (Jessop et al. 1995; Jessop 1995), many real installations, demonstrations projects, and assessment studies have been carried out, as introduced in detail in the section of Background and Motivation in Chapter 1. The scientific understanding of using the mine water as a geothermal resource, however, far lags behind its application. The key to the efficiency and sustainability of the exploration is the distribution and variation of the temperature in the mine water (Malolepszy 2003), which highly depend on the movement of the mine water (Hamm and Sabet 2010; Hamm et al. 2008). This water movement is extremely complex and hard to predict, since it is not well understood. This is because this water movement is driven by temperature and salinity differences (Reichart et al. 2011), i.e., double-diffusive natural convection, and can be influenced by the configuration of the mining space (Wolkersdorfer 2008; Kories et al. 2004), interaction between the mine water and pore/surface water (Jessop et al. 1995; Renz et al. 2009), and exploration strategies (e.g., locations of water in/out, pumping rate), etc. The mine water in a shaft, for example, can form one to several cells/layers, within which water is well mixed (Wolkersdorfer 2008). However, the formation and change of the layers within the mine water are not well understood. This raises a scientific question regarding a multiphysics approach of the coupling between water in porous materials and the hydrodynamics of bulk water in large underground spaces with complicated structures, which has not been well studied. The existing studies have concentrated on either the buoyancy-driven flow in the mine water or the heat transfer in the mine water/geologic formation, instead of a multiphysics approach for the whole system. In addition, field measurements for the purpose of geothermal energy explorations are rare. A comprehensive study, including the site exploration, the site geology and field conditions, the energy reserve estimation, a demonstration project, a field study, and multiphysics framework development and numerical analyses for a specific site, is still lacking.

This chapter presents the first three part of a comprehensive study utilizing an abandoned underground copper mine located in the Upper Peninsula of Michigan (U.P.). This copper mining region was the first major copper mining region in the U.S., which started in the 1840s and ceased in 1968. Hundreds of deep mines were developed during this time period with some mines reaching depths of 2.4 km. These mines have now filled with groundwater and are available for the use in geothermal applications. The intent of this chapter is to share what we have learned from this ongoing project in the U.P., which to the best of our knowledge is a unique energy application in the U.S. The complete study covers the essential components of the site for this application and includes the site's geology, the technical details of the demonstration project, an economic analysis, field measurements, a theoretical framework and numerical simulations. This chapter introduces the first three components. First, the geologic conditions that are critical for an understanding of the natural system and to the recovery of the geothermal energy are investigated. Relevant geologic information is summarized and discussed in terms of the overall geologic conditions, distribution, and properties of representative soils and rocks, faults and fissures, and hydrogeology to provide a detailed geological background of the area. Second, a detailed discussion of the mine in which the research is based, including its mining history, the structure of underground mining spaces, and economic potential, is provided. Finally, the results from the demonstration project conducted at a different underground copper mine but located within the same geologic formation, which has been running since 2009 to provide heating and cooling to an 11,000 square feet building, are presented.

2.2 Site Geology

Geologic conditions, i.e., bedrock geology, distributions and properties of the rocks, faults, and fissures, and hydrogeology, consists of the background for discussing the geothermal energy recovery in flooded mines. The background provides material properties of the geologic formation that holds the mine water, parameters for economic analysis, and initial and boundary conditions of the mine water and mine structure for numerical simulations. This geologic information is thus necessary and will render the study a valuable reference for future studies on this energy renovation. In the following sub-sections, the key background information is introduced with an emphasis on the Hancock mine located in Hancock, MI and the Quincy Mine located just to the north of the Hancock Mine.

2.2.1 Bedrock Geology

The first copper mines in the U.P. mined native copper were located in the Portage Lake Lava Series (PLLS), a part of the Keweenawan Series of the late Precambrian age. It was estimated that over 344 million metric tons of copper ore have been mined from the PLLS (White 1968). This results in a potential underground mined volume of 1.28×10^{8} m^3 in the area, which is about 95% filled with groundwater. The PLLS is associated with the Midcontinent Rift System that stretched from Kansas through the Lake Superior Basin into Lower Michigan a distance of 2000 km (Bornhorst and Barron 2011). As the Rift developed, large quantities of basaltic lava erupted from the center of the Rift forming hundreds of flows known as the Portage Lake Volcanics (see Figure 2.1). These flows are further interspersed with red clastic sedimentary rocks. As the volcanic activity ceased, the basin subsided and was filled in with sediments overlying the PLLS. The last phase of the Midcontinent Rift was strong compressional loading along the Grenville Front (Cannon 1994). This compressional loading caused the Lake Superior Basin to be uplifted, resulting in reverse faulting along the basins edges and resulting in new fracturing, faulting and minor folding of the PLLS and the overlying sedimentary rocks. A major geologic feature of this area is the Keweenaw fault that formed on the southeast flank of the basin, as shown in Figure 2.1. In the Keweenaw Peninsula, the Keweenaw fault's surface expression can be seen from the Keweenaw County in the northeast end to the Ontonagon County in the southwest with a length of 100 miles (White 1968). All of the native copper mining was conducted in the PLLS, mostly in the basaltic flow tops but also in some of the interbedded sediments.

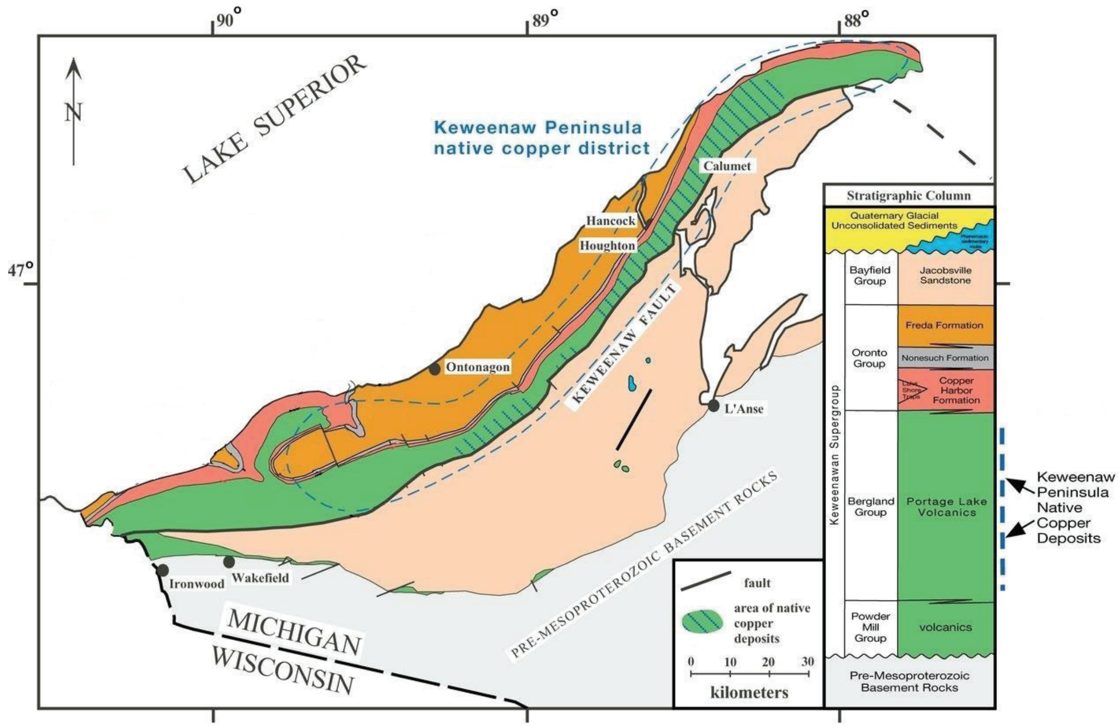

Figure 2.1. Geologic context of bedrock in the U.P. for copper mining areas [revised after Bornhorst and Williams (2013)].

2.2.2 Distributions and Properties of Soils and Rocks

As part of the geologic make-up of the U.P., soils and rocks, especially those close to mines or within mines, provide key information to help understand the numerical model configurations, boundary conditions and possibly the reason for flooded mines in the site. In particular, the permeability of soils and rocks is critical, which dictates the ability of water seeping into mines. Also, the properties of those materials, e.g., the specific heat and density, are crucial to evaluate the heat reserve and renewability for the application (Ghomshei and Eng 2007).

The soil of Keweenaw County is comprised mostly of gravelly, fine, sandy loam and cobbly muck sitting on bedrocks such as conglomerates and sandstones (Tardy 2006), leading to the soil layer in this area with high permeability. In the Houghton County, the soils are mostly loam, sand, and muck (Tardy 2006), resulting in moderate to high permeability in most places. In the place close to the Quincy mine, the Paavola series in Quincy Township consists of dark-reddish brown, loamy, fine sand and pinkish-gray, dry sand at the top, and reddish-brown, loamy, fine sand with films of clay at the bottom with a thickness of 19 to 48 inches (48 to 122 cm). This soil is very permeable at the surface and decreases in permeability toward the bottom. The deer park series close to the Hancock mine consists primarily of sand particles that are black, pale brown, and yellowish brown in color, which has moderate to high permeability.

Rocks are a key component in the flooded mine system providing pathways for water and heat flowing into mines. According to the Keweenaw fault (see Figure 2.2), rocks in this area primarily include Freda sandstones, Allouez conglomerates, Kearsarge amygdaloids, No. 8 conglomerates, No. 3 conglomerates, and the Lower Keweenawan on the west side. The Quincy mine and the Hancock mine are made up of cellular and unclassified amygdaloids, fragmental amygdaloids, and scoriaceous amygdaloids. The permeability for these amygdaloids is very different, which highly depends on cracks and fissures in the rocks. The permeability is relatively low for intact rocks but extremely high at locations where cracks and fissures exist. The permeability of the rock layers is as follows, from the highest to the lowest permeability: fissures, fragmental amygdaloids, felsitic conglomerates, coalescing amygdaloids, sandstones, scoriaceous amygdaloids, cellular amygdaloids, amygdaloid traps, shales and fault gouges. Because of its highest permeability, fissures primarily determine the ability of the geologic formations around mining spaces to allow water and energy transport. Such key information is introduced in the next section.

2.2.3 Fissures and Faults

The distribution and nature of faults and fissures in the mines in the Houghton and Keweenaw Counties are overseen in Figure 2.2. Due to the Keweenaw fault running the entire length of the Keweenaw Peninsula, the area between Eagle River and Eagle Harbor contains many faults and fissures.

In the Houghton County, Shaft 7 of the Quincy mine (Figure 2.3) includes the Hancock fault (Figure 2.2), which runs through the shaft at Portage Lake level. The fault reaches 2000 feet (610 m) in depth. A fissure cuts through Shaft 6 at Drift 55 and cuts through the levels below-extending upward and cutting through Drift 1 of Shaft 2. Another fissure cuts through Shaft 8 at Drift 24, cutting through only three drifts; one on the east side of the shaft and two on the west. More detailed information regarding fissures in the Quincy mine will be introduced in Section 2.3.1. Some drifts of the Hancock mine (Figure 2.3) are connected with those of the Quincy mine. The layers of rock around the Hancock mine have a half-parabolic shape.

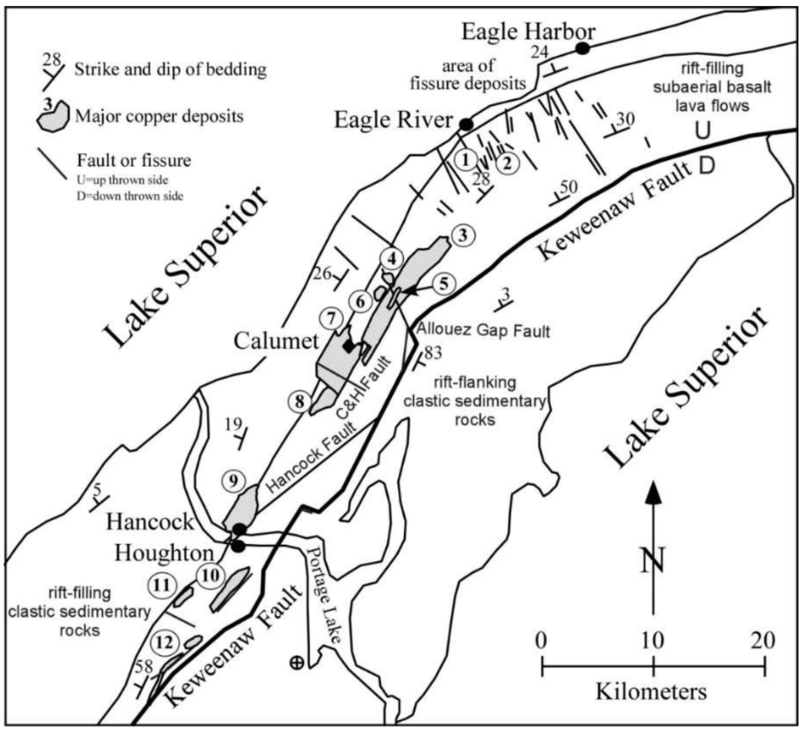

Figure 2.2. Faults and fissures distributed in the Keweenaw Peninsula (MNA 2010).

2.2.4 Underground Hydrogeology around Mines in the U.P.

According to local geological and mining experts, about 95% of the underground working spaces in the area are filled with water. The underground hydrogeology around the mines and its influence on the mass and heat transport in the mine water-geologic formation system determine the reserve and sustainability of the geothermal energy in the mine water. The key information is summarized below.

Due to the draining of groundwater into the Lake Superior watershed, glacial deposits and bedrock constitute much of the groundwater supply in the Keweenaw County. However, in the Houghton County, the Jacobsville sandstone aquifer is the major contributor of groundwater and reaches 900 feet (274 m) in depth followed by a layer of 600 feet (183 m) thick Nonesuch shale. Other suppliers of groundwater are the two lava flows of the Copper Harbor conglomerate, and the underlying andesitic and basaltic lava flows in the northern part of the County as well as the Keweenaw moraine in the central and southern part. Kames, kame terraces, eskers, and kettles are also found throughout the County (Apple and Reeves 2007). The groundwater will flow in the direction toward the Keweenaw fault and toward the greatest depth, which is located toward the top of the peninsula. This can give the groundwater a northeastern movement. It will not go straight into the fault, but will instead move toward the deepest parts or where permeability is greater. Based on the report data from GWMAP (2005), the estimated depths to water table in most regions of the Houghton County range from 0 to 15 feet (0 to 4.6 m). This information indicates that a great amount of water is available to mines in the area.

2.3 Site Exploration of Typical Mines in the U.P.

In addition to the geologic information, explorations of typical mining sites, especially those close to populated areas, are necessary for more practical evaluation of the geothermal energy in the mine water. In this section, the Quincy mine was chosen for the assessment of its potential for geothermal applications.

2.3.1 Background on the Quincy Mine

The Quincy mine started in 1848. Pewabic mine discovered the Pewabic lode of amygdaloid copper that was 12 to 15 feet thick. Contained within it was native copper. Part of this lode was on the Quincy property, giving them profitable amounts of copper from 1856 to1858. Around 1945, Quincy reached as low as 9,260 feet (2,822 m) in depth, the deepest mine in the area at that time. Due to a poor market in 1920, Quincy closed and reopened from 1937 to 1945 due to the high copper demand during World War II (Butler and Burbank 1929). Since the closure of mining activities in this area, the shafts and stopes of the mine have been slowly filled with groundwater. The water has currently filled the mine up to the seventh level, making all lower levels inaccessible.

Shown in Figure 2.3 is the layout of the underground mining spaces of the Quincy mine and the Hancock mine close to the downtown of Hancock City. The underground mining structures are projected to a horizontal plane, which is roughly parallel to the ground surface. Most roads and buildings of the downtown of Hancock are distributed on the upper right corner. The scale is 300 feet to 1 inch (91 m to 2.54 cm) in the original picture. The green lines and black dotted lines marked the major mine shafts (projection). The black curly lines are the horizontal drifts (projection), which are parallel to each other and perpendicular to the shafts. The shafts are connected by the horizontal drifts. The projection of the mining structures on the horizontal plane manifests itself as interconnected nets because most of the shafts are inclined and dip to the northwest.

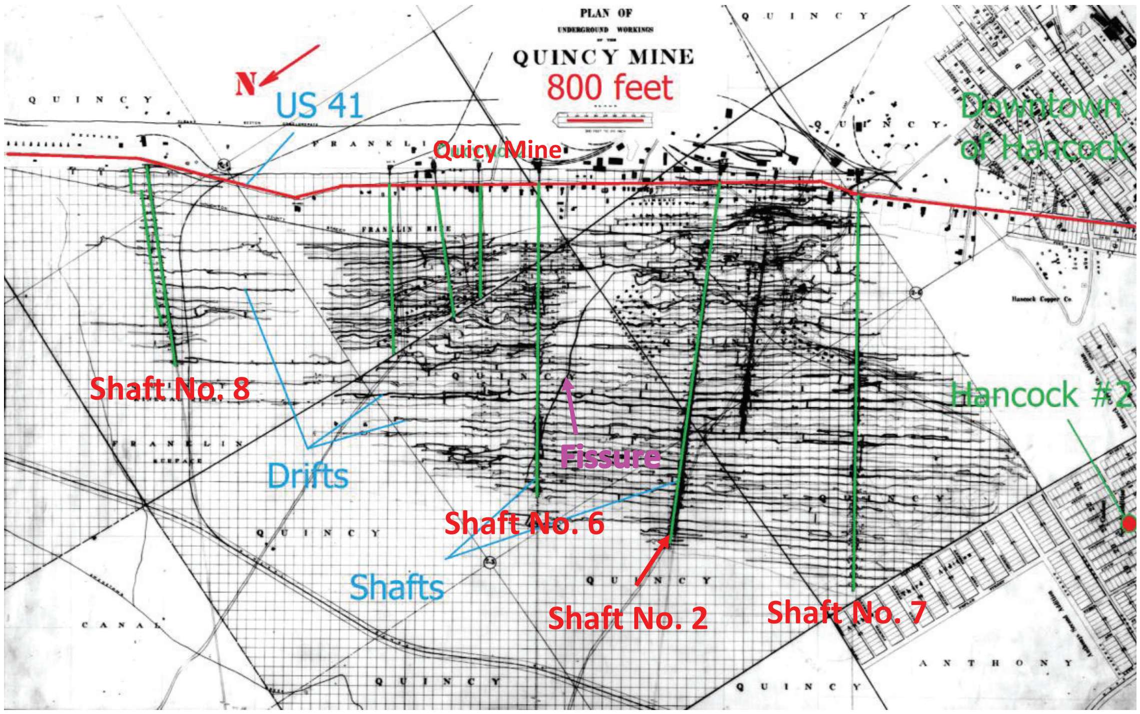

Figure 2.3. Layout of underground mining spaces of the Quincy mine [Keweenaw Digital Archives No. 27P].

The Quincy mine consists of several major mine shafts, i.e., Shaft 2, 6, 7, and 8, and some unlabeled shafts adjacent to these major shafts, as shown in Figure 2.3. The major shafts from left to right in Figure 2.3 are Shafts 8, 6, 2, and 7. According to Butler and Burbank (1929), Shaft 8 consists of 75 drifts and reaches a depth of 6,600 feet (2,012 m). Shaft 6 has a depth of 7,650 feet (2,332 m) and 81 drifts. The distance between Shaft 6 and Shaft 2 is 1,890 feet (576 m). Shaft 2 is the deepest shaft, 9,260 feet (2.82 km or 1.75 miles) along the dip of the deposit on a 55-degree inclination with 85 drifts, when the mine ceased production in 1945. Shaft 7 has a depth of 6,130 feet (1,868 m) and consists of 70 drifts. Those unlabeled shafts, which include approximate 35 drifts for each, have a relatively shorter depth than the major ones. Most of the deep copper mine shafts are inclined at an angle, ranging between 28 to 73 degrees. Due to the depth of the lodes, copper mines in this area are often deeper than other types of mine shafts in the U.S., leading to a reachable depth with a very high temperature in the geothermal field for bulk mine water.

Figure 2.3 also shows some fissures. One of the unlabeled fissures, for example, cuts through Drift 11 at 290 feet (88 m) from Shaft 8 toward the right and at Drift 13 right where the drifts start from Shaft 8. The same fissure also crosses the adjacent shafts. Another fissure, which was marked in Figure 2.3, cutting through Shafts 6 and 2 starts at Shaft 2 and moves downward and toward the southwest, crossing into Shaft 6. Many drifts of Shaft 6, such as Drifts 9 and 13, are cut through by this fissure. Due to the reason that many drifts of Shaft 6 are connected with those of Shaft 2, this fissure cuts through many drifts such as Drifts 1, 3 and 16 on the left of Shaft 2. Drift 45 of Shaft 2 corresponds to Drift 31 of Shaft 6, where the fissure cuts through the shaft.

After the closure of the mining activities, groundwater started to fill the underground mining spaces. The Quincy mine has been filled to the 7th level, where an adit was developed for drainage. It thus is concluded that a great amount of water is stored in the underground spaces. The top layer of the mine water is strongly influenced by air temperature. But when it reaches a specific depth, i.e., 200 feet (60 m), it is reasonable to assume that water therein is independent of temperature variations in the atmosphere. As the depth further increases, the water temperature turns to be more influenced by geothermal gradients. According to some miners, the temperatures at the bottom of some shafts were estimated to be as high as 100 ^{o}F (38 ^{o}C). It is therefore predicted that a tremendous amount of geothermal energy is stored in the abandoned mining spaces, making them potential low-enthalpy geothermal reservoirs. But it is worthwhile to mention that the temperature distribution and its variation in the mine water are still a key but little-understood issue and require further investigations.

2.3.2 Estimation of Thermal Energy Reserve

2.3.2.1 Estimation Using Conventional Volume Method

The conventional way to estimate the thermal energy of the mine water is the volume method (Raymond and Therrien 2008). Due to the complexity of the underground mine structures, the volume of the mine water in the Quincy mine cannot be calculated directly, but rather, can be estimated based on the amount of the production of Pewabic amygdaloid lodes from this mine. According to Butler and Burbank (1929), the total production of lodes from 1862-1906 and 1911-1925 was estimated to be 27,268,298 tons. Accordingly, the volume of the mine water is 9.81×10^{6} m^{3} if the density of these lodes is assumed to be 2,780 kg/m^{3}. The geothermal gradient in this area was around 0.015 degree Celsius per meter of a depth according to Van Orstrand (1920). If the temperature at the surface of the mine water is 9 ^{o}C according to field measurements of the site (see Figure 3.2 in Section 3.2), the temperature at the bottom of Quincy (2,822 m) can reach 49.5 ^{o}C, which is much higher than that estimated by the local miners (38 ^{o}C). The static energy storage of the mine water then can be estimated using the following equation:

$$H_w = \eta c \rho V (T_h - T_c) \tag{2.1}$$

where H_w is the energy (kWh), $\eta = 0.0002778$, which is the unit conversion factor (kWh/kJ), c is the specific heat of the mine water (kJ/(kg °C)), V is the volume of the mine water (m^3), T_c and T_h are the temperature (°C) of the mine water on the top and at the bottom, respectively, and ρ is the density of the mine water (kg/m^3), which in fact varies with its temperature and is slightly higher than that of distilled water (Wolkersdorfer 2008). For simplicity, ρ was assumed to be 1,000 kg/m^3 for the thermal energy estimation.

Table 2.1. Estimation of the thermal energy in the mine water from the Quincy mine.

Parameter	**Unit**	**Case 1**	**Case 2**	**Case 3**	**Case 4**
Temperature difference	°C	40.5	42.5	44.5	46.5
Specific heat	kJ/(kg °C)	4.2			
Volume	m^3	9.81E+06			
Energy	kW h	4.64E+08	4.86E+08	5.09E+08	5.32E+08
Household (10000 kW h/year)	-	4.64E+04	4.86E+04	5.09E+04	5.32E+04
Heat conversion to other energy resources	natural gas [m^3 (ft^3)]	1.33E+8 (4.68E+9)	1.39E+8 (4.91E+9)	1.46E+8 (5.14E+9)	1.52E+8 (5.38E+9)
	petroleum [m^3 (gallons)]	1.28E+5 (3.37E+7)	1.34E+5 (3.53E+7)	1.40E+5 (3.70E+7)	1.46E+5 (3.87E+7)
	coal [tons]	2.41E+05	2.52E+05	2.64E+05	2.76E+05

Note: The heat conversion of the thermal energy of the mine water was made according to the U.S. Energy Information Administration.

Table 2.1 shows the thermal energy of the mine water estimated using Eq. (2.1) and its conversion to the equivalent heat content of other energy resources. When the temperature difference in Case 1 is 40.5 ^{o}C, the thermal energy is 4.64×10^{8} kW h, which is comparable to the heat content from 1.33×10^{8} m^3 (4.68×10^{9} ft^3) of natural gas, 1.28×10^{5} m^3 (3.37×10^{7} gallons) of petroleum, or 2.41×10^{5} tons of coal. According to the U.S. Energy Information Administration, the annual energy consumption for a U.S. residential utility household is 10,000 kW h, this amount of energy in Case 1 can satisfy 46,400 residential utility customers. However, the geothermal gradient in this area is possibly much greater than 0.015 ^{o}C/m. It is thus necessary to estimate the thermal energy using a higher geothermal gradient, which is reflected as a greater temperature difference. In Cases 2, 3 and 4, the temperature differences were assumed to be 42.5 ^{o}C, 44.5 ^{o}C, and 46.5 ^{o}C, respectively. Accordingly, the thermal energy reserves of Cases 2, 3 and 4 are estimated to be 4.86×10^{8} kW h, 5.09×10^{8} kW h, and 5.32×10^{8} kW h, respectively, leading to a higher estimate than that of Case 1. The number of residential utility households also increases accordingly.

It is also worthwhile to mention that, for Cases 1-4, the volume of the mine water was estimated only considering the periods of 1862-1906 and 1911-1925, which did not include 1856-1861, 1907-1910, and 1937-1945 due to a lack of available data. Some underground spaces in the mine for transportations and operations were also not included. These three periods plus such huge underground spaces probably correspond to a much larger volume of the mine water. In addition, $T_c = 9\,^{o}$C, which was used for the above estimates, is still high, and thus, can be decreased in practice to yield a higher thermal energy estimate. Due to the above reasons, the thermal energy reserve of the mine water in the Quincy mine is expected to be greater than the current estimates.

2.3.2.2 *Estimation Considering Thermal Energy Recharge*

The above static energy reserve estimation using Eq. (2.1) is conservative. The water in the Quincy, in fact, is similar to a big "battery" that will be recharged with the heat by the surrounding geologic formations, which, however, is not considered in the static energy reserve with Eq. (2.1). According to Muffler and Cataldi (1978), the energy recharge to the mine water can quickly reach over 10% of the original total thermal energy if the heat flux from the rocks is considered. Therefore, the Thermal Energy Recharge (TER) deserves to be considered, which will be discussed in this section.

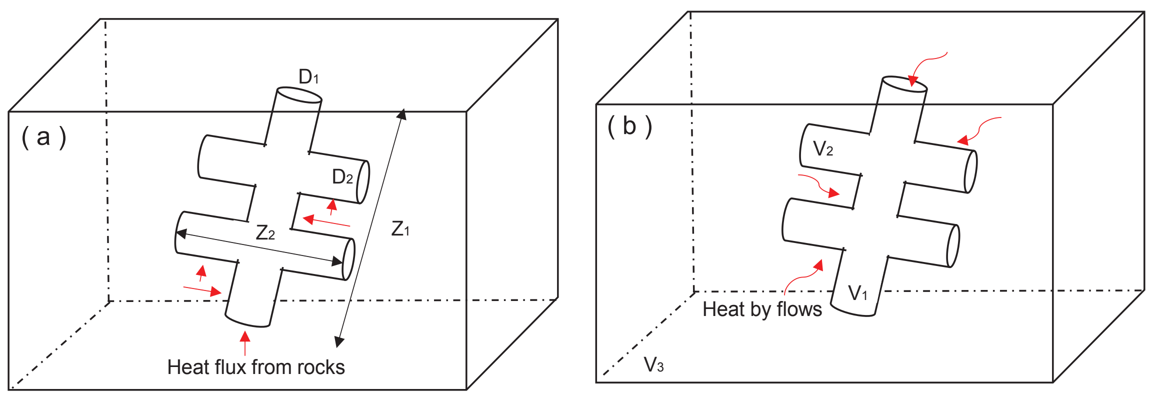

Figure 2.4. Conceptual view of the thermal energy recharge from (a) the surrounding rocks and (b) fluid transport through the surrounding rocks

To include the TER, we consider the dynamic energy recharge from the surrounding rocks and from the fluid transport through the surrounding rocks with high temperatures. Figure 2.4 shows the conceptual geometry of a representative shaft with these two major types of the TER. The geometry of the mine water is thus needed to calculate the TER. However, the structure of the Quincy mine is extremely irregular. To solve this, the mine shaft and drifts were assumed to be cylindrical, as shown in Figure 2.4, because previous studies such as Hamm and Sabet (2010) usually simplified the mining spaces as interconnected cylinders. To compute the TER, 9 shafts in the Quincy mine were adopted according to Butler and Burbank (1929). The TER to the whole mine water is equivalent to the sum of the TER to the mine water in each shaft. According to Muffler and Cataldi (1978), the total thermal energy reserve E_{tot} is:

$$\begin{cases} E_{tot} = H_w + H_r + H_f \\ H_w = \sum_{i=1}^{m} c\rho V^i (T_h^i - T_c) \\ H_r = \sum_{i=1}^{m} (\phi_q \pi D_1^i Z_1^i + n^i \phi_q \pi D_2^i Z_2^i) t \\ H_f = \theta c_r \rho_r V_3 (T_r - T_c) \end{cases} \tag{2.2}$$

where H_w is the thermal energy calculated using Eq. (2.1); H_r is the TER conducted from the surrounding rocks (Figure 2.4a); H_f is the TER convected by water flow from rocks with high temperatures (Figure 2.4b); t is the time (s); ϕ_q is the conductive heat flow (W/m^2); n^i is the number of horizontal drifts (the superscript means the i^{th} shaft); D_1^i and D_2^i are the diameter of a shaft and a drift, respectively; Z_1^i and Z_2^i are the length of a shaft and a drift, respectively; θ is the rechargeable factor; c_r is the specific heat of rocks (kJ/(kg ^{o}C)), ρ_r is the density of rocks (kg/m^3), V^i and V_3 (m^3) are the volume of the i^{th} mine water and rocks, respectively; T_r is the temperature of rocks (^{o}C) at the bottom; m is the number of shafts and $m = 9$ for the Quincy mine; and T_h^i is the bottom temperature, which can be estimated with the depth of each shaft and the geothermal gradient.

To evaluate H_r, $Z_1^i = 5Z_2^i$ was assumed and n^i for each shaft was chosen according to Section 2.3.1. Also, $5D_1^i = D_2^i$ was assumed because of the relatively large dimensions of stopes in the Quincy mine according to Butler and Burbank (1929). The ratio between H_r and H_w thus can be calculated to evaluate the rate of the TER regarding H_r with respect to time using the following equation:

$$\frac{H_r}{H_w} = \sum_{i=1}^{m} \frac{(\phi_q \pi D_1^i Z_1^i + n^i \phi_q \pi D_2^i Z_2^i)t}{c\rho V^i (T_h^i - T_c)} = \sum_{i=1}^{m} \frac{4\phi_q t(1+n^i)}{c\rho D_1^i (1+5n^i)(T_h^i - T_c)} \tag{2.3}$$

where $V^i = \pi D_1^{i2} Z_1^i / 4 + n^i \pi D_2^{i2} Z_2^i / 4$. Figure 2.5 shows that H_r / H_w varies as a function of t and ϕ_q when $D_1 = 5$ m. Five typical ϕ_q values were adopted according to Muffler and Cataldi (1978). As can be seen, H_r / H_w linearly increases with time. In addition, the rate of the recharge increases with the increase of ϕ_q. H_r / H_w can reach 10% within 4 years if $\phi_q = 0.063\ \mathrm{W/m^2}$. The time for the TER due to H_r significantly decreases when ϕ_q increases from $0.063\ \mathrm{W/m^2}$ to $0.84\ \mathrm{W/m^2}$. These observations reveal that ϕ_q is a key parameter to determine the rate of recharging such a big "battery" from the rocks, which primarily depends on the heat transfer coefficient. According to Zhang et al. (2015), the heat transfer coefficient for the water-rock interface mainly depends on the flow velocity. The mine water, in reality, is not stagnant (Wolkersdorfer 2008). Therefore, increasing the mine water velocity is a way to increase ϕ_q.

It is seen that the TER can easily reach the level of the static reserve estimate in the conventional method within a few years even with only H_r. Therefore, it is very necessary to consider the TER for evaluating the geothermal energy reserve in the mine water.

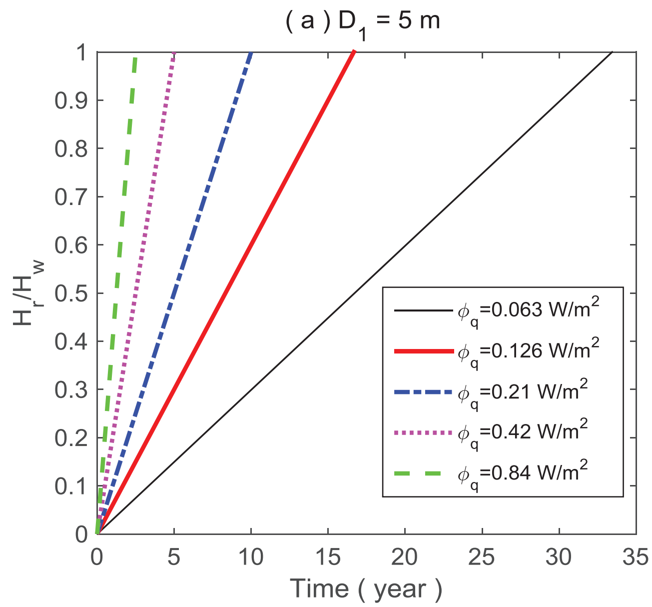

Figure 2.5. H_r / H_w as a function of t and ϕ_q to the mine water when $D_1 = 5$ m

H_f is also considerable, because the water in the mine primarily comes from flow transport through the permeable rocks, especially fissures and faults. Similar to H_r, H_f was evaluated with the reference to H_w. According to Muffler and Cataldi (1978), the influence of H_f can be formulated using a rechargeable factor θ:

$$\frac{H_f}{H_w} = \frac{\theta c_r \rho_r V_3 (T_r - T_c)}{c\rho V_{tot} (T_h - T_c)} = \frac{c_r \rho_r}{c\rho} R\theta \tag{2.4}$$

where V_{tot} is the total volume of the mine water; $T_r = T_h = T_{h|\max}$ (T_h is from Eq. (2.1)), where $T_{h|\max}$ is the bottom temperature of the mine water of the deepest shaft; and $R = V_3 / V_{tot}$. Figure 2.6a plots H_f / H_w as a function of θ with three values of R. H_f / H_w linearly increases as θ increases. To obtain a certain amount of H_f, the needed value of θ decreases with the increase of R. More specifically, when $H_f / H_w = 0.1$, which is of practical significance according to Muffler and Cataldi (1978), θ decreases with the increase of R (see Figure 2.6b). This is because, while heat is eventually from rocks, a larger rock volume provides a better energy resource, leading to the higher TER. In a small range of R, e.g., $R = 1$, θ is equal to 18%. However, this value of R seems geologically unreasonable because the volume of rocks should be larger than that of the mine water. When $R = 10$, θ is approximately equal to 1.8%. To understand the TER due to H_f, Figure 2.7 shows the TER in the static energy reserve for Case 1 in Table 2.1 considering H_f. It is seen that this TER is obvious. Among them, the TER is 25 GWh, 65 GWh, and 130 GWh at $\theta = 5\%$ when R is equal to 2, 5, and 10, respectively. Therefore, it is indicated that the TER due to H_f will be significant in this large natural system at reasonable values of R.

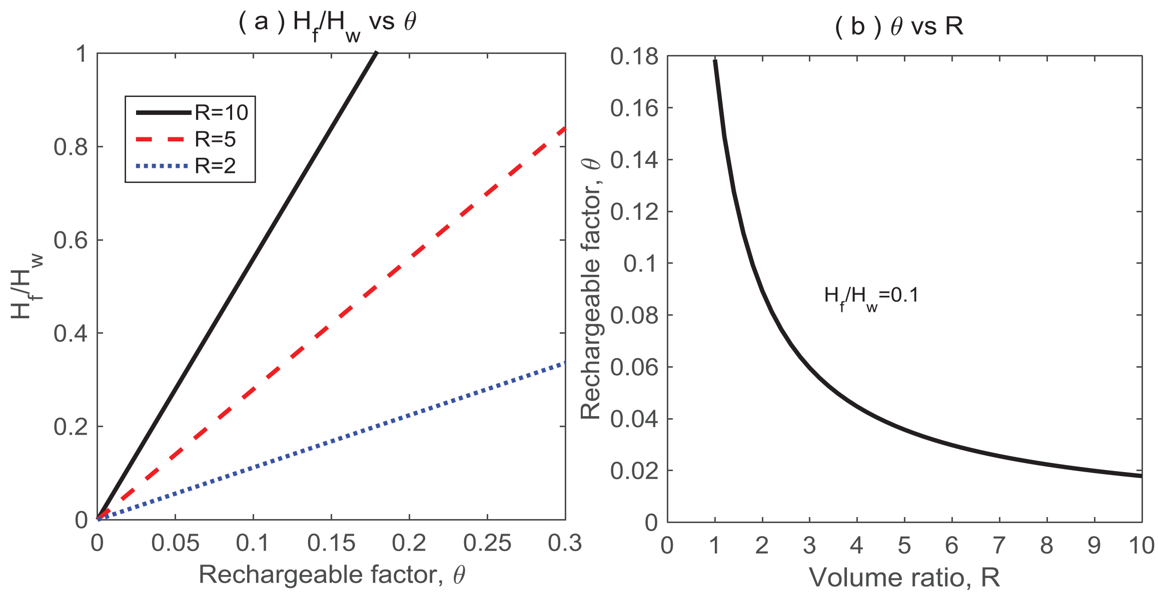

Figure 2.6. Estimation of H_f: (a) H_f / H_w as a function of θ and R and (b) θ vs R when $H_f / H_w = 0.1$

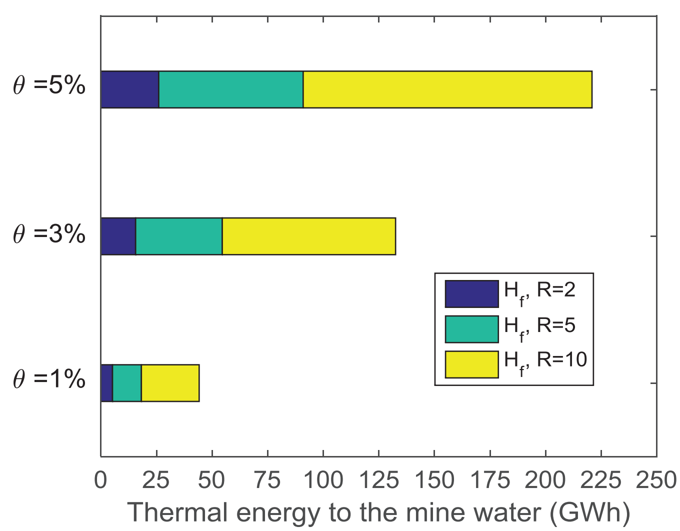

Figure 2.7. TER to the static energy reserve considering H_f with three different R at three different θ.

Another helpful angle for the thermal energy estimation is to compare the energy of the mine water incorporated with the energy recharge with that of a small-scale power station. The energy produced by a power station can be estimated using the following equation:

$$G = 365Ch \tag{2.5}$$

where G is the annual electricity generation produced by a power station (GWh), C is the power capacity (GW), and h is the working hours per day (hour) and h=12 was assumed in this chapter. For the comparison, three power stations in Michigan, i.e., GM Pontiac, White Pine, and Escanaba Paper, were adopted, which have the power capacity of 29 MW, 40 MW, and 54 MW, respectively (U.S. Energy Information Administration).

The energy reserve in the Quincy considering the renewability of the energy is comparable to a small-scale power station. Figure 2.8 shows the energy comparison between the mine water and these power stations. In this comparison, we use the total thermal energy of the mine water estimated based on Case 1 in Table 2.1. This total thermal energy was divided by the duration of time in Figure 2.5a under three different ϕ_q to obtain the annual energy. As can be seen, the energy of the mine water approximates a half of that of GM Pontiac when $\phi_q = 0.21\ \text{W/m}^2$. As ϕ_q increases to $0.84\ \text{W/m}^2$, the energy of the mine water exceeds that of GM Pontiac and of White Pine, but is less than that of Escanaba Paper. The results from Figure 2.7 and Figure 2.8 show that the TER to the mine water is very significant, and thus, cannot be neglected, leading a favorable increase in the potential of geothermal energy for the application.

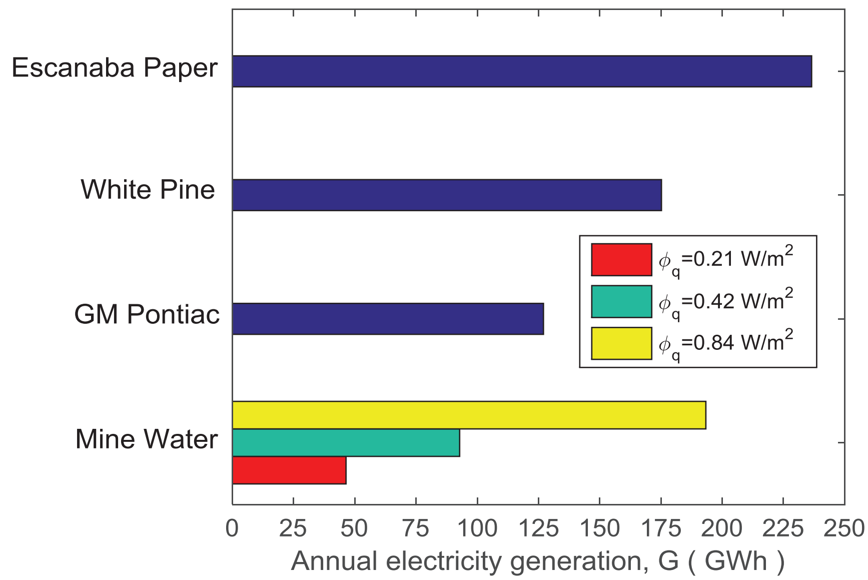

Figure 2.8. Energy comparison between the mine water with three different ϕ_q and three power stations in Michigan.

2.4 A Demonstration Project

It is a worldwide issue to revitalize historical mining areas, especially considering the common socioeconomic issues in these areas such as the "dirty energy" tags, poverty and shortage of energy, on a basis of local conditions specific to mining such as far and remote locations and abandoned mining facilities. In the U.P., besides waiting for a rebound in the mining industry, many great efforts have been made to revitalize such areas and to enhance the well-being of the residents. Among attempts, a demonstration project was launched by the Keweenaw Research Center (KRC) in the U.P. in 2009 to explore the possibility of using geothermal energy from a flooded mine in the region. In this project, geothermal energy was tapped from the mine water to provide heating and cooling for an 11,000 square feet building near the Houghton County Airport from the New Baltic No.2 mine shaft.

Shown in Figure 2.9 is the schematic of the set-up of heat pumps and pipe distribution system for geothermal applications using the mine water in the KRC. The set-up of heat pumps and pipe distribution system are similar to that of the GHP applications. The geothermal pipes were distributed in the engineering center of the KRC including a reception area, offices, conference rooms, computer centers, lunch rooms, and bathrooms. Air ducts were installed in those areas to transfer thermal energy from the mine water to the surrounding air for the purpose of space heating. The mine water was piped into a big heat exchanger. Through this heat exchanger, the mine water heats a closed loop system within the building. Due to a low temperature outside, a special attention was made to ensure that the water of this closed loop system moves smoothly inside the pipes. The water always moves inside the pipes and is mixed with glycol to avoid freezing. The water-glycol mix circulates and runs through heat pumps throughout the building for heating purposes.

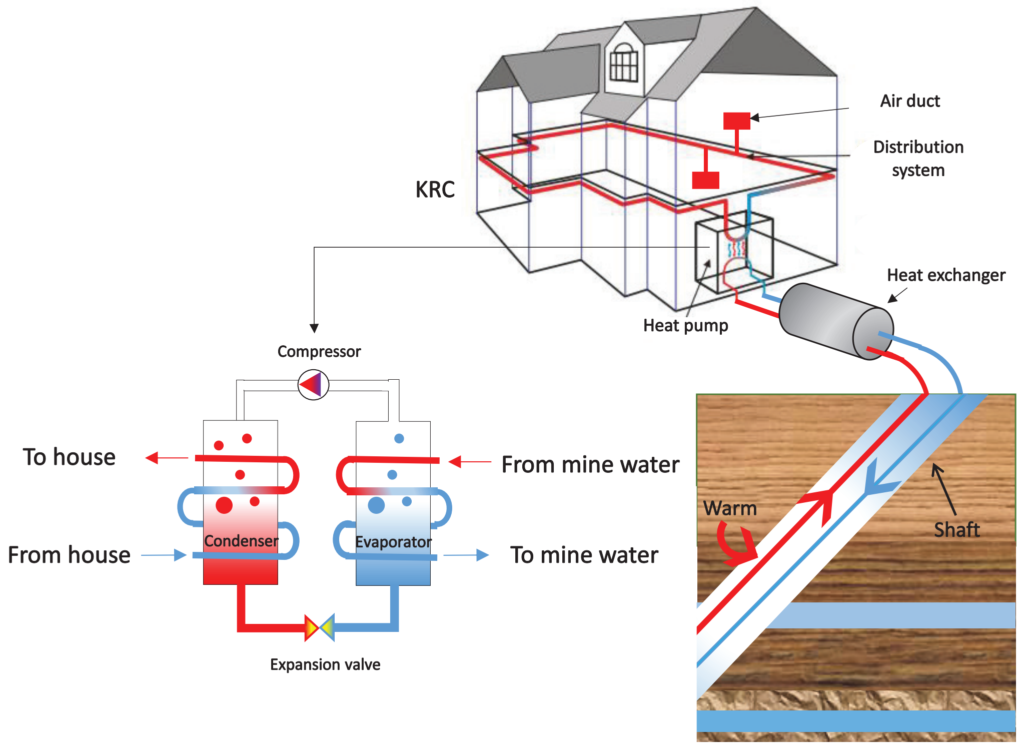

Figure 2.9. Schematic of the use of the mine water for geothermal applications in the KRC.

The initial KRC geothermal system installation consisted of 14 heat pumps with a nominal heating capacity of 435,000 BTU/hr. A 90 gpm (gallon per minute) pump pulls the mine water from a 300 feet depth and sends it through a double wall plate heat exchanger. On the building side of the heat exchanger, a 160 gpm pump circulates water to all the heat pumps. The initial heating design point was based on an entering water temperature of 40 ^{o}F (4.4 ^{o}C) and a leaving water temperature of 34.6 ^{o}F (1.4 ^{o}C), which is typical for geothermal heat pumps. When the actual entering water temperature turned out to be near 55 ^{o}F (12.8 ^{o}C), the coefficient of performance of the heat pumps increased by 20%. In 2014, a 4,000 sq-ft addition required the installation of four more heat pumps with a heating capacity of 149,000 BTU/hr. While the primary temperature conditioning in the region is the need for heating, the multiple heat pump systems simultaneously heat and cool different portions of the building, which frequently happens as the computer server room always needs cooling while the offices need heat. The KRC geothermal system cost approximate \$100,000 to install during the building's construction phase. Based on the condition of its service, the director of the KRC estimated that a payback period is three to five years and the rough installation cost savings are about 30% over a conventional natural gas system. Because of its benefits, the KRC is intended to expand this mine water-based geothermal on the site to install a new and smaller system in a separate building.

For geothermal heating using the mine water, a higher average annual temperature indicates a higher energy output-input ratio, i.e., the coefficient of performance. The U.P. has a primary need of heating with a low average temperature, so it possibly represents an extreme situation that is less economical. Despite this extreme situation, a demonstration project launched by the authors still indicated that heating using the mine water is very economically attractive. An estimate of economic benefits was made and is shown in Table 2.2. The estimate of cost (M) was calculated using the following equation:

$$M = r\delta H_w \tag{2.6}$$

where r is the dollar per unit consumption of a heating resource, e.g., \$/gallon for oil, and δ is the efficiency factor. For heating, the financial benefit of geothermal application (with mine water) in the U.P. is better than heating with electricity, propane or diesel fuel. Table 2.2 was made under the condition that the western portion of the U.P. had the second highest electrical price in the nation and a very low cost of fuel. As most costs of the geothermal-mine water system occur during installation and later system operation using electricity, a lower electrical rate could significantly reduce the cost, making the application of the technology in other parts of U.S. a possibly even much more economical option. The geothermal energy from the mine water may provide an effective way to alleviate the socioeconomic issues in mining areas.

Table 2.2. Residential heating cost comparison for the Upper Peninsula of Michigan.

Heating Method	\$ per Million BTU	Comments
Electric Heating	\$ 58.61	Electrical rate of \$0.20/kWh, 100% efficiency
Heating Oil	\$ 30.19	#2 Fuel Oil at \$3.54/gallon, 85% furnace efficiency
Propane	\$ 28.62	\$2.25/gallon, 85% furnace efficiency
Mine Water Geothermal	\$ 15.08	55°F mine water, COP=4.7, \$0.20/kWh, electricity
Natural Gas	\$ 8.24	\$0.70/Therm, 87% furnace efficiency

The project has been running well and data have been continuously monitored. Though not well known by outsiders, this effort is of great significance as it proved the feasibility of recovering geothermal energy from the mine water in the U.P. More than that, it has a scientific and practical significance beyond the territory of the area. It is one of the limited numbers of real projects in the world for such applications with the mine water in deep hard-rock mining and a groundbreaking one in the U.S.

2.5 Conclusions

This chapter presents a comprehensive study, which has been conducted in the Upper Peninsula of Michigan, for exploring the use of water from deep abandoned mine shafts for geothermal applications in-house heating/cooling. Three major components, relevant geologic information, i.e., properties of representative rocks, faults faults and fissures and underground hydrology, the site exploration and its energy reserve estimation, and a real project demonstration, were presented to provide a complete background and preliminary results for understanding the recovery of the geothermal energy from the deep abandoned mines in the site. The results indicated that there is a great amount of thermal energy potential stored in the Quincy mine in the U.P., which can be used for geothermal applications. The effort of this chapter is of great significance because it not only proved the feasibility of recovering geothermal energy from deep abandoned mines in the U.P., but set up a paradigm in the U.S. for recovering geothermal energy from abandoned mines in other mining areas. It is the first time that the economic value of this energy renovation is validated by comparing to other heating options based on a large-scale demonstration project and that the high power of this type of low-enthalpy geothermal energy reservoir is investigated and reported for deep mines.

3 Heat Potential Evaluation and Understanding of Heat Transfer Mechanisms

This chapter introduces the scientific part of a large-scale study in the Upper Peninsula (U.P.) of Michigan, a historical mining area, for exploring the water in deep abandoned copper mines as a geothermal energy resource. The main focus of the chapter is placed on the scientific understanding of the natural mine water-geologic formation system, especially the transport of heat and mass in this large-scale natural system. For this purpose, this chapter presents the results of a field study involving measurements of temperatures and chemicals in a local mine shaft in the U.P. and numerical analyses to preliminarily investigate the quasi-equilibrium water movement in this local mine shaft due to geothermal gradients to provide insights into the phenomena observed in the field study.

3.1 Introduction

Geothermal energy recovery from flooded underground mines has been gaining momentum worldwide since the pioneering work in Canada in 1989 (Jessop et al. 1995). The application of the use of the water in flooded mines, i.e., mine water, as a geothermal resource is a variation of the Surface Water Heat Pump (SWHP) system (Zheng et al. 2015), which falls into the category of low-temperature geothermal applications (ASHRAE 2009). The SWHP is less common than other Geothermal Heat Pump (GHP) systems, i.e., Ground-Water Heat Pump (GWHP) system and Ground-

Coupled Heat Pump (GCHP) system, as the SWHP involves environmental and legal concerns when accessing natural waters (e.g., lake, pond, and river). Moreover, the SWHP SWHP can represent a higher-quality geothermal energy resource because bulk water provides a better medium for heat transfer than the pore water used in the GWHP and the water in pipes and backfill soils in the GCHP. As a variation of SWHP, the concept of the geothermal application in this study is to pump the water from deep abandoned mines and exchange heat between the pumped water and buildings for heating/cooling purposes. This type of SWHP application thus takes advantage of abandoned facilities (Malolepszy et al. 2005; Raymond et al. 2008), provides more economical energy compared to the conventional heating methods (e.g., fuels) (Behrooz et al. 2008), and avoids many concerns with natural water bodies in the conventional SWHPs (Jessop et al. 1995). But some aspects of this type of SWHP for its application need to be considered. Especially, the scientific questions behind the application are much different from those behind the conventional SWHPs, because the mine water-geologic system possibly represents a much more delicate system due to the extremely low velocity of the mobile water, high geothermal gradients, and complicated geologic and mining situations.

However, there is no doubt that the use of the mine water as a geothermal resource inherits most of the socioeconomic and environmental benefits of conventional GHP applications: safe (Limanskiy and Vasilyeva 2016), green (Ramos and Falcone 2013), relatively renewable and adaptable (Burnside et al. 2016; Burnside et al. 2016). In addition, from a technical perspective, the nature of this type of SWHP application provides more attractive advantages, making it a much higher grade geothermal resource: eco-friendly and environmental utilization of waste materials (abandoned mine water), higher-quality geothermal energy (higher geothermal gradient), highly efficient exploration (heat transport of bulk water), and economical utilization (utilization of existing facilities). The mine water has a unique feature which can even further magnify the above benefits: it can move due to both natural convection (caused by geothermal gradients and salinity) and forced convection (water from surrounding geologic formations, surface water, and the energy extraction process) (Hamm and Sabet 2010; Reichart et al. 2011). This feature (i.e., bulk water movement due to both natural convection and forced convection), in fact, is very useful and highly desirable. This is because natural convection in bulk water triggers warm water (at the bottom with a higher temperature) to move upward to heat cold water (at the top); forced convection caused by the heat extraction process will lead to a greater temperature difference, which can further expedite this natural convection process. Therefore, the heat transfer due to this feature can exceed that in the conventional GWHPs and GCHPs by many orders. Though still far from being satisfactory, numerical simulations have been adopted to understand the underlying mechanisms. Hamm and Sabet (2010) modeled the hydraulic behavior of the mine reservoir and the mine water temperature in a production shaft. Their study revealed the impact of the natural convection, the production flow rate, and the permeability of the surrounding rocks on the geothermal potential for explorations. More efforts have been made with an emphasis on several critical issues for the topic. One example is that Streb and Wieber (2011) investigated the locality for extracting the mine water at a required temperature without causing a decrease in the potential of the discharge using a hydraulic model. The lifespan of the required temperature supply from the mine water in the flooded coal mines was also discussed by Arias et al. (2014) and their numerical results indicated that the studied mine water-based geothermal system would serve over 30 years.

Despite several real demonstration projects launched worldwide for the mine water-based geothermal application (Jessop et al. 1995; Jessop 1995), a thorough scientific understanding of the mechanisms associated with recovering geothermal energy from the mine water is still absent. However, such an understanding is critical to the practical implementation of the energy technique. Since economic paybacks are usually the major driving force for the application, the first two things of interest are usually what will be the water temperature available for the geothermal heat pumps (efficiency) and how will that temperature vary as the exploration proceeds (sustainability). However, as mentioned above, the mine water has a unique feature when it is considered as a geothermal resource: energy is convected by moving fluid elements of the mine water. The significance of this factor is not predictable. The major phenomenon in the mine water was summarized as 'thermohaline staircases' caused by a thermosolutal flow (Reichart et al. 2011). To be more specific, a buoyancy-driven flow, which results from the density difference due to temperature (thermal) and salinity (solute) differences, is proposed to be the major process of interest in the mine water. Experimental and numerical studies suggested that seepage from surrounding geological formations (Jessop et al. 1995; Renz et al. 2009) and the configuration of the mine working spaces (Wolkersdorfer 2008; Kories et al. 2004) may also play significant roles.

Due to the complexity of and limited accessibility to the underground mining space, the underlying uncertainty may only be disentangled by means of numerical simulations with the help of limited site measurements. Though a very few, numerical studies have been made to investigate either the sustainability concern regarding the energy recharge from the geologic formations around the mine water (Malolepszy 2003), or the efficiency concern regarding the hydrodynamics (buoyancy-driven flow for heat variation) in the mine water (Hamm and Sabet 2010; Hamm et al. 2008). In particular, two numerical studies have been conducted to understand non-isothermal hydrodynamics of the mine water, which is a key in this geothermal application by controlling the temperature variation and distribution. Hamm and Sabet (2010) investigated the temperature variation of the mine water in a vertical shaft using non-isothermal hydrodynamics without the thermal coupling between the mine water and the surrounding geologic formations. In the other study, Reichart et al. (2011) investigated the temperature variation of the buoyancy-driven flow triggered by both temperature and salinity using a small scale of the mine water (around 1 m). However, these studies were concentrated on either geologic formations or mine water, instead of the multiphysics of the whole system. This fact is possibly attributable to several reasons: 1. the complexity of the physical mechanisms in the natural process, 2. high computational cost, and 3. limited data from the field. In addition, numerical simulation of this type is mostly separated from field studies due to the limited accessibility to abandoned underground mines. A comprehensive study of mine water-based geothermal applications (i.e., a variation of SWHP system), including a field study, the theoretical understanding, and numerical analyses, is highly desirable. This chapter will fill this knowledge gap by presenting such a study. A field test on Hancock Shaft 2 is presented. A theoretical framework is developed for the thermo-hydrodynamic process in the mine water coupled with heat transfer in the surrounding geologic formations. A preliminary assessment of Shaft 2 is presented to shed light on the buoyancy-driven flow.

3.2 Field Study on Hancock Shaft 2

It is known from Section 3.1 that the temperature distribution within the water in deep abandoned mines is a key issue to this geothermal application. However, it is usually difficult to obtain such data. This is because abandoned underground mining working spaces may partially collapse after flooding and very limited information can be obtained regarding what structures remain after the mine is closed. Some field data are available indirectly from those environmental and mining investigations into water stratification in abandoned mines (Wolkersdorfer 2008). However, few field measurements can be found for the purpose of recovering geothermal energy from flooded mines, let alone field measurements conducted in parallel to other site explorations and numerical analyses.

This section introduces a field study for measuring the temperature and chemical distributions in an abandoned copper mine shaft located in the Upper Peninsula (U.P.) of Michigan. This copper mining region was the first major copper mining region in the U.S., which started in the 1840s and ceased in 1968. Hundreds of deep mines were developed during this period with some mines reaching depths of 2,400 m due to the depth of the lodes. Among them, the Quincy mine was the most famous copper mine, which had the deepest shaft (i.e., Shaft 2 in Figure 3.1) with a depth of 2.82 km, when it ceased production in 1945. Another copper mine on the southwest of the Quincy mine was the Hancock mine, which had two major shafts (Shaft 1 and Shaft 2). These mines were with groundwater soon after their closures and are available for the potential geothermal energy resource.

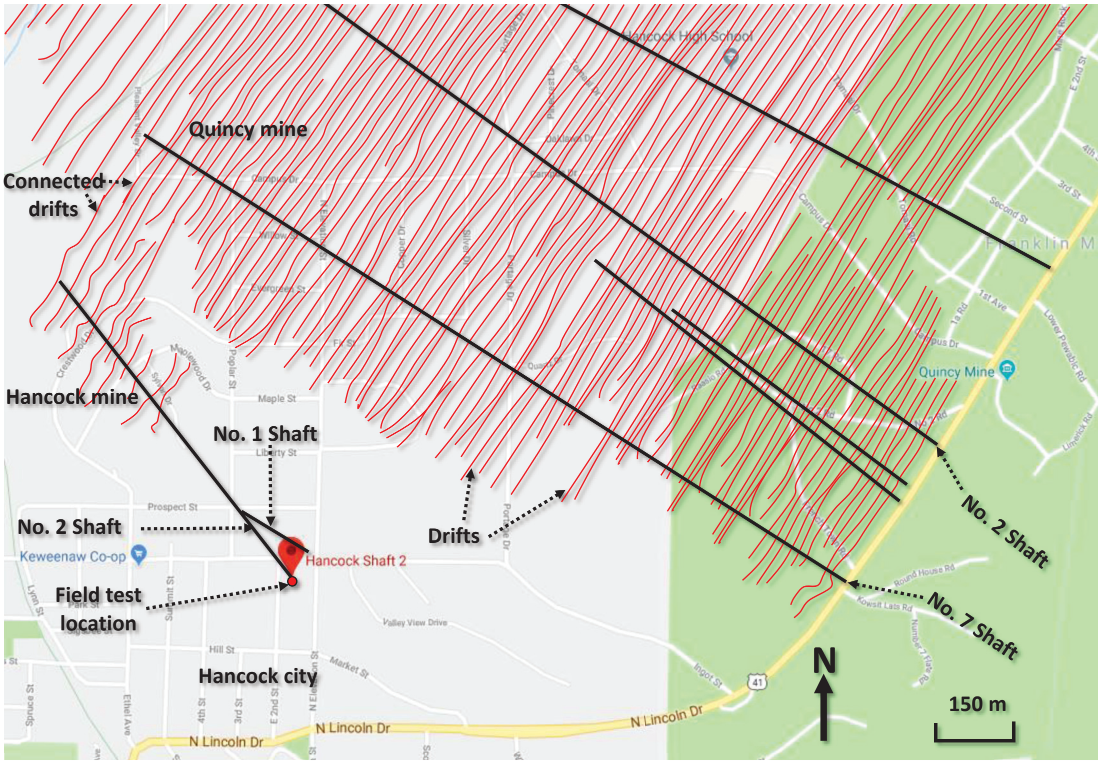

Figure 3.1. Layout of underground mining spaces of Quincy and Hancock mines [Developed with Google map].

Shown in Figure 3.1 is the layout of the underground mining spaces of the Quincy mine and the Hancock mine close to the downtown of Hancock City. The 3D underground mining structures are projected to the map for visualization. The black lines from the southeast to the northwest are the major mine shafts, e.g., Hancock Shaft 2 and Quincy Shaft 7 (projection). The red lines are the horizontal drifts (projection) from the southwest to the northeast. The drifts are parallel to each other and perpendicular to the shafts. The shafts are connected by the horizontal drifts. In this study, a nearly vertical shaft, i.e., Hancock Shaft 2 in the lower left corner of Figure 3.1, was chosen for the measurements. The field measurement location was marked by a red dot, which is located in the Hancock City.

Technically, the Hancock Shaft 2 was not "abandoned" but sealed many decades ago. The excavation for the shaft was started in December of 1906, which reached 400 feet (122 m) deep by the end of the year. By November of 1908, it reached 1,300 feet (396 m) with the shaft being sunk to the massive dimensions of 29' 6" by 9' 6" (9 m by 2.9 m) and contained four hoisting compartments and one service duct. Another main shaft in the Hancock mine group, i.e., Hancock Shaft 1, is close to Hancock Shaft 2. These two shafts are connected on the 13th level. In 1915, the 63rd level of the Hancock Shaft 2 at a depth of 1 km was drilled through to a drift that corresponds the drift of the Quincy Shaft 7 to form the connected drift (see Figure 3.1), and the two were, from then on, worked as one. The final depth of the Hancock Shaft 2 was estimated to be 4,000 feet (1219.2 m).

There is a practical reason for choosing this vertical shaft, though it is not typical in the U.P.: it is very hard to lower equipment down into the shaft which could be over thousands of meters long. Attempts have been made in the U.P. to send robots down non-vertical shafts, which might overcome this issue. However, it was found that most parts of the submerged mining structure are covered with a thin layer of silt and the propulsion of the robot can easily stir the silt up and make the mine water almost invisible. Therefore, this vertical shaft was chosen for the test.

Sensors for temperature and electrical conductivity were sent down into the shaft using a pulley system, which is similar to the wireline system in the oil industry (Clark 1988; Dines et al. 1988). Based on one ongoing real project for this geothermal application in the U.P., it was estimated that 1,000 feet (305 m) are a limit, beyond which pumping costs would overcome the economic gain of the geothermal application with the mine water in the U.P. Notwithstanding, the sensors were lowered to a depth slightly over 3,000 feet (914 m) for a better understanding of the water movement and temperature distribution. The temperature transducers had a slow response time to a temperature change. The depth was not recorded with the temperature transducer. But instead, the best effort was made to correlate the temperature and the depth based on time. An encoder was deployed on the pulley system to accurately calibrate for depth. Two temperature sensors, i.e., the HOBO U12 stainless temperature data logger and the Aqua TROLL 200 temperature sensor, were used. The HOBO temperature sensor has a measurement range of -40^{o}C~125^{o}C and can work appropriately under a maximum pressure of 2200 psi. Its measurement resolution and accuracy are 0.03^{o}C at the measurement range of 0~20^{o}C and ±0.25^{o}C at the measurement range of 0~50^{o}C, respectively. The Aqua temperature sensor has a measurement resolution of 0.01^{o}C and an accuracy of ±0.1^{o}C. It has a maximum working pressure of 500 psi and a measurement range of -5^{o}C~50^{o}C. The Aqua TROLL 200 conductivity sensor was utilized for electrical conductivity measurements. This sensor has a measurement range of 5~100,000 $\mu S/cm$. Its measurement accuracy and resolution are ±1.005 $\mu S/cm$ and 0.1 $\mu S/cm$, respectively. The above three sensors were all internal memory data logging devices and were calibrated before the test. A pressure gage (related to depth) was used to ensure that the sensors were not "hung up" on anything.

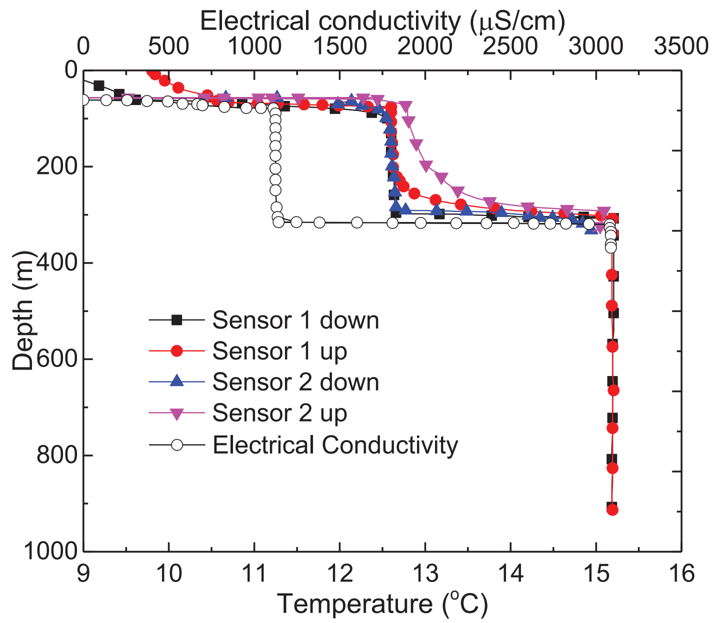

Figure 3.2. Measured distributions of temperature and electrical conductivity.

The measured variations of the temperature and electrical conductivity with depth are shown in Figure 3.2. It is seen that the water level is at 200 feet (60 m) below the ground surface. Therefore, data at positions above that point are of limited value. The water temperature is not linearly distributed along the depth, as predicted for stagnant water surrounded by rocks with a linear temperature distribution because of an approximately constant geothermal gradient. Instead, the data clearly demonstrate the existence of two constant temperature zones with an average temperature of 54.7°F (12.6°C) and 59.3°F (15.2°C), respectively. The existence of the two constant temperature zones indicates that the water is stratified. This stratification is also supported by the distribution of the electrical conductivity. The value of the electrical conductivity indirectly reflects the distribution of the total salt concentration. As can be seen, the changes in the temperature and electrical conductivity happen at about the same depths. The distributions of both the temperature and electrical conductivity led us to the same deduction: water moves relatively fast within individual layers (zones or cells) and consequently, resulting in a constant temperature and electrical conductivity in each layer. There are slight differences in the temperatures measured by different sensors and in those measured by the same sensor but in different runs (i.e., up or down). The major reason is the slow temperature response of the transducers that were continuously raised or lowered, leading to temperature-depth profiles that are not highly accurate.

In order to provide cross-references, water was sampled at 200 (61 m), 577 (176 m), 750 (229 m), 1,000 (305 m), and 3,000 (914 m) feet using a Kemmerer water sampler. The numbers of collected samples from the above corresponding depths were one, three, four, five, and six, respectively. The samples were analyzed at the White Water Associates in Amasa (certification number #65802), Michigan. pH and alkalinity were measured with potentiometry using a standard hydrogen electrode (4500-H+B) and with the Titration Method (2320B), respectively. The metals contained in the samples were determined with the method 6010B using an Inductively Coupled Plasma (ICP). The Method Detection Limit (MDL), which determines the minimum concentration of a substance with 99% confidence, was used to evaluate the measurement accuracy. All the measurements were conducted by the White Water Associates under the procedure of each standard method. The results from the measurements present direct evidence for the distributions of different minerals in the mine water. As shown in Table 3.1, the results support the deduction obtained above regarding the water stratification. More than that, the results from Table 3.1 also help provide a direct estimate of the quality of the mine water in the site for the safe use, which is another concern for exploring the mine water for geothermal applications. The concern could be raised when the acid mine water is pumped out and chemicals, such as heavy metals, are stirred up or pumped out from the mine water in the deep mining space. Table 3.1 shows that the concentration of Mn varies with depth, where it is less than 0.53 mg/L before 1,000 feet (305 m) and increases to 1.6 mg/L at the depth of 3,000 feet (914 m). The above values of the concentration of Mn are much lower than the upper limit value (59 mg/L) calculated using Rule 57 for evaluating the quality of non-drinking surface water according to Department of Environmental Quality, Michigan. In addition, according to Piatak et al. (2006), a range of pH values for water samples collected from the Pike Hill copper mines in Vermont in the U.S. is 3.1-4.2, which is undesirable as it is too acid. However, as shown in Table 3.1, the range of the measured pH of this mine water is 6.8-7.1. Such a range is very safe as the mine water is close to neutral rather than acid. This is because the mine water quality possibly has rebounded due to the mine water "rebound" process (i.e., flooding) with low alkaline (pH range:7.0-7.5 according to (Kubitz et al. 1995)) water in the local area. Therefore, the range of the measured pH of this mine water is very close to local surface water.

Table 3.1. Measured results for chemical concentrations in the mine water.

Depth	CO_3	HCO_3	pH	mg/L	Cl	F	Fe	Mn	Na	K	NO_2 NO_3	SiO_2	SO_4
	mg/L	mg/L			mg/L	mg/L	mg/L	mg/L	mg/L	mg/L	mg/L	mg/L	mg/L

Feet	Carbonate Alkalinity	Bicarbonate Alkalinity	pH	Hard ness	Chloride	Fluoride	Iron (t)	Manganese (t)	Sodium (t)	Potassium (t)	Nitrate Nitrite-N	Silica (d)	Sulfate
200	0	190	7.1	300	170	0	1	0.12	41	0.97	0.22	15	37
577	0	200	6.9	470	280	0	14	0.52	62	0.85	0	16	0
750	0	200	7.1	450	280	0	11	0.46	61	0.78	0	17	0
1000	0	200	7.1	490	310	0	11	0.53	64	0.77	0	17	0
3000	0	210	6.8	1300	920	0	34	1.60	150	0.87	0	33	0
MDL	5	5	0.1	0.3	4	0.006	0.01	0.0013	0.15	0.12	0.1	0.03	15

Note: MDL=Method Detection Limit

3.3 Numerical Analysis: Thermo-Hydrodynamic Modeling

This chapter presents the scientific part of a large-scale study in the Upper Peninsula (U.P.) of Michigan, a historical mining area, for exploring the water in deep abandoned copper mines as a geothermal energy resource. The main focus of the chapter is placed on the scientific understanding of the natural mine water-geologic formation system, especially the transport of heat and mass in this large-scale natural system, which is critical to the efficiency and sustainability of the energy renovation. A theoretical framework for the thermo-hydrodynamic process in the mine water coupled with heat transfer in the surrounding geologic formations is developed to outline a mathematical description for studying the scientific issue. Also, simulations are conducted, based on the real geologic information for Hancock Shaft 2 introduced in Chapter 3, to preliminarily investigate the quasi-equilibrium water movement in this local mine shaft due to geothermal gradients to provide insights into the phenomena observed in the field study in Section 3.2.

3.3.1 Theoretical Formulation of Underlying Mechanisms

From a multiphysics viewpoint, the scientific understanding of the problem in this study possibly involves heat transfer, water movement, particle transport, chemical reactions, and mechanical responses in both the mine water and the surrounding geologic formations. It is a so-called thermo-hydro-diffuso-chemico-mechanical problem in the water-geologic formations system (Renz et al. 2009; Reichart et al. 2011). However, a comprehensive consideration of the above mechanisms is nearly impossible due to constraints in the computational resources. It is believed that hydrodynamics in the mine water is a critical part of the geothermal energy recovery while the multiphysical processes in the geologic formations are possibly much less significant in this application. In addition, multiphysics frameworks in porous materials have been successfully implemented and validated in the previous studies, e.g., Liu and Yu (2011) and Liu et al. (2012), therefore, it is less urgent to implement such multiphysics frameworks in this study. Due to the above considerations, the focus in this chapter is placed on the hydrodynamics of the mine water.

A few numerical studies have been conducted previously to evaluate the efficiency of the energy application by studying the hydrodynamics (buoyancy-driven flow) in the mine water or to investigate the sustainability of the system by studying the heat transfer in the geologic formations (Hamm and Sabet 2010; Hamm et al. 2008). However, these studies for heat transfer are focused on either the mine water or the geologic formations and consequently, they fail to reflect the real thermal field in the system. In fact, the whole mine water-geologic formation system needs to be considered by including the hydrodynamics in the mine water, heat transfer in the surrounding geologic formations, and their couplings.

To capture these mechanisms, this section outlines a theoretical framework for the thermo-hydrodynamic process in the mine water coupled with heat transfer in the surrounding geologic formations. Overall, this framework is intended for a multiphysical process involving the thermal field in both the geologic formations and the dynamics of water movement in an open mining space. The thermo-hydrodynamic framework includes the transient natural convective motion of water and heat in the system. The transport of salts is also included in this theoretical framework but is not considered in the later simulations. The governing mechanisms in the system can be mathematically described by a multiphysics framework as follows.

The movement of the mine water in deep underground mining spaces could be considered as large-scale hydrodynamics. For this large-scale hydrodynamics, water can be reasonably assumed to be incompressible. The continuity equation for the incompressible flow is formulated as:

$$\nabla \cdot \mathbf{U} = 0 \tag{3.1}$$

where $\mathbf{U}$ is the velocity of the mine water (m/s). The momentum balance of water is described as:

$$\frac{\partial \mathbf{U}}{\partial t} + \nabla \cdot (\mathbf{U}\mathbf{U}) - \nabla \cdot [\frac{\mu_{\mathrm{eff}}}{\rho}(\nabla \mathbf{U} + \nabla \mathbf{U}^T) - \frac{2}{3\rho}\mu_{\mathrm{eff}}(\nabla \cdot \mathbf{U})\mathbf{I}] = -\frac{1}{\rho}(\nabla p_{\mathrm{d}} + \rho_{\mathrm{eff}}\mathbf{g}) \tag{3.2}$$

where ρ is the density of the mine water (kg/m^3); $\mathbf{I}$ is the identity matrix; μ_{eff} (Pa s) is the effective viscosity represented using $\mu_{\mathrm{eff}} = \mu_{\mathrm{laminar}} + \mu_{\mathrm{turbulent}}$, in which μ_{laminar} and $\mu_{\mathrm{turbulent}}$ are the laminar dynamic viscosity and the turbulent dynamic viscosity, respectively; p_{d} is the dynamic pressure (Pa) and is formulated by $p_{\mathrm{d}} = p - \rho g h_e$, in which g is the acceleration (m/s^2), h_e is the elevation (m), and p is the total pressure (Pa); and ρ_{eff} is the effective density (kg/m^3), which is a function of temperature T (K) and salinity S and can be described using the following equation:

$$\rho_{\mathrm{eff}} = \rho_{\mathrm{eff}}\left(T, S\right) \tag{3.3}$$

The governing equation for salt transport is formulated as:

$$\frac{\partial S}{\partial t} + \mathbf{U} \cdot \nabla S = \nabla \cdot \left(\alpha_S \nabla S\right) \tag{3.4}$$

where α_S is the solute diffusivity coefficient of the mine water (m^2/s), which is given by $\alpha_S = \alpha_{\mathrm{laminar}}^S + \alpha_{\mathrm{turbulent}}^S$. Generally, the salinity of the mine water increases with depth, leading to a higher density in the salty water when compared to the fresh water. The fresh water thus overlays the salty water. This suppresses the natural convection in the mine water. The governing equation for salt transport is presented here to complete the framework. For simplicity, the difference in the mine water due to salinity is excluded in the later simulations in this study.

The energy conservation within the moving fluid element can be formulated in terms of the temperature T (K) as follows:

$$\frac{\partial T}{\partial t} + \mathbf{U} \cdot \nabla T = \nabla \cdot (\alpha_T \nabla T) \tag{3.5}$$

where α_T is the thermal diffusivity of the mine water (m^2/s) and is given by $\alpha_T = \alpha_{\text{laminar}}^T + \alpha_{\text{turbulent}}^T$.

Heat transfer in the surrounding geologic formations is coupled to the heat transfer in the mine water. To be more specific, the heat conduction happens across the interface between the surrounding geologic formations and the mine water if the temperatures on two sides of the interface are different. Thermal conduction in geologic formations is governed by the following equation:

$$\rho_{\text{s}} c_{\text{p}} \frac{\partial T}{\partial t} = \nabla \cdot (k_s \nabla T) \tag{3.6}$$

where ρ_{s} is the solid density (kg/m^3), c_{p} is the specific heat of the solid (J/(kg K)), k_s is the thermal conductivity of the solid (W/(m K)). Figure 3.3 illustrates the thermal coupling process at the interface between the two regions, i.e., the mine water and its surrounding geologic formations. As can be seen, the energy rate ϕ_w via convection for the mine water and the energy rate ϕ_c via conduction for the surrounding rocks are formulated as:

$$\phi_w = hA(T_i - T_{wc}) \tag{3.7}$$

$$\phi_c = \frac{k_s}{\delta} A(T_{rc} - T_i) \tag{3.8}$$

where h is the convective heat transfer coefficient (W/(m^2 K)), A is the area (m^2), T_i is the temperature at the interface, T_{wc} and T_{rc} are the cell-center temperature in the water region and the solid region adjacent to the interface, respectively, and δ is the distance

(m) between the face-center (the center of a face of a finite volume cell) at the interface and the cell-center in the solid region. At the interface, $\phi_w = \phi_c$, we obtain

$$T_i = \frac{k_s / \delta}{h + k_s / \delta} T_{rc} + \frac{h}{h + k_s / \delta} T_{wc} \tag{3.9}$$

At every iteration, Eq. (3.9) was used to determine the temperature at the interface, which will be used as the boundary temperature to solve a transient heat equation in each region. The value of k_s is constant and given (see Table 3.2 in Section 3.3.3) while the initial values of h for each cell are calculated with Eq. (3.7) using the given initial T_i at the first iteration. After that, the values of h (calculated with T_i from the last step) and T_i are updated automatically by iterations. In such a way, the interface between the two regions is thermally coupled.

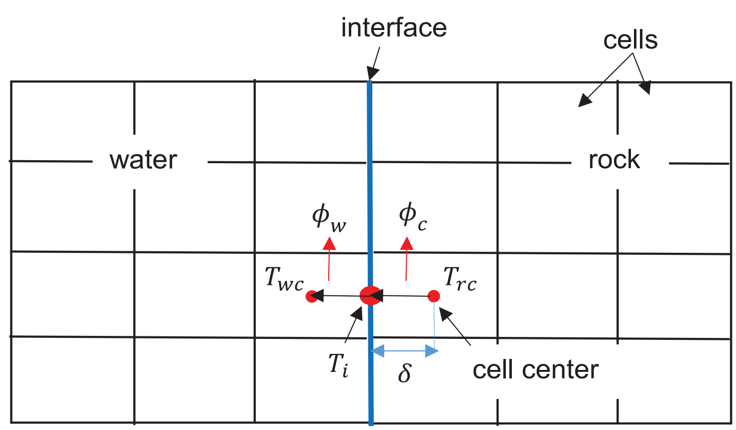

Figure 3.3. Schematic of thermal coupling between the mine water and surrounding rocks.

3.3.2 Numerical Framework Validation

The validation of the developed model in the above section against a documented experiment is presented in this section. Braga and Viskanta (1992) conducted an experiment to investigate transient natural convective heat transfer in water (near its maximum density) in a rectangular cavity with inside dimensions of 150 mm in height, 300 mm in length, and 75 mm in depth. The experiment consisted of three major parts as shown in Figure 3.4, i.e., a cold wall in which the temperature was maintained at 273.15 K, a hot wall (opposite to the cold wall) in which the temperature was maintained at 281.15 K, and water between the two walls in which there was a small gap (3 mm) between the top insulation and water to produce a free water surface. The walls around water were insulated and several thermocouples were inserted into the top, middle and bottom of the water body to measure temperature variations with respect to time at these points.

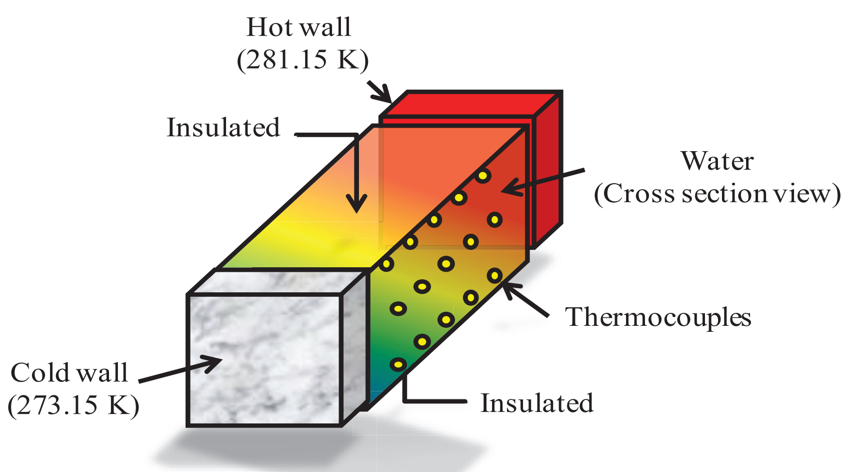

Figure 3.4. Schematic cross-section view of the experiment conducted by Braga and Viskanta (1992).

This experiment was performed to investigate heat transfer and water movement triggered by temperature differences. To visualize the flow patterns, the water was mixed with an amount of neutrally buoyant particles (Braga and Viskanta 1992), which was scanned by the laser beam so that the flow patterns can be visualized through the front and back insulations. The Boussinesq approximation (see Eq. (3.11)) is valid in most cases to simulate natural convection as the density of fluids decreases linearly with increasing temperature. However, this approximation is invalid for this experiment due to the effect of density inversion. To be more special, the maximum density of water appears at 277.13 K so that the density fails to linearly vary with temperature, which significantly affects the natural convective motion at locations near to the density extremum (Braga and Viskanta 1992). In order to accurately simulate this experiment, the relationship between the fluid density and the corresponding temperature was corrected using Eq. (3.10) (McDonough and Faghri 1994):

$$\begin{cases} \rho_{\mathrm{eff}} = \rho_{\mathrm{ref}}[1+\beta_1 T+\beta_2 T^2+\beta_3 T^3+\beta_4 T^4]^{-1} \\ \rho_{\mathrm{ref}} = 999.972(kg/m^{-3}) \\ \beta_1 = -0.67896452\times 10^{-4}(°C^{-1}) \\ \beta_2 = 0.907294338\times 10^{-5}(°C^{-1}) \\ \beta_3 = -0.964568125\times 10^{-7}(°C^{-1}) \\ \beta_4 = 0.873702983\times 10^{-9}(°C^{-1}) \end{cases} \tag{3.10}$$

The initial and boundary conditions in the current simulation were set up according to the real conditions. An initial temperature of 281.15 K was uniformly distributed within the water body. Non-slip was used on all boundaries between the water and walls. For the boundary conditions of flow on the free surface, the velocity normal to the surface was set up zero while zero gradients were defined for velocities in the other directions. Due to the negligible dimensions in the surrounding solids, heat transfer in the solids was not considered in this case. The parameters regarding thermal and transport properties used in the model were adopted from Braga and Viskanta (1992). 78,120 cells were generated for the water body and 0.1 s was selected as the time step. Such a mesh and time step were tested and a good accuracy and computing cost were obtained with them.

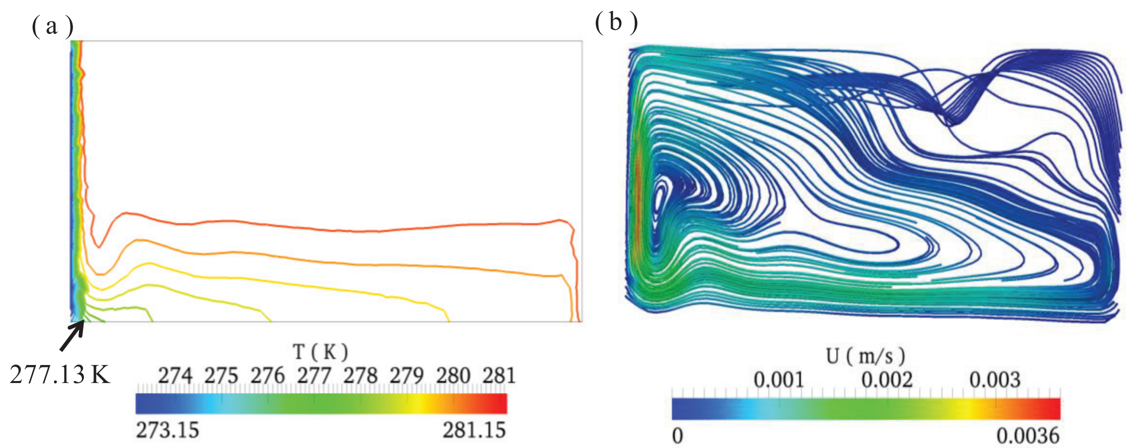

Figure 3.5. Numerical simulation results on a cross-section of height at t=5 min: (a) temperature distribution and (b) streamlines.

The water density distribution with temperature in the cavity has been presented in Figure 3.5a based upon transient isotherms. The maximum density appears at the 277.13 K isotherm at a location close to the corner, which separates the water body into two parts with different flow patterns. But during this period, heat conduction was predominant within the water body in the process. Therefore, these two separate parts with different flow patterns in the cavity is not explicit. This result also can be validated by the corresponding transient streamlines presented in Figure 3.5b. It can be clearly seen that the flow circulates anticlockwise from the hot wall to the cold wall, which verifies that heat conduction was dominant and convection was initiated during this period. Unfortunately, no results regarding flow patterns were obtained in the experiments during this period.

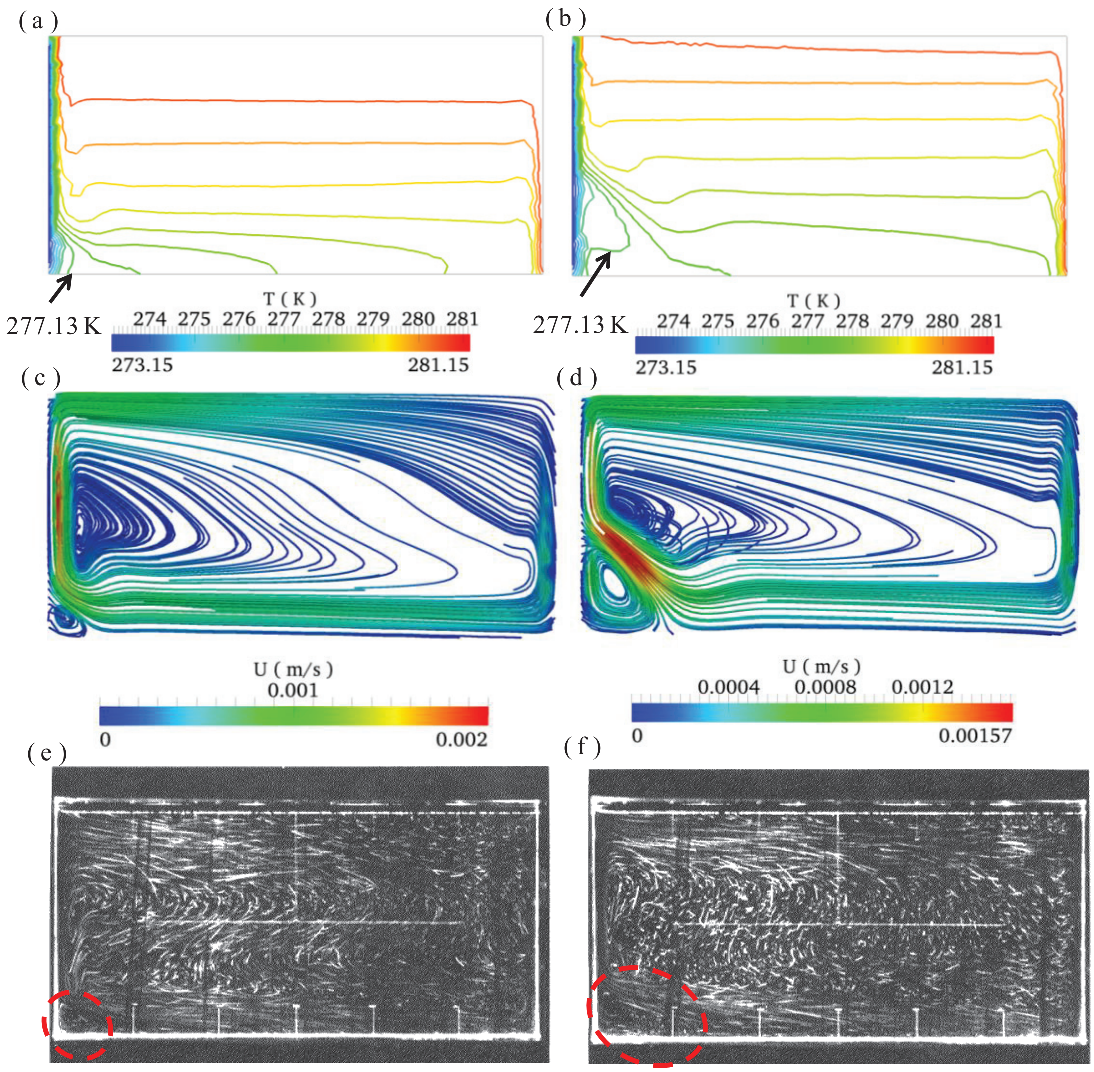

Figure 3.6. Numerical simulation results on a cross section of height: (a) temperature distributions at t=15 min; (b) temperature distributions at t=30 min; (c) streamlines at

t=15 min; (d) streamlines at t=30 min; (e) observed streamlines at t=15 min; (f) observed streamlines at t=30 min (observed photos are copied from Braga and Viskanta (1992)).

Interesting flow patterns caused by natural convection were observed as time elapsed. At t=15 min, the fluid that had been cooled to the density inversion (Figure 3.6a) exhibited two circulations. One circulation is that the flow along the cold wall at the corner is forced to move up and then to move down along the 277.13 K isotherm due to buoyancy as shown in Figure 3.6c. The other circulation followed a similar flow pattern obtained at t=5 min. The flow patterns at t=15 min show very good agreement with the observed flow patterns in Figure 3.6e. This phenomenon is also confirmed by the results obtained at t=30 min in Figure 3.6b and Figure 3.6d. Due to the heat convection, two separate flow circulations are more obvious. The observed flow patterns in Figure 3.6f reaffirm this phenomenon with very a good comparison.

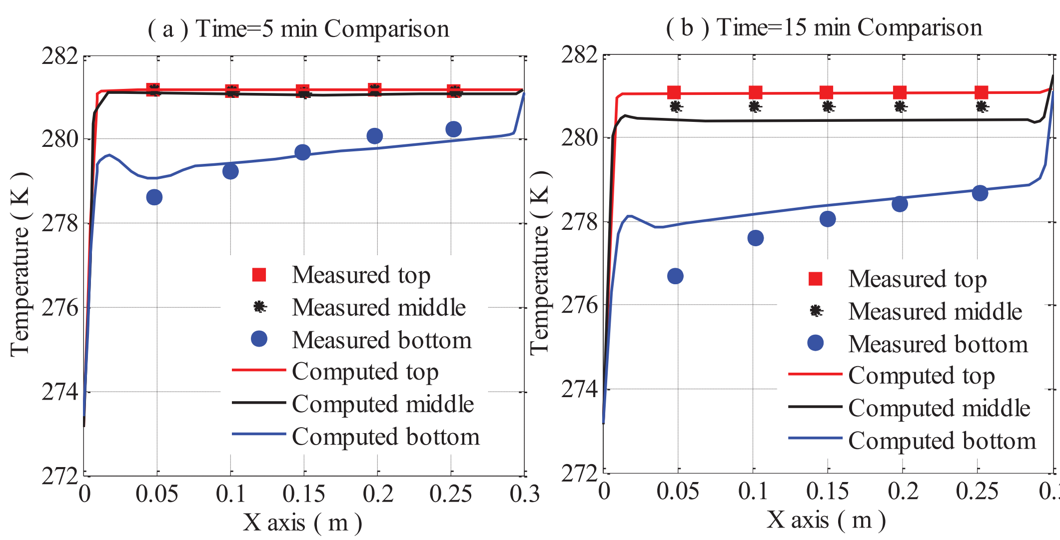

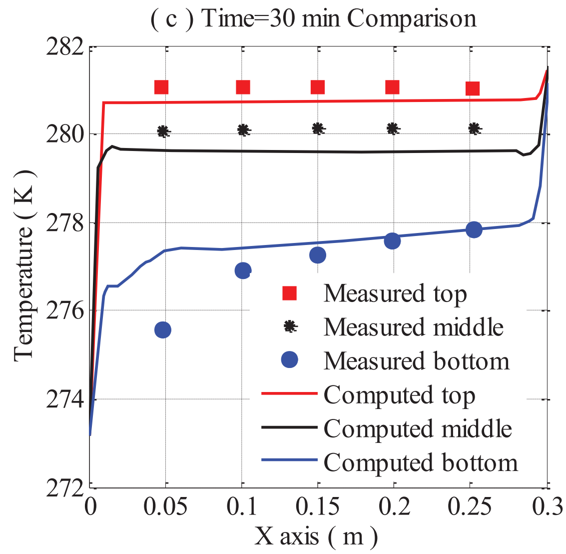

Figure 3.7. Computed temperatures compared with measured temperatures: (a) t=5 min; (b) t=15 min; and (c) t=30 min (measured data are reproduced from Braga and Viskanta (1992)).

Good comparisons between the computed and measured temperatures further proved the good accuracy of the model. As presented in Figure 3.7, it can be clearly seen that the distributions of computed temperatures match very well with that of measured temperatures at all different positions for all different times. A slight difference in the comparison between the computed temperatures and measured temperatures at the bottom was primarily caused by heat conduction along the thermocouple probes (Braga and Viskanta 1992). This heat conduction is particularly significant at locations close to the lower left corner where the density inversion appears. Therefore, the measured temperatures are slightly smaller than the computed values.

3.3.3 Preliminary Assessment of Hancock Shaft 2

The above section validated a theoretical framework laid down in Section 3.3.1 for simulating the complicated physical processes in the mine water-surrounding geologic formation system. The following work was carried out to meet the urgent need for testing the performance of the above framework for hydrodynamics in a mine water environment affected by the heat from the surrounding rocks, especially for the buoyancy-driven flow, which is believed the dominant mechanism. The purpose is to reproduce the quasi-equilibrium water movement process, in which the mine water is well mixed due to the temperature difference caused by the geothermal gradient. Moreover, it will be of practical interest if simulations based on the theoretical framework can provide insights into the data obtained from the field study introduced in Section 3.2, even though a direct comparison is difficult due to the lack of data. Such transient simulations have been conducted and preliminary results are presented in this section.

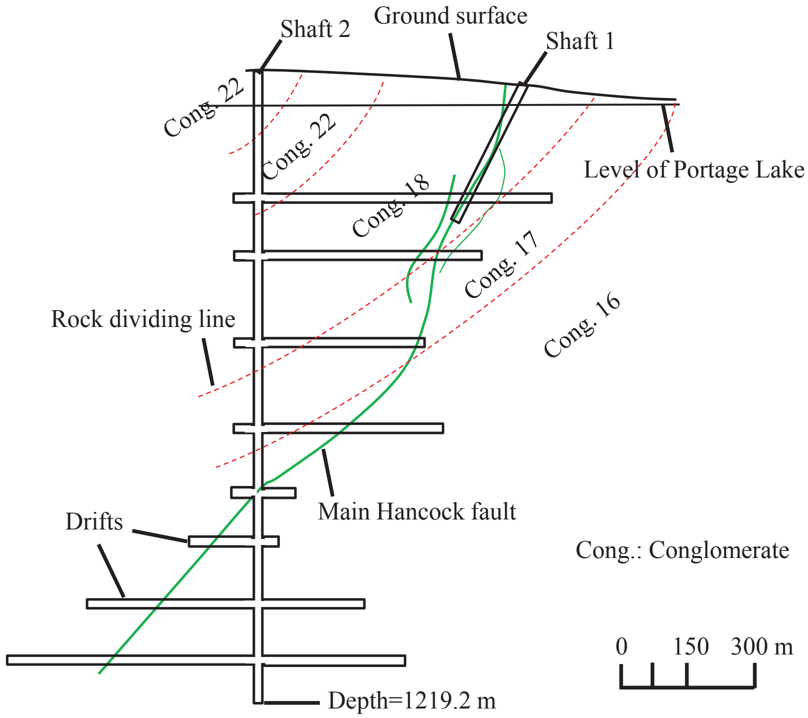

Figure 3.8. Underground structure layout of a cross-section of the Hancock mine according to (Butler and Burbank 1929).

Thermo-hydrodynamic modeling of the mine water in the Hancock Shaft 2 in the U.P. was preliminarily implemented. According to Butler and Burbank (1929), as shown in Figure 3.8, the Hancock Shaft 2 is almost vertical and connects eight horizontal drifts at different depths. Shaft 1 is also connected with Shaft 2 via the upper drifts, where faults are located. It is known that the geometry of these horizontal drifts is extremely irregular due to those faults and blasting activities, so is that of the shafts. A cylindrical shaft and drifts were adopted in the current simulation for analyses in this study, which is similar to the previous studies, e.g., Hamm and Sabet (2010), without considering Shaft 1 and those faults, as shown in Figure 3.9. As can be seen, the configuration and position of the shaft and drift were determined based on the real conditions in Figure 3.8. The dimensions of the shaft were adopted according to the documented data (Butler and Burbank 1929), while the dimensions of drifts were assumed based on Hamm and Sabet (2010). To allow for the complicated geologic conditions, the surrounding rocks include major rock layers, i.e., conglomerate No. 22, No. 18, No. 17 and No. 16, according to Figure 3.8. Because the water level is 60 m below the ground surface according to the field data in Figure 3.2, soils and the rocks above the water surface in the mine were not included in this case, therefore, the geological formations were only rocks in the simulation. The total length of the mine water in the shaft is 1159.2 m, as shown in Figure 3.9. In addition to the surrounding rocks, the bottom rocks (conglomerate No. 16) that are in contact with the bottom surface of the mine water were included. The coupling between the mine water and the surrounding rocks deserves special attention. This is because heat transfer occurs cross those two regions and affects the movement of the mine water via conduction. This coupled heat transfer between two regions was solved using Eq. (3.9) introduced in Section 3.3.1. For the dimension of finite volume cells, the model was configured with a high resolution of 1.5 m for the mine water body and the solid regions in the surrounding rocks very close to the mine water and with a relatively low resolution of 3-5 m for the rocks far from the mine water.

To consider the geothermal gradient at the domain, the internal temperature in both the water body and the surrounding rocks was assumed to be linearly distributed with depth from 282.15 K (9 ^{o}C) to 288.15 K (15 ^{o}C), in which the temperature was adopted according to the field study in Figure 3.2. The temperature of the bottom rocks (200 m×754 m×50 m ($x \times y \times z$)) was assumed to be uniform within the domain and fixed at 288.15 K at the bottom.

Our trial calculations indicated that the temperature variations in the surrounding rocks (200 m×754 m×1159.2 m) only occur within a few tens of meters away from the shaft. Due to this reason, a Neumann type of boundary with no heat flux was used at the exterior side boundaries of the surrounding rocks.

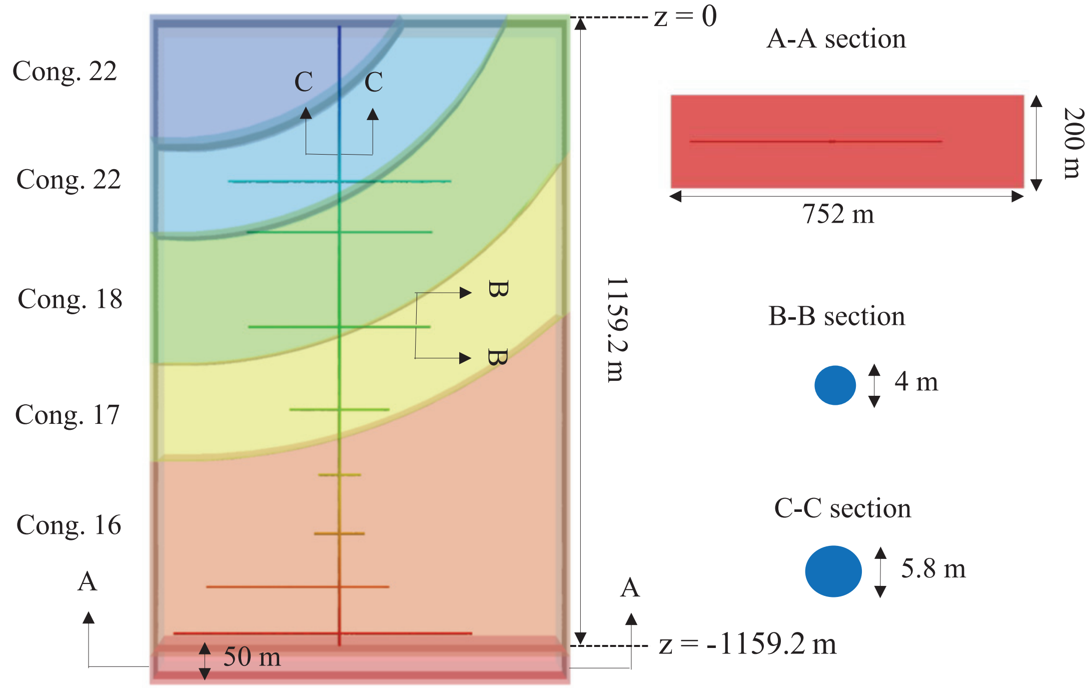

Figure 3.9. Configuration of the mine water-layered rocks system and its dimensions (the red line in A-A section is the projection of the bottom drift on the bottom rocks).

For the hydrodynamics, the dependence of the water density on temperature is a critical auxiliary relationship, which determines the overall process of the buoyancy-driven flow. As introduced above, salinity will not be included in this case. The classic Boussinesq approximation was used to formulate the relationship between the fluid density and temperature, in which this relationship is assumed to be linear. The effective density ρ_{eff}

is formulated using a reference density at a reference temperature and the thermal expansion coefficient β (K^{-1}) in the following equation (Oliveira and Issa 2001):

$$\rho_{\mathrm{eff}} = \rho_{\mathrm{ref}}[1-\beta(T-T_{\mathrm{ref}})] \tag{3.11}$$

where ρ_{ref} is the reference density and T_{ref} is the reference temperature. The simulation was conducted by implementing the framework outlined in Section 3.3.1 with an open-source finite volume method C++ library, OpenFOAM. The PISO algorithm was used in this study to solve the iteration of the system (Oliveira and Issa 2001; Ferziger and Peric 2012). The framework validation is not presented here but can be found in detail in the study of (Bao and Liu 2016). The laminar flow was considered in the current simulation. The thermodynamic properties of the mine water slightly vary with the temperature. However, this temperature dependence of the thermodynamic properties of the mine water was treated as negligible in this study except for ρ_{eff} in Eq. (3.2). The thermal conductivity of the rocks varies with porosity (Schön 2015). According to Manger (1963), the porosity of sedimentary conglomerates has a range of 0.5-1.1%. The existence of water in voids of the rocks also influences the thermal conductivity of the rocks (Robertson 1988). The thermal conductivities of the sedimentary rocks in this study were estimated within the above porosity range considering water in voids of the rocks according to Robertson (1988). The parameters used in this case are detailed in Table 3.2. Due to the high computational cost of the large-scale simulation, this study investigates a process lasting 46 days.

Table 3.2. Parameters used in the current simulation.

	Conglomerate type	Thermal conductivity (W/(m K))	Specific heat (J/(kg K))	Density (kg/m^3)		Reference density (kg/m^3)	Reference temperature (K)	Specific heat (J/(kg K))	Prandtl number	Dynamic viscosity (Pa s)
Rock	No. 16	1.69	841	2800	Mine water	999.8396	273.15	4181	6.62	9.59×10^{-4}
	No. 17	1.58	839							
	No. 18	1.57	843							
	No. 22	1.22	840							

Simulation results for the initial and final temperature contours of the system are depicted in Figure 3.10. As can be seen in Figure 3.10a, the initial internal temperature distributions in the mine water and the surrounding rocks are identical and linear with depth because they were defined to have the same linearly distributed internal temperature from 282.15 K (9 ^oC) to 288.15 K (15 ^oC). After 46 days, the temperature distribution in the mine water changes obviously because of the thermal natural convection caused by the density difference in the mine water (Figure 3.10b). The temperature distribution in the surrounding rocks, however, almost remains unchanged. This comparison indicates that the natural convection, which only exists in the mine water, is a much more dominating heat transfer mechanism in the mine water. Without it, the rate of heat transfer in the mine water would be comparable to that in the rocks.

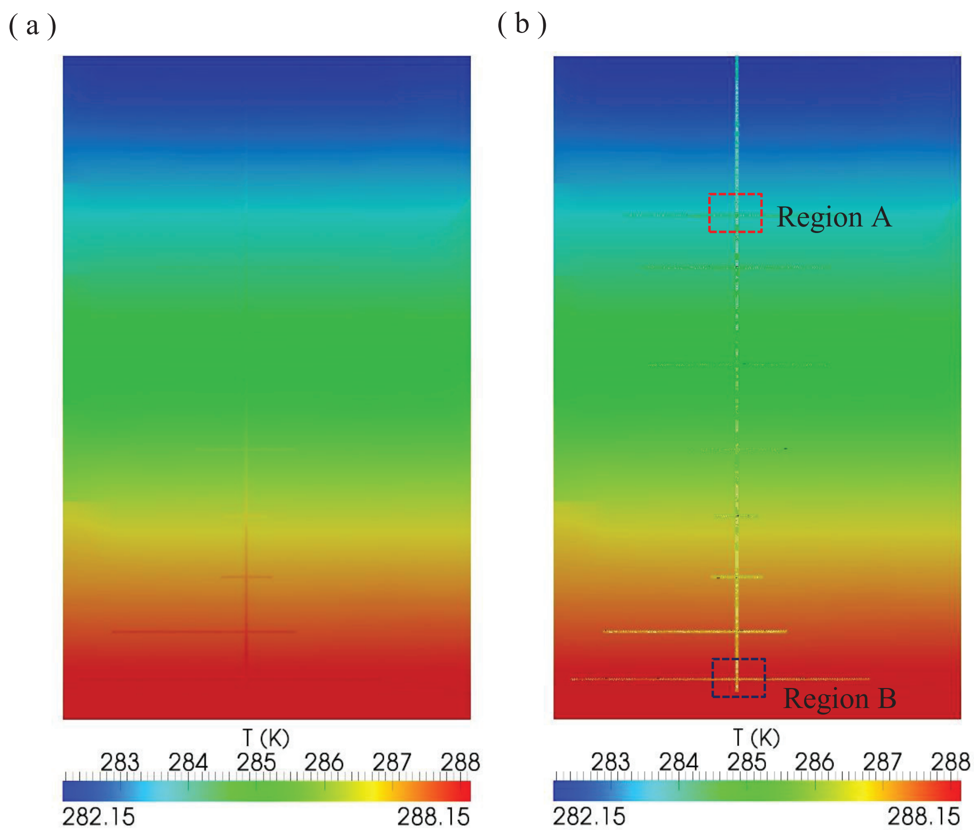

Figure 3.10. Temperature profiles of the system: (a) initial conditions and (b) *t*=46 days.

Typical simulation results for the flow patterns at different times in two representative areas, i.e., Region A and Region B in Figure 3.10b, are depicted in Figure 3.11 and Figure 3.12, respectively. Due to the density difference caused by the geothermal gradient, the mine water is not stagnant. As can be seen in Figure 3.11 and Figure 3.12, the mine water circulates in the shaft. To be more specific, the water at the bottom with high temperatures moves upwards, because this water is relatively lighter compared to that at the top with low temperatures. By contrast, the water at the top with low temperatures moves down. Then the water from the bottom is mixed with and cooled by the cold water at the top. The water from the top is mixed with and heated by the warm water at the bottom. The water, which has been cooled at the top, tends to be heavier and therefore moves down and returns to the bottom. This water circulation is faster at t=1 hour and 1 day when compared to those at t=15 and 46 days, which can be seen from the magnitudes of the velocity of the mine water. This larger velocity is caused and triggered by the larger temperature difference defined in the initial condition. As time elapses, the temperature difference decreases. Overall, this water circulation is triggered by the geothermal gradient and will approximate a quasi-equilibrium state gradually in which water is moving by following a relatively stable pattern.

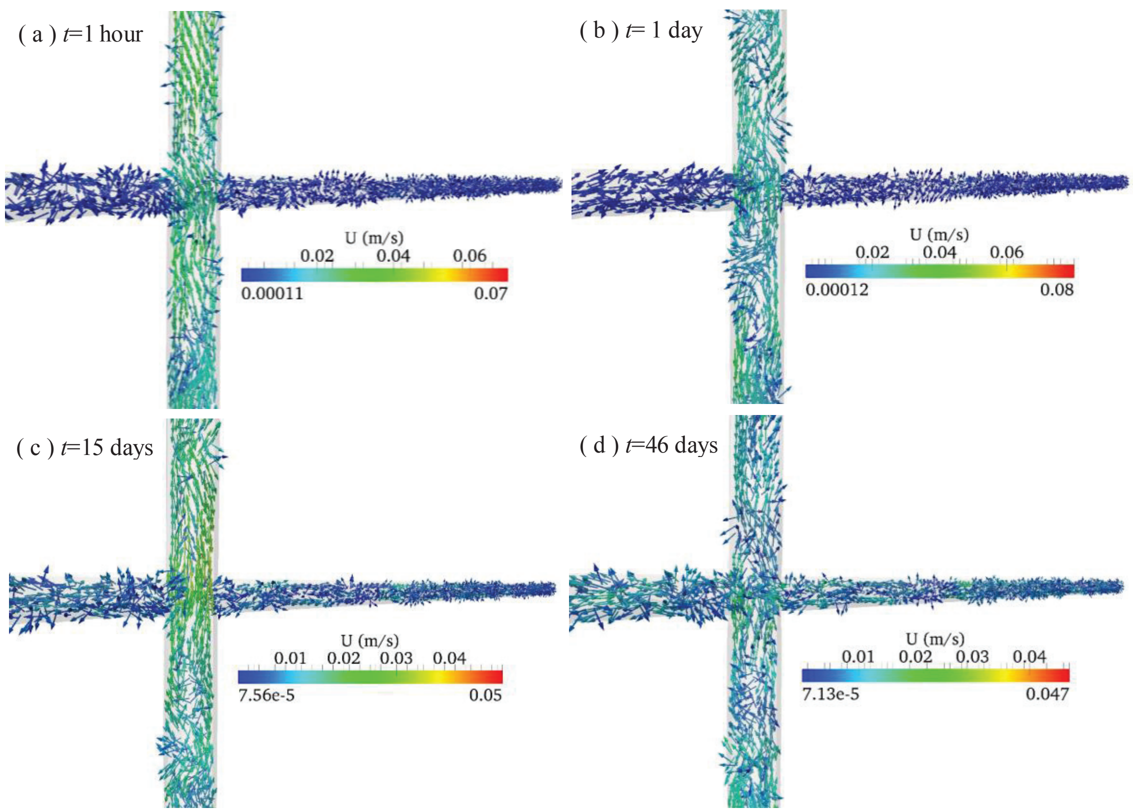

Figure 3.11. Flow patterns of Region A in the water body: (a) t=1 hour, (b) t=1 day, (c) t=15 days and (d) t=46 days. Note that for visualization, the temperature profile of the water body is not included.

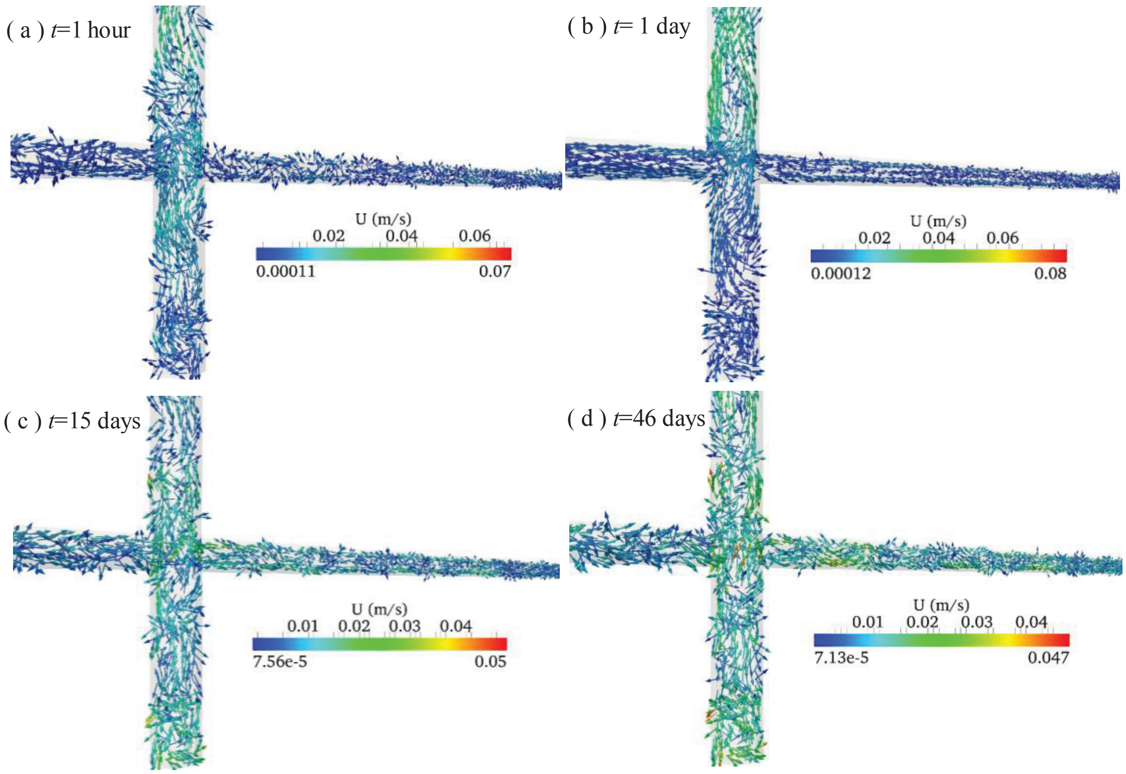

Figure 3.12. Flow patterns of Region B in the water body: (a) t=1 hour, (b) t=1 day, (c) t=15 days and (d) t=46 days. Note that for visualization, the temperature profile of the water body is not included.

On the other hand, the surrounding rocks influence the mobile mine water via heat conduction. Figure 3.13a presents temperature distributions along the horizontal axis in Figure 3.10 through both the surrounding rocks and the mine water at an evaluation of 5 m below the mine water surface (z=-5 m). As can be seen, the temperature along this horizontal axis is same at t=0, except for regions at two sides due to the effect of boundary conditions. Because of the circulation of the mine water caused by the temperature difference, the temperature of the mine water increases significantly from 282.17 K to 284.3 K within 46 days. During this period, the surrounding rocks at z=-5 m affect the mine water via heat conduction. However, this conduction to the mine water is much less significant when compared to heat convection in the mine water, because the temperature of the rocks at the interface also increases (Figure 3.13a). This can also be seen in Figure 3.13b using the temperature variation of the node at the interface between the mine water and the surrounding rocks. The surrounding rocks at z=-5 m are intended to make the mine water stable at this elevation via heat conduction to this node. However, Figure 3.13b shows that the temperature of the node increases quickly rather than remains stable. This observation further indicates that heat conduction from the surrounding rocks to the mine water is not predominant when compared to heat convection. This heat convection in the mine water, therefore, dominates the thermal process of the mine water.

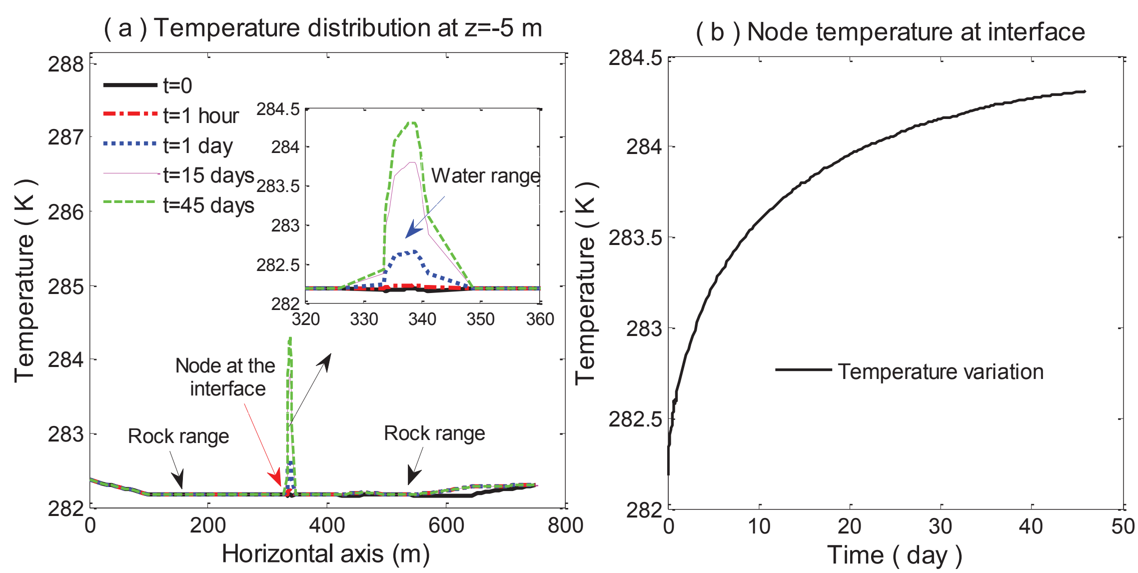

Figure 3.13. Temperature changes in the domain: (a) temperature distributions along the horizontal axis through the domain at z=-5 m and (b) temperature variation of the node at the interface.

The temperature distributions on different cross-sections at different times can help understand how the thermal energy of the mine water is distributed and varies in a three-dimensional way, which triggers and maintains the buoyancy-driven flow. The temperature contours of the mine water on the horizontal cross-sections at the top, middle and bottom of the shaft are plotted in Figure 3.14, Figure 3.15 and Figure 3.16, respectively. As can be seen in Figure 3.14a, at t=0, the temperature is the same in the cross-section at the top. To solve the coupled heat transfer at the interface between the mine water and the surrounding rocks, the initial temperature value of 282.15 K is defined at this interface, while the temperature in the water body along the shaft is linearly distributed with depth from 282.15 K (9 ^{o}C) (top) to 288.15 K (15 ^{o}C) (bottom). Due to this reason, at t=0, the temperature is not the same in the cross-sections in the middle (Figure 3.15a) and at the bottom (Figure 3.16a). This also leads to the temperature difference on these three cross-sections (top, middle, and bottom) at t=0. As time elapses, the temperature at the top increases from 282.15 K to 282.33 K at t=3 hours. The temperature in the top cross-section continuously increases to 284.31 K at t=46 days, as shown in Figure 3.14. The opposite phenomenon was observed in the cross-section at the bottom in Figure 3.16. The temperature at the bottom decreases from 288.15 K to around 287 K when t=46 days. The temperature in the middle cross-section almost remains unchanged during the same process, as shown in Figure 3.15. This is because the water movement will approach a quasi-equilibrium state gradually to form one layer with almost the same temperature. Eventually, this temperature is approximately equal to the initial temperature in the cross-section in the middle. It is also seen that the temperature contours, e.g., Figure 3.14b or Figure 3.16b, are not symmetric. This is because the relatively large (resolution is around 1.5 m) and unstructured (tetrahedron) cells were used in the simulations for the mine water to save the computational cost. Therefore, the asymmetric temperature contours were observed in Figure 3.14 and Figure 3.16.

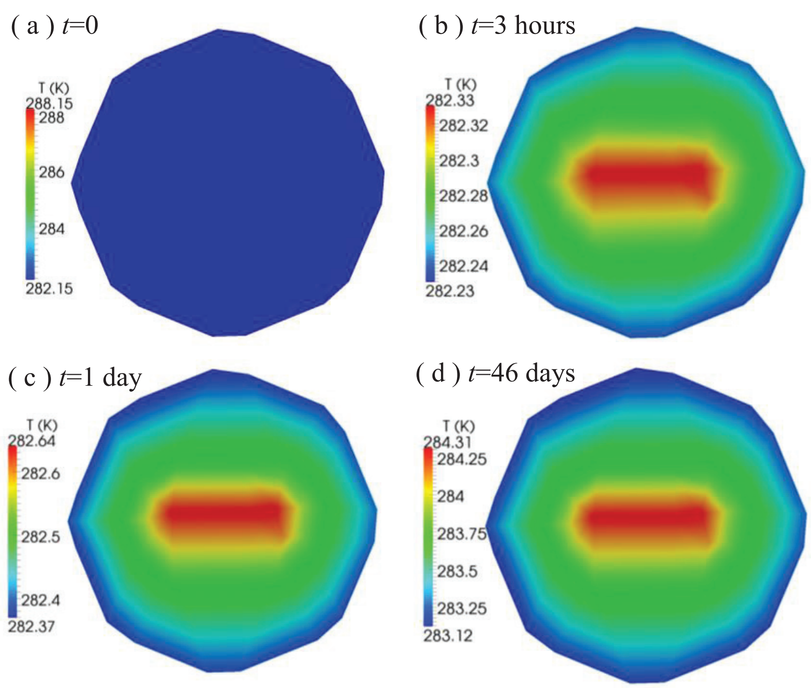

Figure 3.14. Temperature contours in cross-sections at the top of the water body at different times.

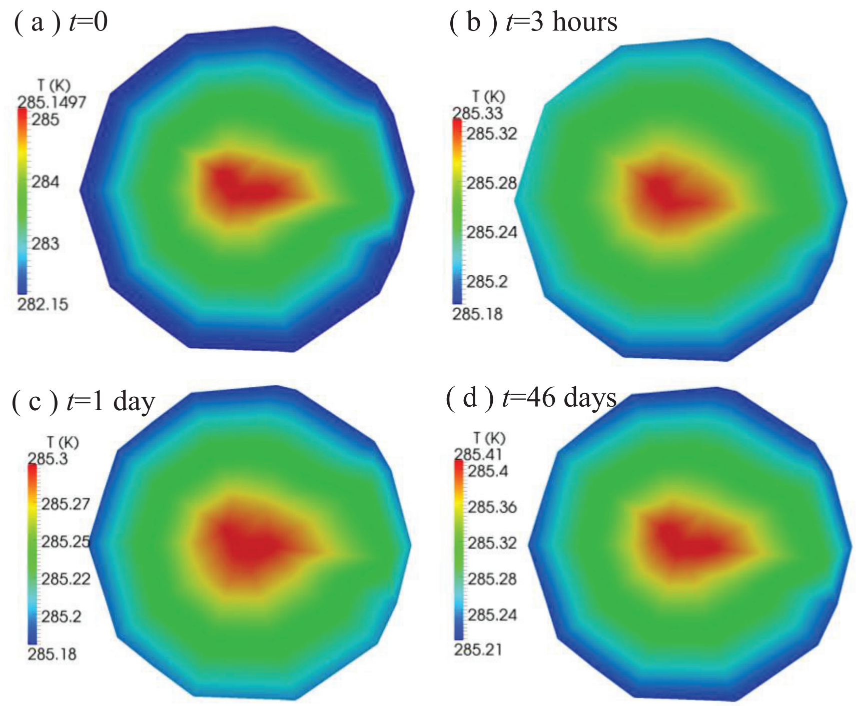

Figure 3.15. Temperature contours in cross-sections in the middle of the water body at different times.

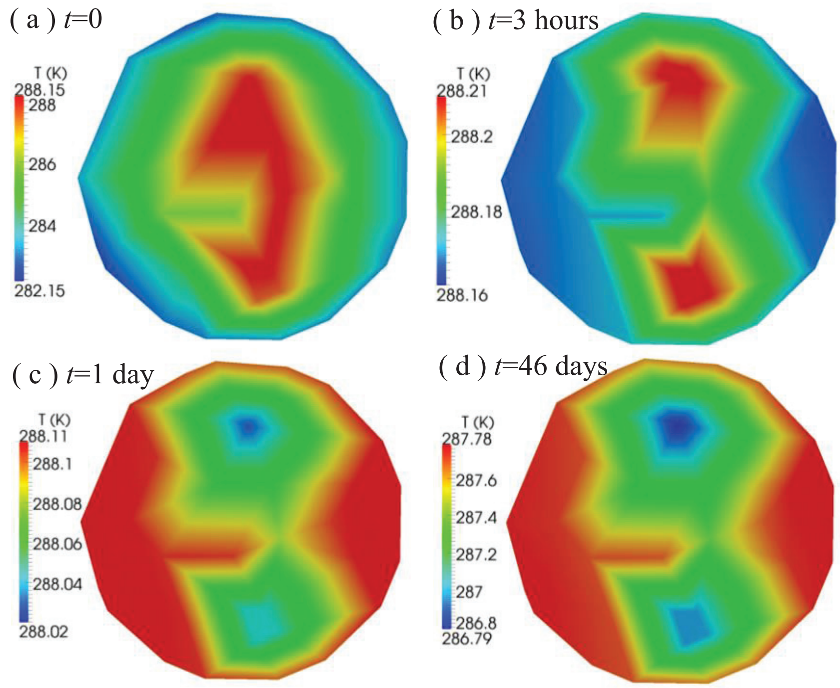

Figure 3.16. Temperature contours in cross-sections at the bottom of the water body at different times.

At t=3 hours, t=1 day or t=46 days, the temperatures in the cross-section at the top and bottom are non-uniform, as shown in Figure 3.14 and Figure 3.16. The reason is that the surrounding rocks with a relatively low temperature cool the mine water at the top, while the surrounding rocks with a relatively high temperature heat the mine water at the bottom. These rocks affect the temperature of the mine water via heat conduction. However, this heat conduction is much slower than the heat convection in the mine water. As a result, the temperature of the mine water varies significantly. At t=46 days, the difference between the temperatures at the top and bottom is approximately 2.5 K. These temperature variations at the top and the bottom further confirmed that the warm water and the cold water in the shaft are well mixed to a nearly uniform temperature. As a result, the quasi-equilibrium water movement status will be approached and maintained.

Another angle for directly showing the energy and mass flow within the mine shaft is the temperature variations with time. Five representative positions were chosen from the axis of the shaft water body to investigate the temperature variations with time. As shown in Figure 3.17a, the temperature at z=-1159.2 m (z=0 m on the surface of the mine water and z==-1159.2 m at the bottom of the mine water) decreases rapidly at the beginning and relatively slowly afterward. The opposite temperature variation was obtained for the temperature at z=0 m, which increases rapidly at the beginning and then slowly. The results at z=-289.8 m and z=-869.4 m exhibit a similar trend to those at z=0 m and z=-1159.2 m. However, the temperature at z=-579.6 m almost remains unchanged. These results help explain the simulated flow pattern in Figure 3.11 and Figure 3.12. The temperature distributions along depth at different times in Figure 3.17b also help explain the flow patterns observed in Figure 3.11 and Figure 3.12 and the temperature variations in Figure 3.14, Figure 3.15, and Figure 3.16. The difference between the temperatures at z=0 m and z=-1159.2 m decreases from 6 K to 2.5 K as time elapses, which is also similar to what we observed in Figure 3.14, Figure 3.15, and Figure 3.16. The mine water is mixed because its temperatures tend to gradually approach a constant due to the natural convection. This good mixing condition is consistent with most field observations in flooded mines (Wolkersdorfer 2008).

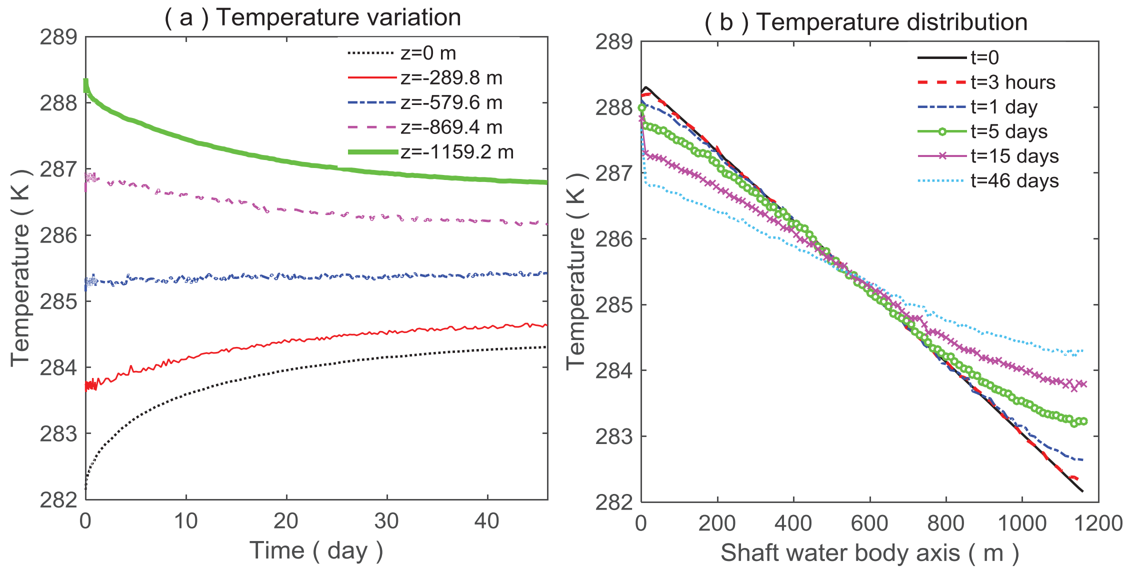

Figure 3.17. Computed temperatures: (a) temperature variation at different positions, and (b) temperature distribution along the shaft water body.

The circulation of the mine water due to the natural convection (Figure 3.11 and Figure 3.12) essentially mixes the water and significantly speeds up the heat transfer in the water. For the case shown in Figure 3.17, the temperatures of the whole water body in the shaft will approach an equilibrium value, making all the water in this shaft appear as one layer (cell). The mechanism inferred from the above simulation well explains the mixing of the mine water within each stratified layer in the field study, in which the temperature and chemical concentrations are approximately constant. These simulation results serve as a rough assessment to validate the buoyancy-driven flow in the mine water, which include complicated geologic conditions for the first time. Such a preliminary assessment has succeeded in reproducing the major mechanisms explaining heat and mass transfer in the complicated multiphysical processes and shedding light on what we observed from the field study.

3.4 Conclusions

This chapter introduces the results on the scientific understanding of the natural mine water-geologic formation system, especially the transport of heat and mass in this large-scale natural system, for exploring the water from deep abandoned copper mines as a geothermal energy resource in the U.P. of Michigan, a historical mining area in the U.S. Three essential components for understanding the physical processes involved in the geothermal application of the mine water were introduced: a field study, a theoretical framework, and numerical simulations. The field study yielded measurements of temperatures, electrical conductivity, and chemical concentrations in a local mine shaft in the U.P. The main purpose is to understand the key scientific issue in the use of the mine water as a geothermal resource, i.e., the temperature distribution in the mine water. The theoretical framework development provided a mathematical description for the thermo-hydrodynamic process in the mine water coupled with the heat transfer in the surrounding geologic formations for studying the scientific issue. Simulations were conducted to preliminarily investigate the quasi-equilibrium water movement in the mine shaft due to geothermal gradients to shed light on the phenomena observed in the field study.

The simulation based on the proposed framework provided explanations to the data obtained in the field from a scientific perspective, which is of practical meaning to the success of this energy renovation with water in deep mines. No research is reported prior to the current study to include the comprehensive information as detailed in this study. This study fills this gap with simulations accompanied by field studies on the same deep flooded mine shaft, a pioneering one in the United States. Also, a theoretical framework for the mine water-surrounding geologic formation system has been successfully implemented to test a realistic case. Serving as a solid cornerstone, this study will be further continued for a scientific understanding to help predict the efficiency and sustainability of the energy exploration from abandoned underground mines using the mine water as a safe, green, relatively renewable and adaptable geothermal resource.

4 Numerical Simulation of Thermohaline Stratification via Double-Diffusive Convection: Key Heat and Mass Transport Mechanisms

In this chapter, the main purpose is to explore the formation of thermohaline stratifications in the large-scale mine water using the multiphysics simulation with unique non-isothermal and non-isosolutal hydrodynamics. The thermohaline stratification is the layering phenomenon and commonly observed in flooded mines. That is, both temperature and salinity in the mine water are stratified to form separate layers with significant gradients between layers. However, the formation of thermohaline stratifications in the mine water is still a big scientific myth that remains little understood in the past three decades. The nomenclature of equations used in this chapter can be found in the following table.

Nomenclature

h_{rf} rock-flow heat transfer coefficient [W/m^2/K]	S_t top salinity [%, w/w]
h_f^T flow-flow heat transfer coefficient [W/m^2/K]	S_b bottom salinity [%, w/w]

h_f^S salt transfer coefficient [m/s/%]

$\mathbf{g}$ gravitational acceleration vector [m/s^2]

G heat or salt gradient [K/m or %/m]

F_r rock heat flux [W/m^2]

F_f^T flow heat flux [W/m^2]

F_f^S flow salt flux [m/s]

ΔF_f^T flow heat flux difference [W/m^2]

ΔF_f^S flow salt flux difference [m/s]

t time [s]

p total pressure [Pa]

p_{d} hydrodynamic pressure [Pa]

T_0 reference temperature [K]

T temperature [K]

T_t top temperature [K]

R represents T_t or S_b [K or %]

z elevation [m]

Dimensionless numbers

N buoyancy ratio

N_c critical buoyancy ratio

Le Lewis number

Pr Prandtl number

Ra Rayleigh number

Sc Schmidt number

Greek symbols

ρ density [kg/m^3]

ρ_0 reference density [kg/m^3]

ν_{eff} effective kinematic viscosity [m^2/s]

β_T thermal expansion coefficient [K^{-1}]

T_b bottom temperature [K]	β_S solutal expansion coefficient [%$^{-1}$]
T_d temperature difference [K]	α_T thermal eddy diffusivity [m^2/s]
$\mathbf{U}$ velocity [m/s]	α_{eff}^T effective thermal diffusivity [m^2/s]
S_0 reference salinity [%, w/w]	α_{eff}^S effective solutal diffusivity [m^2/s]
S salinity [%, w/w]	

4.1 Introduction

As an alternative energy source, geothermal energy provides green, sustainable, eco-friendly and renewable energy for humanity's energy demands (Rybach 2003; Rybach and Mongillo 2006; Lund et al. 2005). Geothermal energy can be used for electric power generation due to its advantages, such as environment-friendliness and cost-competitiveness over conventional sources of energy (Milora and Tester 1977). Exploring geothermal energy for electric power generation needs specific qualifications, e.g., a very high enthalpy fluid or vapor; as a result, only specific locations in about 24 countries could generate electricity by employing geothermal resources (Bertani 2012). Another direct use of geothermal energy is to heat or cool buildings using geothermal heat pumps (Chiasson 1999; Self et al. 2013; Ochsner 2012; Chua et al. 2010). Such apparatus can transfer heat from materials (e.g., water and ground) with low enthalpy to a high enthalpy fluid via the circulation of a working fluid in heat pumps to enable heating/cooling buildings with energy from the low enthalpy (temperature) source. Conventional applications of geothermal heat pumps involve the heat exchange between working fluids in pipes and the surrounding ground (e.g., borehole) in ground-coupled heat pump applications or the heat exchange between working fluids in pipes and well water in ground-water heat pump applications. To obtain the higher energy efficiency, such direct use of geothermal application requires drilling to access a deep location with a greater temperature difference with the working fluids. This raises economic and technical concerns in some areas because of the significant investments in geothermal borehole/well constructions and uncertainties in borehole/well drilling.

Underground mining exists in almost every country. A great number of underground mines in numerous counties were closed and abandoned in the past decades, and many of them were flooded with water after closure (Ramos et al. 2015). Flooded mines usually have hundreds or even thousands of meters deep in the ground. The water in the mines, i.e., mine water, can reach the lower portions of shafts and drifts with high temperatures and can be continuously heated by the Earth's geothermal energy, leading to a stable high temperature contrast with the air without additional drilling work. Due to this benefit, increasing research attention has been paid to the recovery of thermal energy from flooded mines via the mine water for geothermal applications since the pioneering work in Canada in 1989. The mine water with high temperatures can run through a heat exchanger for heating or/and cooling buildings. This novel concept offers more benefits than the conventional ground-water heat pump applications and ground-coupled heat pump applications. Frist, the mine water offers much better heat transfer and a much higher energy reserve because the enormous volume of the mine water provides an enormous bulk and mobile medium for energy storage and transfer than that of well water and soils used in the conventional ones. Also, the mine water is currently treated as a useless material isolated from daily life, the use of the mine water for geothermal applications is thus safe, green, relatively renewable, adaptable, and eco-friendly. Finally, as mentioned above, abandoned mines and the mine water are existing facilities, therefore, no extra cost is needed for their construction, which saves a significant amount of expenditure compared to the conventional ones.

Practical attempts have been made for exploring the mine water as a renewable geothermal resource. A realistic utilization of a flooded mine as a large reservoir of heat was implemented in Canada (Jessop 1995; Allen et al. 2000). This application proved that the extraction of energy from flooded mines beneath the community for heating/cooling buildings is not only feasible but also environmental due to a reduction in carbon dioxide emissions (Jessop 1995; Allen et al. 2000). Observations from later field measurements or evaluations of available geothermal data, such as in Poland (Malolepszy 2003), Netherlands (Bazargan et al. 2008), Germany (Wieber and Pohl 2008), and Spain (Loredo et al. 2011), also revealed that the water in closed mines contains a great reserve of geothermal energy. Additional efforts also have been made in the estimate of the thermal energy reserve and the later energy replenishment from the surroundings (Wieber and Pohl 2008), typical investments and corresponding economic paybacks (Raymond et al. 2008), effective and suitable geothermal energy recovery systems (Hall et al. 2011), effective velocities of the mine water (Hasche-Berger 2013), and potential environmental impacts (Preene and Younger 2014).

However, the scientific understanding of geothermal energy recovery from flooded mines is still far behind its implementations. Though not extensively, a few numerical studies have been carried out to understand the sustainability of the heat extraction from flooded mines (Raymond and Therrien 2008; Raymond and Therrien 2014) and the mechanisms regarding temperature variations in the mine water for the application (Renz et al. 2009; Streb and Wieber 2011; Arias et al. 2014; Bao and Liu 2016). However, the dominant heat transfer mechanism in the mine water, i.e., mine water is usually stratified into layers with different temperatures and salinities (Wolkersdorfer 2008; Reichart et al. 2011), has not been explained in those published studies. As shown in Figure 4.1, each layer has an approximately constant temperature and salinity. Significant changes in the temperature and salinity occur at the interface between two adjacent layers. This observation indicates that the mine water is possibly mobile and well-mixed in each individual layer. This layering phenomenon (i.e., thermohaline stratification) in the mine water yet has not been proven, which is suspected to be similar to the thermohaline staircases in oceans (Radko et al. 2014). The thermohaline stratification could play a crucial role in the geothermal energy recovery. This is because, it governs the temperature distribution and variation, which determine the efficiency and sustainability of this geothermal application.

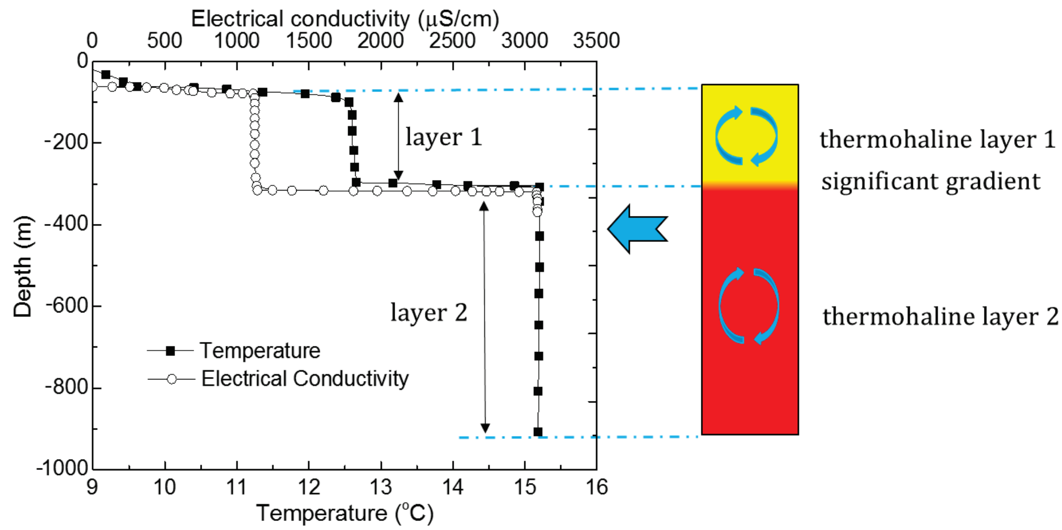

Figure 4.1. Typical thermohaline stratifications from field measurements.

The formation of thermohaline stratifications in the mine water, however, has not been well understood because of the complexity of the physical mechanisms in the natural process and the limited access of flooded underground mining spaces. Hamm and Sabet (2010) modeled the hydraulic behavior of the mine reservoir and the mine water temperature in a production shaft to reveal the influences of the thermal natural convection, the production flow rate, and the permeability of the surrounding rocks on the thermal energy recovery. However, this model (Hamm and Sabet 2010) simulated the thermal natural convection without considering salinity transport. Both heat and salinity transport processes need to be considered as the mine water movement is driven by the buoyancy force that is determined by heat and salinity simultaneously. This coupled process for the mine water movement is called the Double-Diffusive Convection (DDC). Heat and salinity transfer simultaneously in the mine water with different diffusivities, but affect the vertical density gradient of the mine water in an opposite way (Turner 1974). Warm water is lighter compared to cold water, while salty water is heavier compared to fresh water. Reichart et al. (2011) numerically investigated the DDC process in the mine water with a focus on reproducing thermal and solutal convections using a 2-Dimensional (2D) model. However, the scale of the simulated mine water was too small (around 1 m) to reflect the real dimensions (around 1 km) in natural water bodies and thermohaline stratifications were not successfully obtained. Therefore, the formation of thermohaline stratifications of the mine water remains a scientific uncertainty.

In this chapter, we unveil this myth via simulating the DDC process in the mine water using a fully coupled numerical model. The main objective is to explore the formation and evolution of thermohaline stratifications in the large-scale mine water, which is of great significance for the utilization of the mine water for geothermal applications. This chapter is organized as follows. A theoretical framework for the coupled model is described first and then validated against documented experimental and numerical results. Then, two hypotheses for the formation of thermohaline stratifications in oceans are introduced and discussed. Afterward, multiphysics simulation with unique non-isothermal and non-isosolutal hydrodynamics is conducted using the validated model. Based on the simulation, the primary physical mechanisms are investigated and in-depth discussions are made to shed light on the formation and evolution of thermohaline stratifications in the large-scale mine water from a scientific perspective.

4.2 Theory and Method

This section outlines a theoretical framework for modeling the DDC process in the mine water. Due to temperature and salinity gradients, the mine water is triggered to convect naturally with double diffusion in mining spaces. In this situation, the mine water was assumed to be Newtonian and incompressible. The mass of a moving fluid element is conserved according to the continuity equation:

$$\nabla \cdot \mathbf{U} = 0 \tag{4.1}$$

where $\mathbf{U}$ is the velocity of the mine water. The conservation of momentum for the fluid element is formulated using the following equation:

$$\frac{\partial \mathbf{U}}{\partial t} + \mathbf{U} \cdot \nabla \mathbf{U} = -\frac{\nabla p_d}{\rho_0} + \nabla \cdot (\nu_{eff} \nabla \mathbf{U}) + \frac{\rho}{\rho_0} \mathbf{g} \tag{4.2}$$

where ν_{eff} is the effective kinematic viscosity of the mine water; ρ is the density of the mine water; ρ_0 is the reference density of the mine water; $\mathbf{g}$ is the gravitational acceleration vector; and p_d is the hydrodynamic pressure and given by:

$$p_d = p - \rho \mathrm{g} \mathrm{z} \tag{4.3}$$

where p is the total pressure, z is the elevation, and $\rho \mathrm{gz}$ is the hydrostatic pressure. To consider the buoyancy force induced by temperature and salinity gradients, the Oberbeck-Boussinesq approximation (Reichart et al. 2011; Sezai and Mohamad 2000) is used and the density ρ varies linearly with the temperature T and solute concentration S of the mine water:

$$\rho = \rho_0 [1 - \beta_T (T - T_0) + \beta_S (S - S_0)] \tag{4.4}$$

where β_T is the coefficient of thermal expansion; β_S is the coefficient of solutal expansion; and T_0 and S_0 are the reference temperature and salinity, respectively.

The energy conservation of the moving fluid element is formulated as:

$$\frac{\partial T}{\partial t} + \mathbf{U} \cdot \nabla T = \nabla \cdot (\alpha_{eff}^{T} \nabla T) \tag{4.5}$$

where α_{eff}^{T} is the effective thermal diffusivity of the mine water. The solute concentration within the moving fluid element is governed by

$$\frac{\partial S}{\partial t} + \mathbf{U} \cdot \nabla S = \nabla \cdot (\alpha_{eff}^{S} \nabla S) \tag{4.6}$$

where α_{eff}^{S} is the effective solutal diffusivity.

The buoyancy ratio N was defined to evaluate the relative influence of salinity and temperature on the buoyancy force in the system:

$$N = \frac{\beta_S \Delta S}{\beta_T \Delta T} \tag{4.7}$$

where ΔS and ΔT are the salinity and temperature differences between the top surface and the bottom layer of the mine water.

The governing equations presented above were discretized and solved using an open source platform, OpenFOAM. Details regarding discretization of the governing equations can be found in Ferziger and Peric (2012). The PISO algorithm was used in this chapter to solve the iteration of this coupled system (Oliveira and Issa 2001; Ferziger and Peric 2012), which applies a few corrector steps to obtain a desired accuracy of the pressure and velocity.

4.2.1 DDC Framework Validation

In this section, the theoretical framework developed in Section 4.2 is validated against documented numerical results. Steady DDC was experimentally investigated (Lee et al. 1990) in a rectangular enclosure under a vertical salt gradient and a horizontal temperature gradient to reveal the DDC flow structure within the enclosure. A numerical study (Lee and Hyun 1991) was conducted later to verify the observations from the experiment (Lee et al. 1990) by comparing the formation and development of the DDC flow structure. The numerical study provided the transient DDC results and was conducted in a rectangular enclosure with an aspect ratio of (vertical/horizontal) 2:1 under a vertical salt gradient and a horizontal temperature gradient. Different buoyancy ratios were investigated and transient simulation calculations were continued until the quasi-steady state was reached to approximate the steady DDC results of the experiment (Lee et al. 1990).

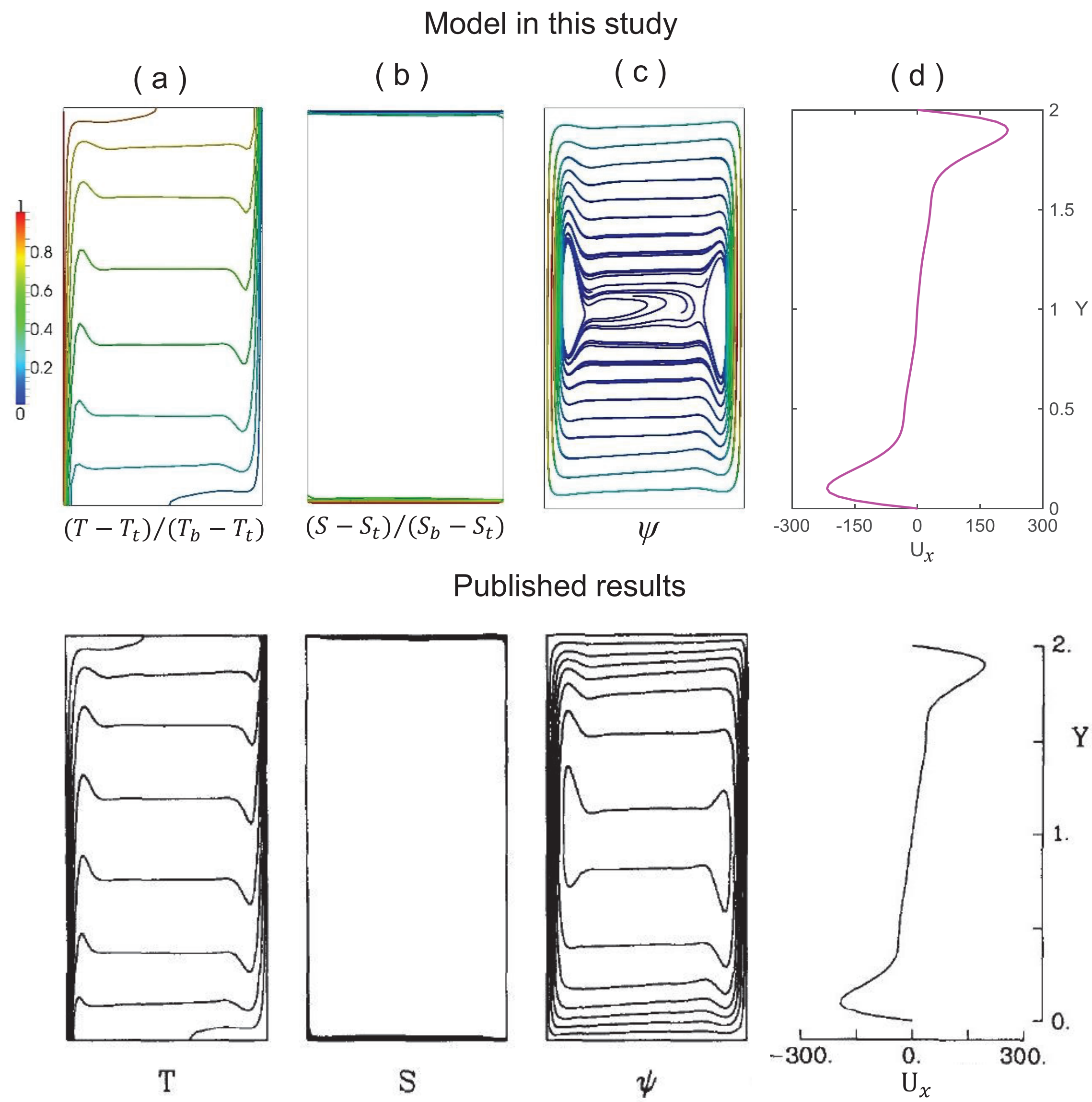

Figure 4.2. Comparisons between the results from the model in the current chapter and the numerical results from Lee and Hyun (1991): (a) dimensionless temperature contour, (b) dimensionless salinity contour, (c) dimensionless streamlines, and (d) dimensionless horizontal velocity vs dimensionless vertical axis.

The simulation in this section is designated for model validation by comparing with the numerical results (Lee and Hyun 1991), in which the same dimensions were used. The adopted parameters for the simulation are as follows: the buoyancy ratio $N = 3$; the Rayleigh number $Ra = 10^7$; the Prandtl number $Pr = 7$; and the Lewis number $Le = 100$, i.e., the Schmidt number $Sc = 700$. For the initial condition, the initial temperature within the enclosure was uniform with T_t, while the initial salinity was linearly distributed from S_t (top wall) to S_b (bottom wall). For boundary conditions, the left wall and the right wall were set up with no solutal flux but with fixed temperatures of T_b and T_t, respectively; the top wall and the bottom wall were set up with the no thermal flux but with fixed salinity values of S_t and S_b, respectively. The above initial and boundary values for the temperatures and salinities were calculated based on N and Ra strictly following Lee and Hyun (1991). 0.1 s was selected as the time step. The grid used for the simulation consisted of 50 and 100 identical cells in the horizontal and vertical directions, respectively.

Shown in Figure 4.2 are comparisons between the results computed by the model in this study and the published numerical results (Lee and Hyun 1991). The dimensionless temperature contour, salinity contour, streamlines, and the horizontal velocity distribution are in good agreement with the published numerical results (Lee and Hyun 1991). Due to a small buoyancy ratio, i.e., $N = 3$, the thermal convection is dominant in the whole cavity, and the iso-solutal lines are located in thin regions adjacent to the top and bottom walls. There is a slight difference in the comparison of dimensionless streamlines in Figure 4.2c. This is because this study adopted a high resolution for streamlines visualization while the resolution of the published results (Lee and Hyun 1991) is unknown. The good agreement in Figure 4.2 indicates the good capacity and accuracy of the newly developed model in Section 4.2 for simulating the DDC process.

4.2.2 Hypotheses of Thermohaline Stratification Formation

The phenomenon of the thermohaline stratification is commonly observed in oceanic regions where temperature and salinity vary vertically in a step-like shape (Merryfield 2000), which thus is called thermohaline staircases in oceans. This phenomenon is associated with dynamic DDC because of the existence of temperature and salinity simultaneously. Two types of DDC can occur if large-scale gradients of temperature and salinity exist in the same vertical direction: (1) the salt-finger type (warm, salty water overlies cold, fresh water) and (2) the diffusive convection type (cold, fresh water overlies warm, salty water). As the salt-finger type is more common and vigorous in the ocean (Kelley et al. 2003), this type, therefore, has been investigated more extensively than the diffusive convection type for understanding the formation of thermohaline staircases in oceanic regions.

To date, two hypotheses, which have been proven by numerical studies to some extent, are available to explain the formation of thermohaline staircases. Merryfield (2000) proposed that thermohaline staircases arise from double-diffusive intrusions caused by lateral temperature and salinity gradients. Radko (2003) recently proposed the second hypothesis that thermohaline staircases are caused by the gamma instability driven by variations in the ratio of the turbulent heat and salt fluxes. For thermohaline staircases modeling in oceans, the second hypothesis (i.e., the gamma) has succeeded in simulating thermohaline staircases in the large-scale oceanic water circulation (Radko et al. 2014) with a surface area of 1,000 km^2 and a depth of 1 km.

As for the mine water, its dynamic DDC belongs to the diffusive convection type due to the geothermal (temperature) and geochemical (salinity) gradients. Though less discussed in oceanography for the diffusive convection type, the major cause of thermohaline staircases in this type is believed to be similar to that of the salt-finger type (Radko et al. 2014). Based on the second hypothesis (Radko 2003), which has succeeded in producing thermohaline staircases (Radko et al. 2014), the gamma is primarily governed by temperature and salinity differences between the ocean surface and ocean bottom. Since a constant flux ratio will not lead to the formation of thermohaline staircases (Radko et al. 2014), the surface temperature and salinity are required to vary in order to obtain a variable gamma (bottom temperature and salinity keep unchanged). A variable gamma is common in oceans because of the wide ocean surface influenced by solar irradiance. However, due to the narrow water surface area constrained by shaft configurations and the negligible influence of solar irradiance, the gamma calculated in the mine water is very likely a constant. This implies that the second hypothesis could not be used to explain the formation of thermohaline stratifications in the mine water. Therefore, we explore the formation of thermohaline stratifications in the large-scale mine water bodies in the following with the first hypothesis, i.e., the major cause is double-diffusive intrusions induced by lateral temperature and salinity fluxes.

4.2.3 Model Description and Configuration

The Hancock mine located in the Upper Peninsula (U.P.) of Michigan was flooded with water after closure due to the high level of underground water table. According to field observations in the U.P. from Hancock Shaft 2 in Figure 3.2, there are at least two layers with approximately uniform temperatures and salinities (indirectly measured by electrical conductivity) in the mine water because of thermohaline stratifications (see Figure 4.1). Therefore, Hancock Shaft 2 was chosen for the simulation in the following sub-section.

Figure 4.3 shows the 2D model configuration and grid developed (Figure 4.3b) based on the realistic underground mine layout and configuration (Figure 4.3a) introduced in (Butler and Burbank 1929). The model was configured to have grids with a resolution of 0.4 m for the mine water in the shaft and drifts, and with a very high resolution of 0.01 m for regions on boundaries. One reason for this configuration is that our trial calculations showed that the DDC flow structure greatly depends on the resolution of grids, therefore, thermohaline stratifications may not be observed with a coarse grid (e.g., the resolution is greater than 1 m in the horizontal direction). Another reason is that such a high resolution of grids on boundaries is helpful for ensuring the numerical stability when considering high lateral heat and salt fluxes from the surrounding water flows, which will be detailed in the following sub-section.

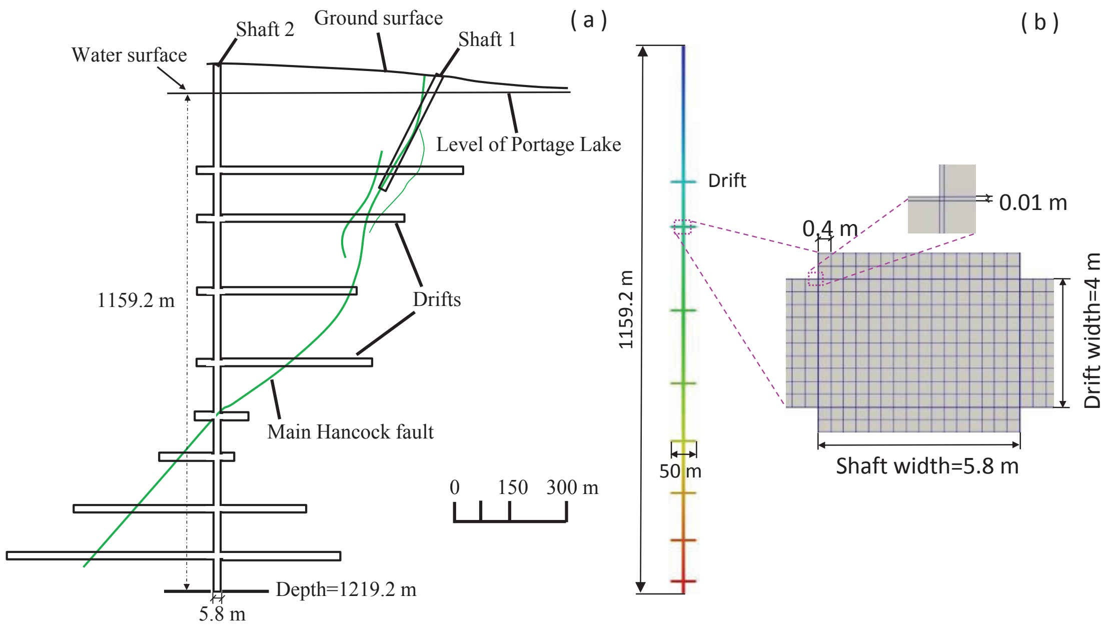

Figure 4.3. Hancock Shaft 2: (a) underground structure layout [modified after (Butler and Burbank 1929)] and (b) model configuration.

The initial temperature and salinity were assumed to be linearly distributed with depths. The temperature distribution was linear from 282.15 K to 288.35 K according to field measurements in Figure 3.2. The top salinity was assumed to be 2%. The bottom salinity was determined by Eq. (4.7) with the known buoyancy ratio N. For example, the bottom salinity is 2.6% when N is equal to 1.26. It is worthwhile to mention that the top salinity here, i.e., 2%, was assumed, which may not be realistic. In fact, the salinity-related buoyancy force depends on the salinity difference (i.e., $\Delta S = S_b - S_t$) between the top and bottom rather than their absolute values (i.e., S_t or S_b). Namely, when the temperature is the same in the domain (i.e., no buoyancy force induced by temperature difference), the buoyancy force calculated by Eq. (4.4) is determined by ΔS rather than S_t or S_b. For convenience, the above top salinity and bottom salinity were assumed for analyses.

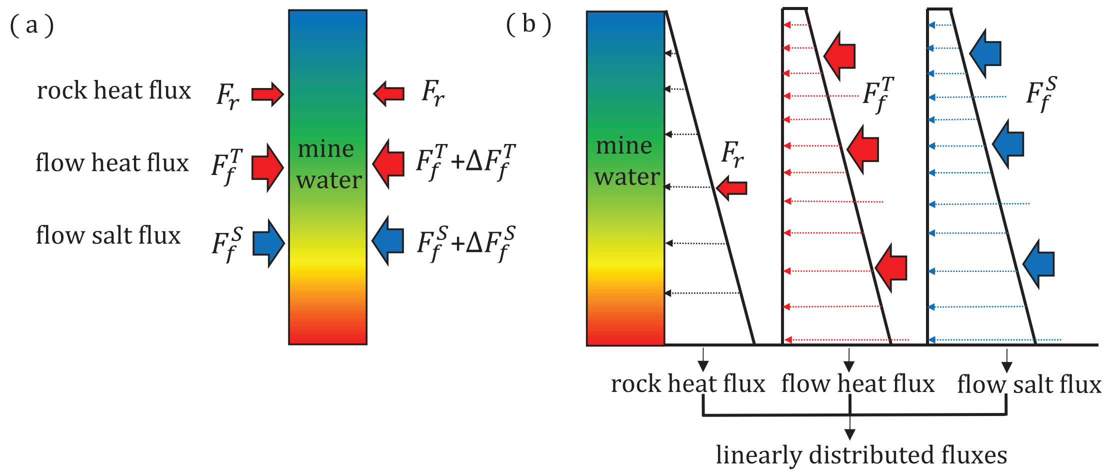

Figure 4.4. Schematic of the boundary conditions of the mine water body in the shaft with double-diffusive intrusions by lateral temperature and salinity fluxes: (a) the whole process of intrusions and (b) linear distribution of fluxes with depths.

The boundary conditions are critical for simulating the thermohaline stratification with the hypothesis assuming double-diffusive intrusions due to lateral temperature and salinity fluxes in Section 3.3.2. Figure 4.4 shows the schematic of the boundary conditions for the simulation with this hypothesis. It is seen in Figure 4.4a that there is neither heat nor salt flux on the top surface or at the bottom. In the lateral directions, as shown in Figure 4.4a, there are lateral heat and salt fluxes on the two lateral boundaries but with a heat flux difference ΔF_f^T and a salt flux difference ΔF_f^S on the two lateral boundaries, which are explained in detail in the following.

For the thermal flux, the initial linearly distributed temperature of the mine water in the shaft can be influenced by the surrounding rock heat flux (i.e., F_r in Figure 4.4a). This heat flux is the same for the two lateral boundaries due to the same geothermal gradient. In addition to the surrounding rocks, the initial temperature of the mine water in the shaft can also be influenced by the heat flux from the surrounding water flows (i.e., F_f^T). The surrounding water flows are the major water source for flooding abandoned mine shafts (i.e., mine water rebound) from groundwater or surface water, e.g., abandoned coal mines flooding in the U.K. (Gandy and Younger 2007) and Poland (Banks et al. 2010). In this situation, the thermal coupling between the mine water and its surrounding flows needs to be considered. However, the consideration of such a thermal coupling is very difficult. The first difficulty is that the effect of convection. For simplicity, we assumed that the heat between the mine water and its surrounding water flows is transferred via conduction only. However, the heat exchange due to this conduction (i.e., the mine water and its surrounding water flows) is much more significant compared to that between the mine water and its surrounding rocks. Therefore, the thermal conductivity of the surrounding water flows should be higher than the rocks. To indirectly consider this higher thermal conductivity, a high heat transfer coefficient was assumed on the lateral boundaries in Figure 4.4a between the mine water and its surrounding water flows. The second difficulty is that locations, where the surrounding water enters the shaft, are unpredictable due to the complexity of underground mine configurations. Any cracks, fissures, faults, or drifts irregularly distributed along the shaft can serve the pathway for the surrounding water flows to enter. For example, Hancock faults and many fissures are distributed along Hancock Shaft 2 according to (Butler and Burbank 1929). To solve this difficulty, as shown in Figure 4.4b, we assumed to use the linear distribution of the thermal flux with depths on the lateral boundaries for approximating the realistic situation. This situation is that the surrounding water flows can enter into the shaft through any possible locations via cracks, fissures, faults, or drifts along it.

In addition, we also assumed that there is a heat flux difference ΔF_f^T on the two lateral boundaries, as shown in Figure 4.4a, which means that the heat flux from the surrounding water flows for the two lateral boundaries can be different. This assumption primarily is attributable to two reasons. First, from a practical perspective, the temperature of the surrounding water flows can be influenced by fissures, fractures, faults or drafts in the flowing process. This process very likely could cause a temperature difference between the lateral surrounding water flows, leading to a heat flux difference for the two lateral boundaries. Second, such an assumption can be mutually proven by the numerical evidence. That is, a heat flux difference is required to reproduce the thermohaline stratification, which will be detailed in Section 4.3.3.

For the salt flux, the initial salinity of the mine water can be influenced by the surrounding flows only. Similar to the heat flux, we assumed that the distribution of the salt flux is linear with depths. Due to the same geothermal and solutal gradients for the surrounding water flows, the difference of heat and salt fluxes on the two lateral boundaries, i.e., ΔF_f^T and ΔF_f^S in Figure 4.4a, can be obtained when the top temperature and top salinity of the surrounding flows on the two lateral boundaries are different. Mathematically, the above assumptions linked to the double-diffusive intrusion due to lateral fluxes in Figure 4.4 are described using the following formulations

$$\begin{cases} F_r = h_{rf}(r(z) - T) \\ F_f^T = h_f^T(r(z) - T) \\ F_f^S = h_f^S(r(z) - S) \\ r(z) = R + zG \end{cases} \tag{4.8}$$

where h_{rf} is the heat transfer coefficient between the mine water and the surrounding rocks, h_f^T is the heat transfer coefficient between the mine water and the surrounding water flows, h_f^S is the salt transfer coefficient, R is the top temperature of rocks, the top temperature of the surrounding water flows, or the top salinity of the surrounding water flows on the two lateral boundaries, $r(z)$ is the linear function of either temperature or salinity in terms of depth z, and G is either the thermal gradient or solutal gradient.

For Hancock Shaft 2 adopted in this study, the parameters for the above boundary conditions were set up as follows: (1) The top surface temperatures of the mine water, surrounding rocks and surrounding flows of one lateral boundary are 282.15 K, while the top temperature of the surrounding flows of the other boundary is 282.65 K, leading to 0.5 K temperature difference in the surrounding flows between the lateral boundaries. (2) The top salinity of the surrounding flows of one lateral boundary, which has the top temperature of 282.15 K, is 2% and the top salinity on the other boundary is 2.3%, resulting in 0.3%

salinity difference. (3) The rocks and surrounding water flows have the same thermal gradient of 5.35×10^{-3} K/m. (4) The surrounding water flows have the same solutal gradient of 5.18×10^{-4}%/m. (5) Due to the low velocity of the mine water caused by the natural convection, h_{rf} was assumed to be 1 W/(m^{2}K) according to (Zhao 2014); while $h_f^T = 50$ W/(m^{2}K) and $h_f^S = 10^{-4}$ m/(s %) were assumed. As illustrated above, $h_f^T > h_{rf}$ should be ensured to indirectly consider the convection effect (i.e., high heat diffusion between the mine water and the surrounding flows).

Table 4.1. Parameters used in the simulation.

Material	Parameter	Value
Mine water	Reference density (kg/m^3)	1088.6
	Reference temperature (K)	333.15
	Reference salinity (%)	15
	Specific heat (J/(kg K))	4181
	Effective viscosity (m^2/s)	3.95×10^{-3}
	Thermal expansion coefficient (K^{-1})	5.24×10^{-4}
	Solutal expansion coefficient (%$^{-1}$)	6.82×10^{-3}
	Effective thermal diffusivity (m^2/s)	4.94×10^{-4}
	Effective solutal diffusivity (m^2/s)	1×10^{-6}

Note: Thermal and solutal properties of the mine water are determined from (Hull et al. 1988).

It is also significant to properly determine the effective kinematic viscosity and effective diffusivities. For the large-scale mine water presented in this study, we did not consider a turbulence model directly. Instead, we assumed the effective kinematic viscosity and effective diffusivities to be constants, which is similar to the numerical modeling of large-scale water circulations in oceans, e.g., Radko et al. (2014). For effective diffusivities (temperature or salinity), Eq. (4.9) can be used to estimate the magnitude of the eddy diffusivities (Vallis 2017), e.g., the thermal eddy diffusivity α_T:

$$\overline{\mathbf{U}'T'} = -\alpha_T \nabla T \tag{4.9}$$

where $\overline{\mathbf{U}'T'}$ is the eddy flux. According to Wolkersdorfer (2008), the maximum measured velocity of the mine water from tracer tests is in a magnitude of 10^{-2} m/s. α_T thus can be estimated under this magnitude. The effective thermal diffusivity is the sum of the eddy diffusivity and the laminar diffusivity, so is that for the effective kinematic viscosity and the effective solutal diffusivity. The eddy kinematic viscosity can be calculated based on the eddy thermal diffusivity and the turbulent Prandtl number. The material properties of the mine water used in this study are tabulated in Table 4.1. Field measurements for chemical concentrations in Table 3.1 showed that sodium chloride is the primary chemical component in the mine water. The simulation, therefore, assumed the salinity in the mine water is caused by sodium chloride.

4.3 Simulation Results and Discussion

4.3.1 Thermohaline Stratification Formation

In this section, transient simulation with non-isothermal and non-isosolutal hydrodynamics is conducted using the validated model detailed in Section 4.2.1. This multiphysics simulation uses the material properties, the initial and boundary conditions introduced in Section 4.2.3. to explore the formation and evolution of thermohaline stratifications in the mine water of Shaft 2.

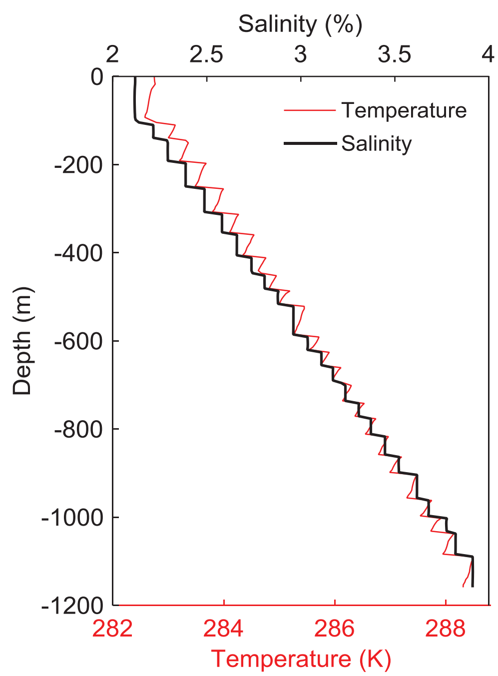

Figure 4.5. Vertical distributions of temperature and salinity along the center axis of Shaft 2 when N=4 at t=4.5 days.

Shown in Figure 4.5 is the vertical distributions of temperature and salinity along the center axis of Shaft 2 when N=4 at t=4.5 days. It is seen that thermohaline stratifications spontaneously form and a “staircase” shape is exhibited. Each staircase represents an individual layer that has almost the same temperature and salinity. There are significant temperature and salinity gradients between two adjacent layers. The number of layers and the location to form layers are highly identical for both temperature and salinity. The structure of layers in Figure 4.5 is very similar to the field observations in Figure 4.1. This indicates that DDC with double-diffusive intrusions by lateral temperature and salinity fluxes can lead to the formation of thermohaline stratifications in the large-scale mine water.

The predicted velocity of the mine water in the simulation also coincide with that of field measurements. Figure 4.6 presents the variations of the mine water velocity with respect to time in the center axis at $z = -470\ \mathrm{m}$. The maximum velocity is around $1\ \mathrm{cm/s}$, which is highly consistent with the maximum magnitude of the mine water velocity from field measurements (Wolkersdorfer 2008; Kories et al. 2004). As can be seen in Figure 4.6, the variation of the mine water velocity is significant before 15 hours due to intrusions by lateral temperature and salinity fluxes. This is because thermohaline stratifications form in this period. After the layer formation, the variation of the mine water velocity tends to be very slow as the mine water orderly circulates in each layer.

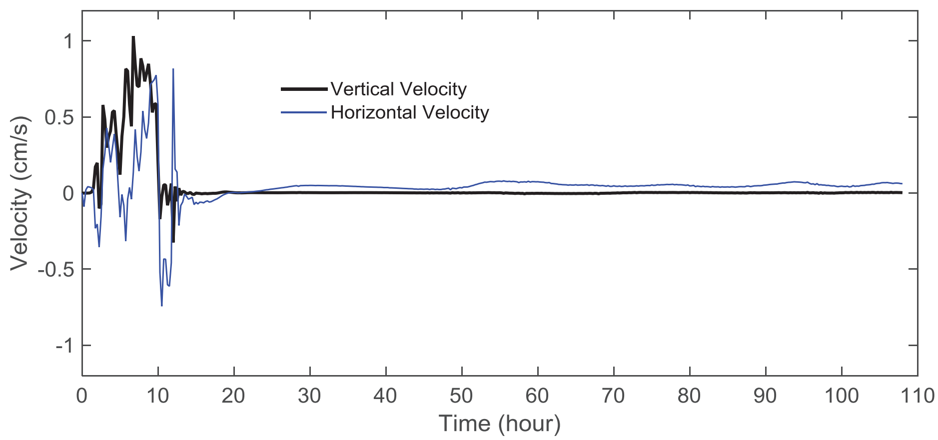

Figure 4.6. Variations of the mine water velocity with time when N=4 in the center axis of Shaft 2 at the location $z=-470$ m.

To clearly illustrate the formation of thermohaline stratifications, Figure 4.7 shows the evolution of stratifications for salinity in the region between $z=-360$ m and $z=-579.6$ m at different times. At $t=7$ hours, layers are observed with different thicknesses (Figure 4.7a). The number of layers decreases at $t=25$ hours (Figure 4.7b). The number of layers further decreases from six (Figure 4.7b) to five (Figure 4.7c) at $t=4.5$ days. These observations in Figure 4.7 indicate that layers merge gradually. Some of the small layers merge to form layers with a larger thickness, leading to a decrease in the number of layers. This phenomenon is similar to the layer-merging event in oceans, in which small layers gradually merge to form large layers (Radko et al. 2014).

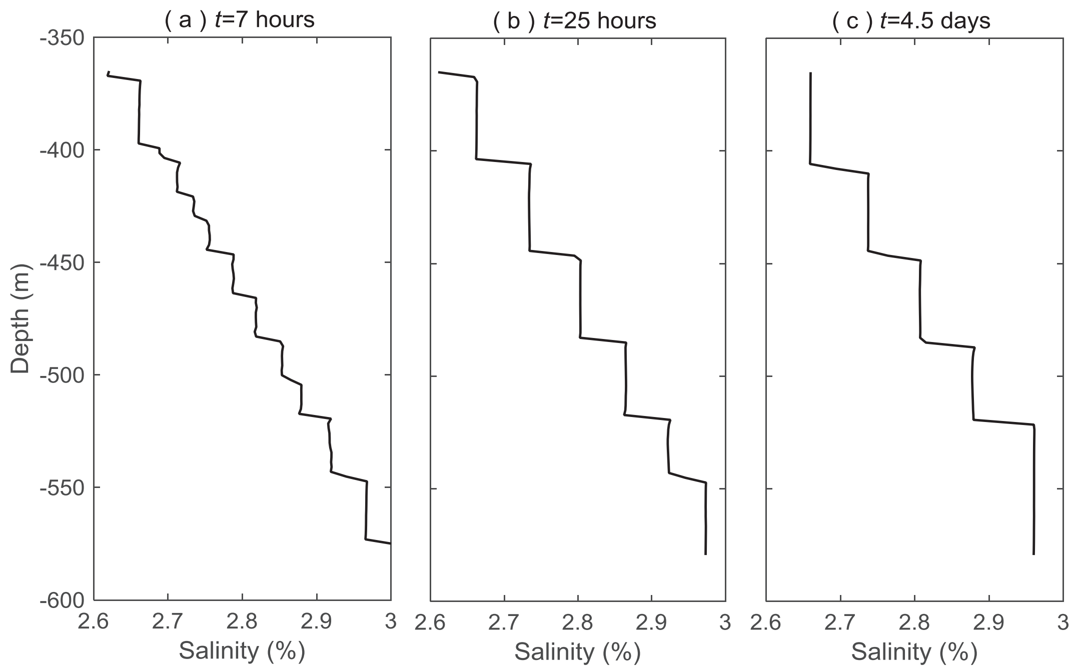

Figure 4.7. Formation and evolution of stratifications for salinity when N=4 in the region between $z=-360$ m and $z=-579.6$ m: (a) t=7 hours, (b) t=25 hours and (c) t=4.5 days.

Corresponding flow patterns in the same region in Figure 4.7 can help illustrate variations of heat and mass in the mine water, which trigger the formation and evolution of stratifications. As shown in Figure 4.8, the mine water is not stagnant because of temperature and salinity differences. The mine water circulates to form separate layers (Figure 4.8a). The water moves relatively fast within individual layers in the clockwise direction; while the velocity is very slow at the layer interfaces (Figure 4.8b). Due to this slow velocity, the connection between two adjacent layers is intercepted. As time elapses from 25 hours to 2.5 days, the layer-merging happens and layers 1 and 2 merge to form one layer with a larger thickness. These observations of flow patterns in Figure 4.8 clearly explain the layer merging event for the salinity distributions and variations in Figure 4.7.

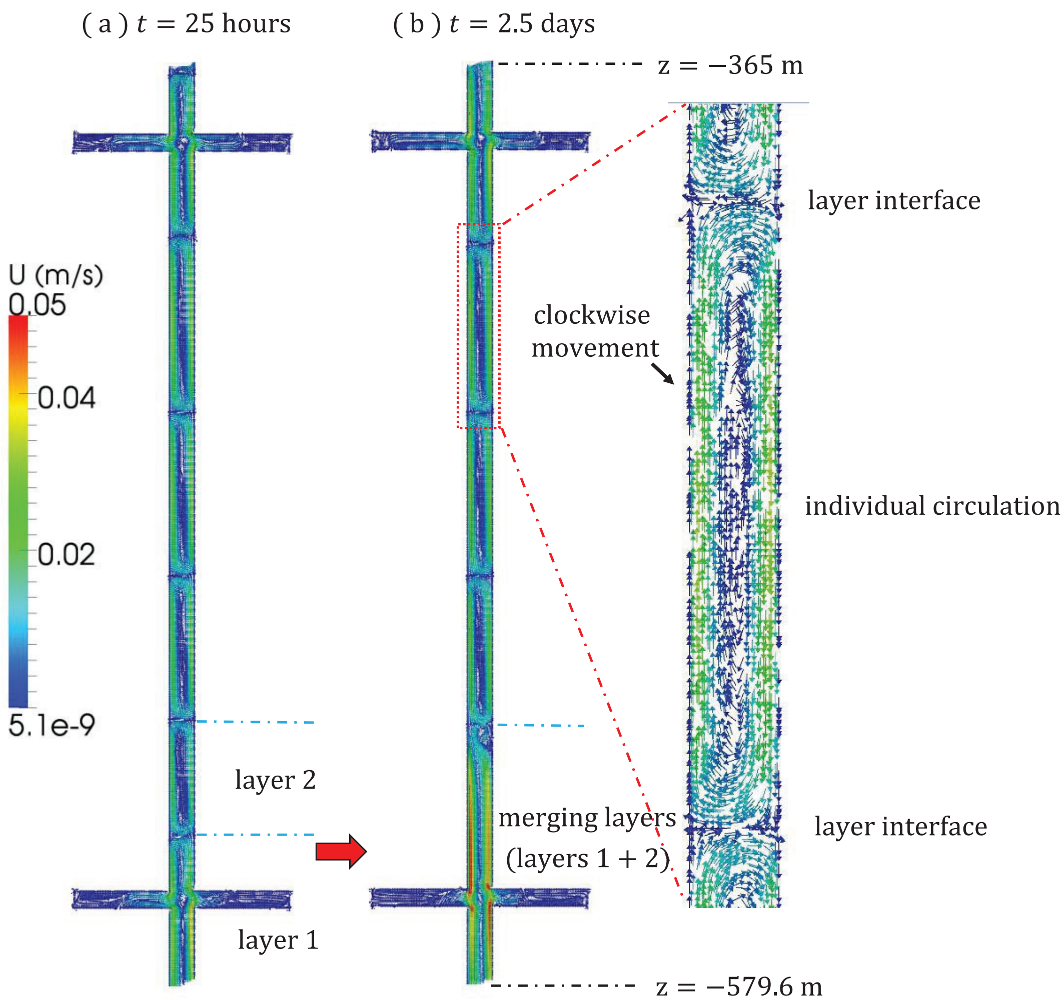

Figure 4.8. Flow patterns of the mine water in the region between $z = -365$ m and $z = -579.5$ m: (a) t=25 hours and (b) t=2.5 days.

Thermohaline stratifications can also be successfully reproduced with a small value of the buoyancy ratio. Figure 4.9 shows the evolution of stratifications for temperature along the center axis of Shaft 2 when N=1.26. N is calculated by Eq. (4.7), in which ΔT remains unchanged while ΔS decreases by reducing S_b. The initial temperature is linearly distributed from 282.15 K to 288.35 K (Figure 4.9 a). As time elapses, the temperature distribution evolves to separate layers with significant temperature differences between layers (Figure 4.9 b and Figure 4.9 c). The layer-merging also happens to form layers with a larger thickness by merging small layers. This interesting phenomenon can also be observed in Figure 4.10 for salinity. The distribution of salinity evolves from the linear distribution to the stratified distribution with separate layers, and then some of the layers merge into larger ones. As time further elapses, thermohaline stratifications presented in Figure 4.11 exhibit the same structure as the field observations in Figure 4.1 with a few (2 or 3) layers.

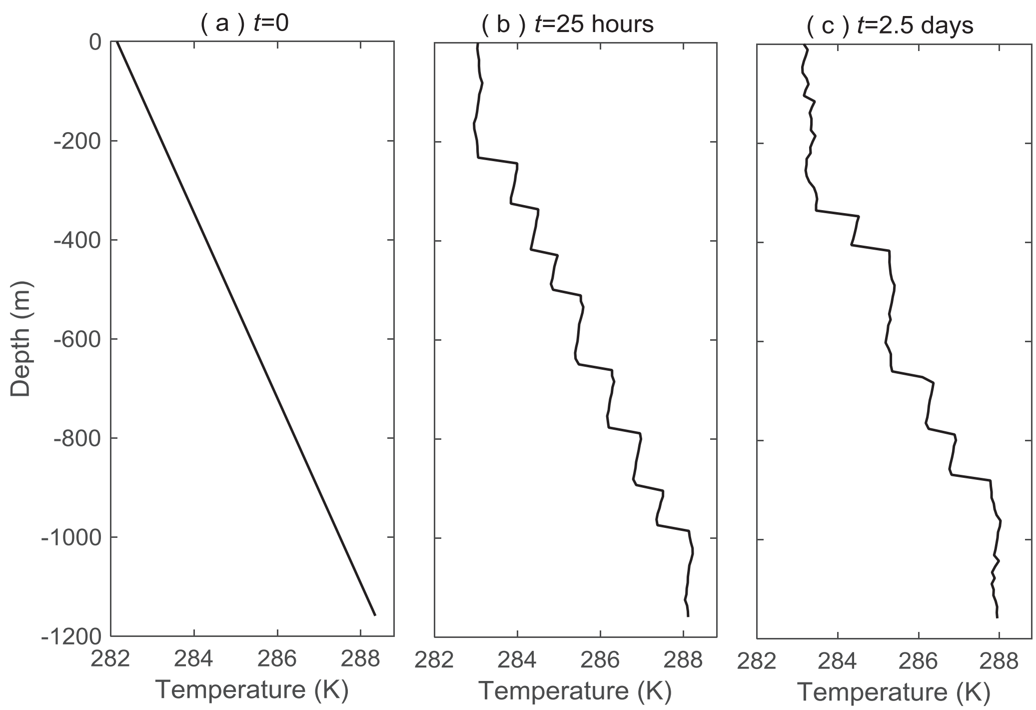

Figure 4.9. Formation and evolution of stratifications for temperature when N=1.26: (a) t=0, (b) t=25 hours and (c) t=2.5 days.

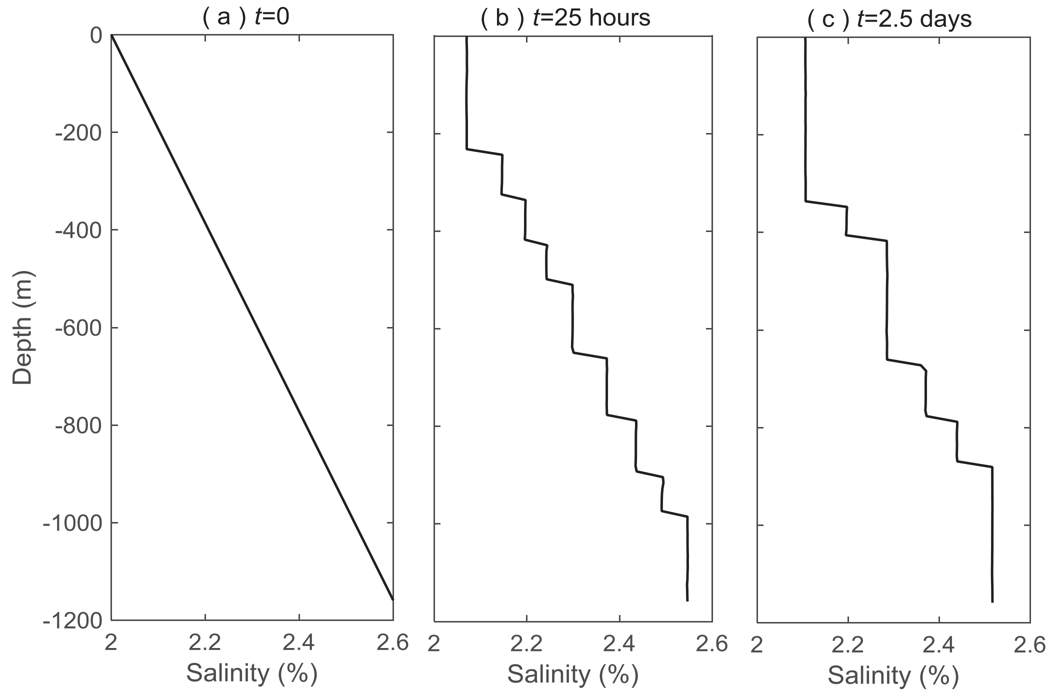

Figure 4.10. Formation and evolution of stratifications for salinity when N=1.26: (a) t=0, (b) t=25 hours and (c) t=2.5 days.

In addition, Figure 4.9, Figure 4.10, and Figure 4.11 indicate that both temperature and salinity are squeezed in the lateral direction during the formation of stratifications. To be more specific, the top temperature and salinity at $z = 0$ increase during this period, which are higher than the initial top values. In contrast, the bottom temperature and salinity at $z = -1159.2$ m decrease, which are lower than the initial bottom values. Therefore, the differences between the top temperature/salinity and the bottom temperature/salinity decrease. In this process, the salinity difference decreases more quickly. This implies that the current N value, which is calculated using Eq. (4.7) based on the field observations of temperature and salinity that are already stratified, is lower than the real N value, which is calculated based on the initial differences in temperature and salinity. Therefore, the real *N* value should be higher than the current *N* value.

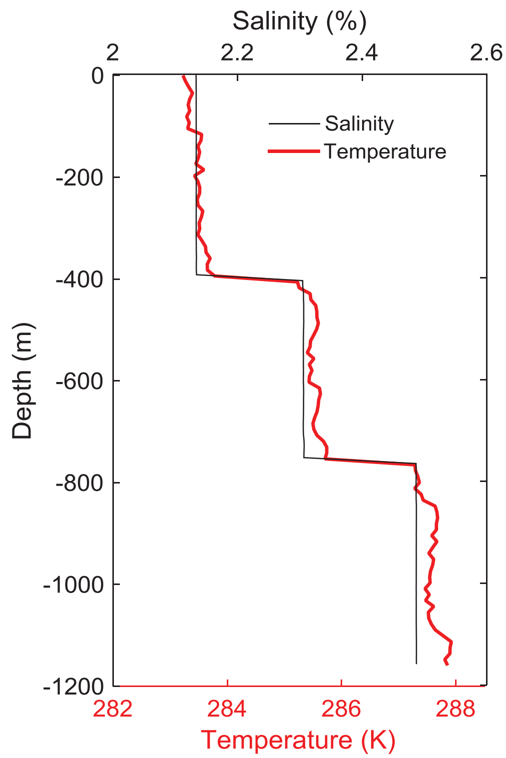

Figure 4.11. Vertical distributions of temperature and salinity along the center axis of Shaft 2 when N=1.26 at t=4.5 days.

Typical temperature and salinity contours are another angle for directly showing the heat and mass distribution within the mine water. As shown in Figure 4.12a, the temperature of each layer is almost the same. A significant temperature gradient exists between two layers, which is consistent with stratifications in Figure 4.9 and Figure 4.10. When t=16 hours, layers 1 and 2 merge to form one layer that has the uniform temperature but a larger thickness (Figure 4.12b). Similar observations also can be seen in Figure 4.13 for salinity contours. A clearly significant salinity gradient is observed between layers (Figure 4.13a). Then, one large layer forms via merging layers1 and 2 when t=16 hours, as shown in Figure 4.13b. These observations clearly show the formation and evolution of stratifications and layer-merging events in the large-scale mine water.

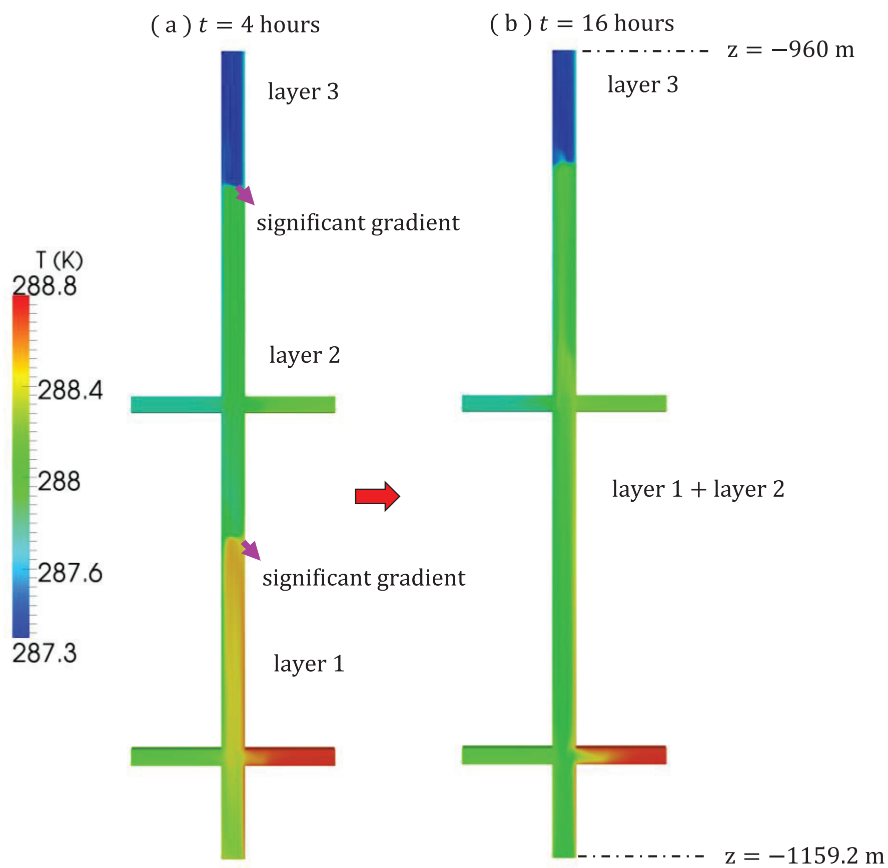

Figure 4.12. Temperature contours in the region between $z = -960$ m and $z = -1159.2$ m: (a) t=4 hours and (b) t=16 hours.

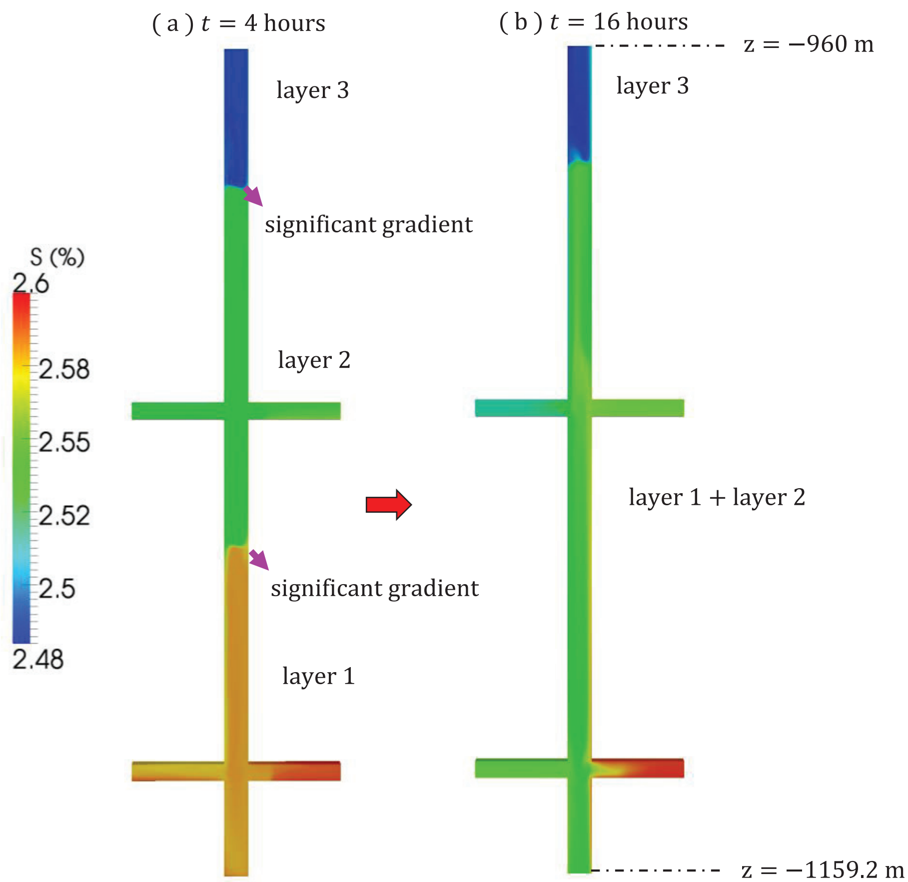

Figure 4.13. Salinity contours in the region between $z = -960$ m and $z = -1159.2$ m: (a) t=4 hours and (b) t=16 hours.

4.3.2 Critical Buoyancy Ratio for Thermohaline Stratification

In oceans, no salt-finger staircases have been reported if the critical buoyancy ratio N_c is lower than 0.5 and N_c needs to be larger than 0.59 to obtain thermohaline staircases (Radko et al. 2014). In this section, we explore the critical buoyancy ratio N_c for the formation of thermohaline stratifications in the large-scale mine water. As the temperature layers are highly identical to the salinity layers in thermohaline stratifications (see Figure

4.9 and Figure 4.10), we focus on the evolution of the temperature distribution in the following.

Figure 4.14 presents the evolution of the temperature distribution along the center axis of Shaft 2 when N differs. As shown in Figure 4.14a, temperature layers cannot be observed during 5 hours when $N = 0.6$. This N value is almost the same as the critical buoyancy ratio for thermohaline staircases in oceans. The results in Figure 4.14 a imply that such a low value of N cannot provide the salinity-induced buoyancy force to suppress the thermal convection. Therefore, the thermal convection is dominant in the whole process when $N = 0.6$. As N increases to 0.8, a few layers may form in local regions, as can be seen in Figure 4.14b, but they are very obscure. Clear layers are observed at the same calculation time when $N = 1$, as shown in Figure 4.14c. The preliminary observations in Figure 4.14 reveal that N_c for the formation of clear layers in the mine water is greater than 0.8 but smaller or equal to 1.0.

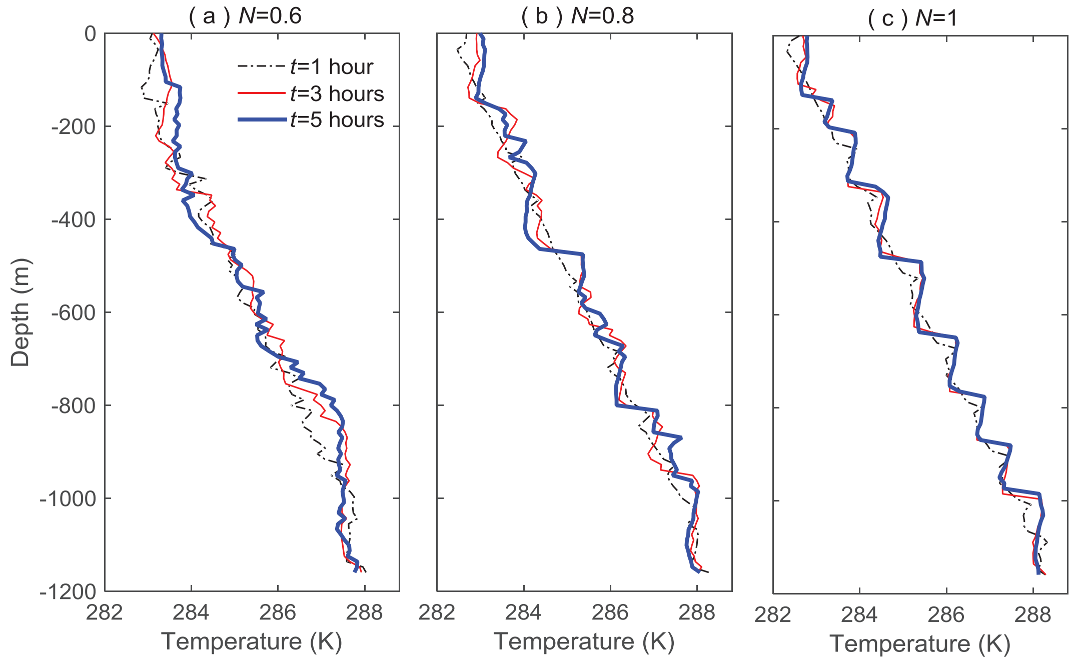

Figure 4.14. Evolution of stratifications for temperature at different times with different N values: (a) N=0.6, (b) N=0.8 and (c) N=1.

In order to accurately obtain N_c for thermohaline stratifications in the mine water, $N = 0.9$, $N = 0.95$ and $N = 1$ were investigated by comparing their temperature distributions and corresponding vertical temperature gradients. Figure 4.15a shows the absolute vertical temperature gradient for $N = 0.9$ at t=5 hours. The vertical temperature gradient in each layer should be very small and close, because the temperature in each layer is almost the same. However, it is unclear to directly determine a temperature layer via the temperature gradient in Figure 4.15a. Therefore, we define a criterion based on the temperature distribution for the layer determination using the corresponding vertical temperature gradient. The temperature distribution for $N = 0.9$ shown in Figure 4.15 exhibits two clear temperature layers, i.e., Layer A and Layer B. Their corresponding vertical temperature gradients are smaller than 0.01 K/m (see Figure 4.15a). Therefore, 0.01 K/m is adopted as the critical value for the criterion to determine the temperature layer. The temperature layer forms if the vertical temperature gradient in a vertical depth range, i.e., around 100 m, is smaller than 0.01 K/m. No layers form beyond 0.01 K/m. Based on this criterion (see the critical line in Figure 4.15a), two temperature layers can be determined when $N = 0.9$ at t=5 hours.

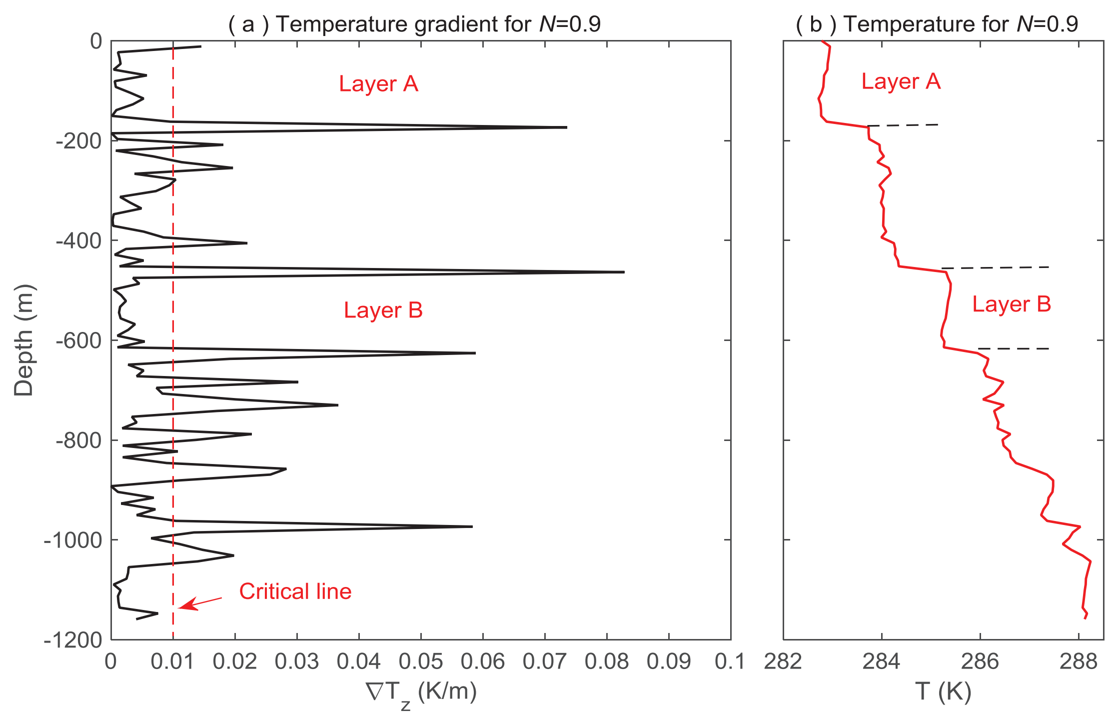

Figure 4.15. Distributions of temperature along the center axis of Shaft 2 for N=0.9 at t=5 hours: (a) absolute vertical temperature gradient and (b) temperature.

For $N = 0.95$ at t=5 hours, it is determined four temperature layers, i.e., Layers A-D, based on the criterion (see Figure 4.16a). The number of layers increases when N increases from 0.9 to 0.95, because the influence of salinity on the buoyancy force increases and the thermal convection is further suppressed. Nine layers can be clearly determined in the whole region at the same calculation time when N increases to 1.0 (Figure 4.17). The results from Figure 4.15, Figure 4.16, and Figure 4.17 indicate that a few layers can be observed when the value of N is located between 0.9 and 1.0. The critical buoyancy ratio N_c is equal to 1.0 to obtain layers in the mine water with a clear and separate structure that is very similar to field observations in Figure 4.1.

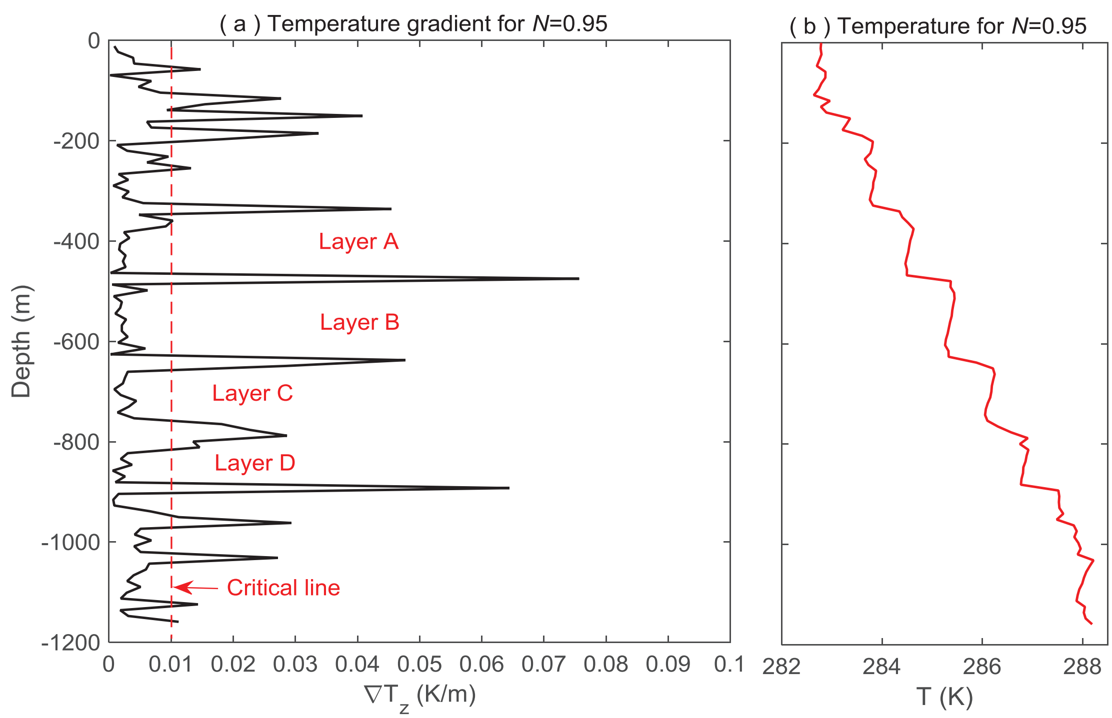

Figure 4.16. Distributions of temperature along the center axis of Shaft 2 for N=0.95 at t=5 hours: (a) absolute vertical temperature gradient and (b) temperature.

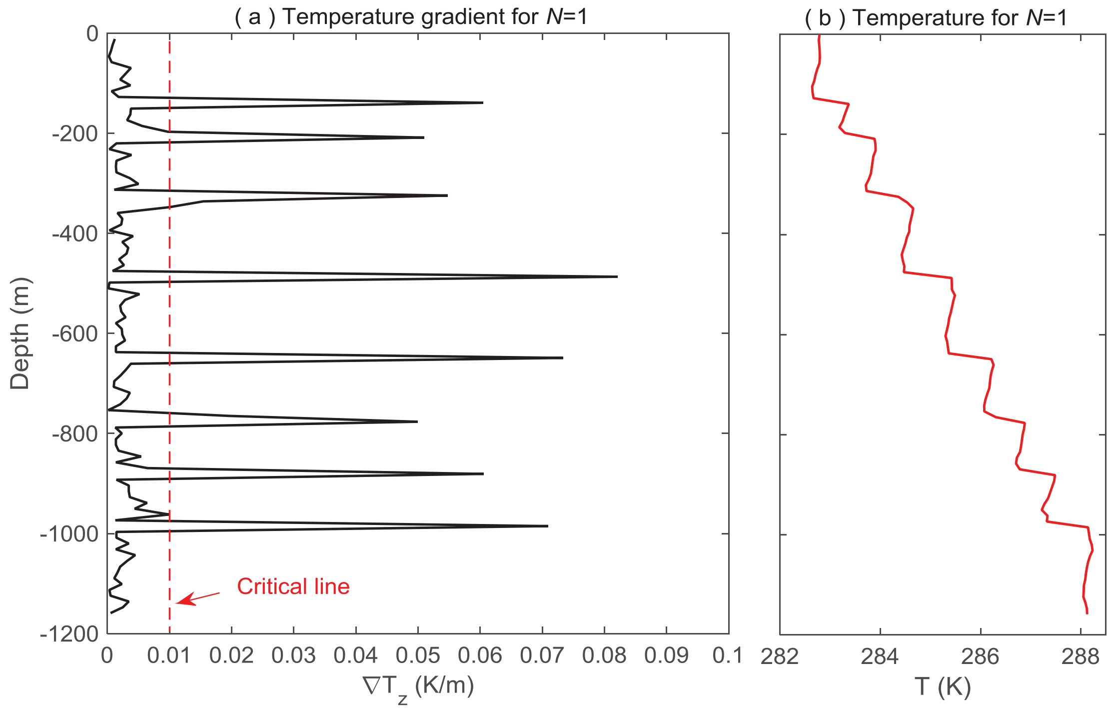

Figure 4.17. Distributions of temperature along the center axis of Shaft 2 for N=1 at t=5 hours: (a) absolute vertical temperature gradient and (b) temperature.

4.3.3 Is the Lateral Double-Diffusive Intrusion Required for the Formation of Thermohaline Stratifications?

According to the first hypothesis (Merryfield 2000) introduced in Section 4.2.2, the major cause for forming thermohaline staircases in oceans is the double-diffusive intrusion due to lateral temperature and salinity fluxes. This has been proven by the transient simulation results in Section 4.3.1. The lateral salinity flux is highly possible in mines flooded by salty underground water, e.g., abandoned mines in southwestern Indiana, U.S. (Bayless and Olyphant 1993). However, this salinity flux is possibly negligible for mines, where the salinity of their mine water is the same as fresh groundwater or surface water, e.g., mines in the U.P. of Michigan. Therefore, this raises an interesting question: "Are the lateral temperature and salinity fluxes required for the formation of thermohaline stratifications?" Such a question will be addressed in this section with N=1.26.

The lateral salinity flux is investigated first. For the purpose, we exclude the lateral salinity flux by employing no salinity flux on the lateral boundaries (see boundary conditions in Section 4.2.3). The simulation results shown in Figure 4.18 reveal that thermohaline stratifications can still form without the lateral salinity flux. By comparing the temperature layers with and without the lateral salinity flux, the only difference is that the layer number differs. The reason is that the inclusion of the lateral salinity flux will increase salinity in the system, which slows down the layer-merging process, so that the layer number with the lateral salinity flux is larger. Therefore, the lateral salinity flux is unnecessary for the formation of stratifications. In fact, the lateral salinity flux for the above simulation results in Figure 4.7 and Figure 4.9 is negligible. This is because the mass transfer coefficient (i.e., 10^{-4} m/(s %) see Section 4.2.3) is very small. Accordingly, the amount of salinity intruded into the mine water via the lateral flux is very small.

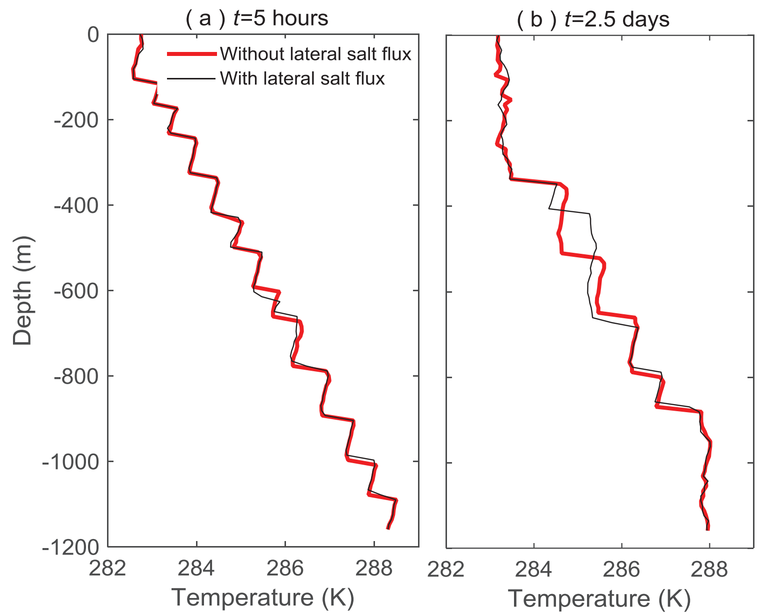

Figure 4.18. Comparisons of temperature layers with and without the lateral salinity flux: (a) t=5 hours and (b) t=2.5 days.

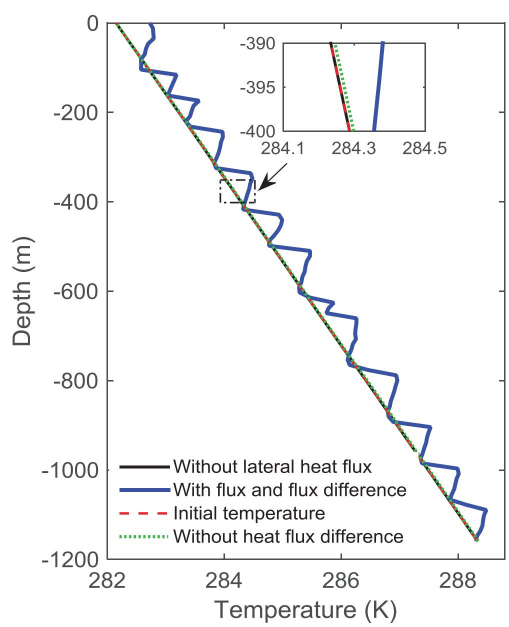

Figure 4.19. Comparisons of the temperature distribution with and without the lateral heat flux at t=5 hours.

For the lateral heat flux, the results in Figure 4.19 for the comparison of temperature distributions with and without this flux reveal that the lateral heat flux is the necessary condition for successfully simulating thermohaline stratifications. Thermohaline stratifications can occur if the lateral heat flux is considered. In addition to that, a difference in this heat flux is also required on the lateral boundaries (see details of this flux for boundary conditions in Section 4.2.3). The temperature distribution without the lateral heat flux is linear and almost the same as the original distribution. A similar observation can be obtained in the situation without the flux difference, as shown in Figure 4.19.

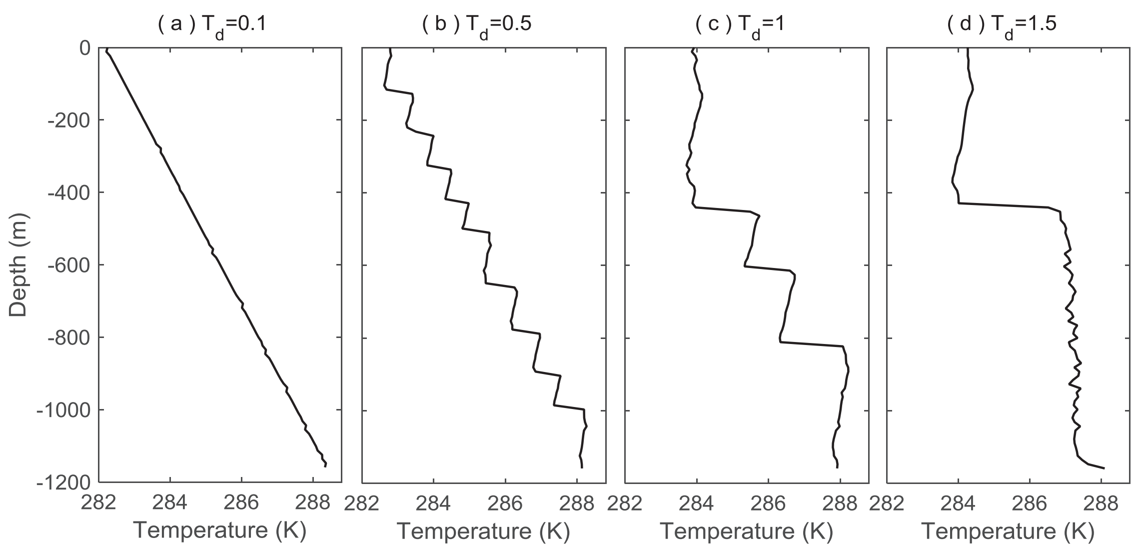

Figure 4.20. Comparisons of temperature layers under the lateral heat flux differences at t=11 hours and the corresponding temperature difference T_d is equal to (a) 0.1 K, (b) 0.5 K, (c) 1 K, and (d) 1.5 K.

Since the formation of thermohaline stratifications requires the lateral heat flux with a difference in this flux, it is also helpful to investigate how the lateral heat flux influences thermohaline stratifications. Figure 4.20 shows the comparisons of thermohaline stratifications under four different in the heat flux conditions by employing different temperature differences. As can be seen that at the same calculation time, a higher difference in the flux, a smaller the number of layers. The reason for this is that a higher difference in the heat flux will increase the temperature in the system, which speeds up the layer-merging process. Therefore, the layer number is smaller. It is also seen in Figure 4.20a that no layers form with a small difference in the heat flux under T_d=0.1. However, as shown in Figure 4.21, layers can be clearly observed when time elapses from 11 hours to 19.5 hours, though these layers are very small. This indicates that the formation of layers under a small difference in the heat flux is very slow. This fact also provides another possible explanation, in addition to the effective kinematic viscosity in Section 5.3.2, for the observation that layers in flooded mines can remain for a long time. Therefore, the results in Figure 4.20 and Figure 4.21 show that layers can form as long as the lateral heat flux with a flux difference is considered.

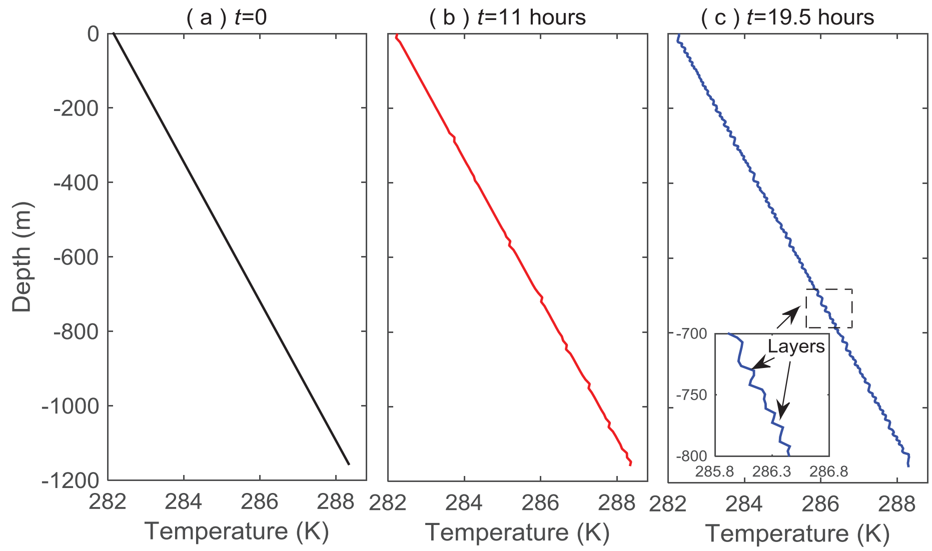

Figure 4.21. Comparisons of the temperature distribution under the temperature difference $T_d = 0.1$ at different times.

4.4 Conclusions

This chapter explores the formation of thermohaline stratifications, which is the key scientific myth that remains little understood in the past three decades in geothermal energy recovery via the mine water from abandoned mines. The thermohaline stratification is very significant for recovering geothermal energy, because it determines the temperature distribution and consequently the reserve and efficiency of the energy resource. In this chapter, a theoretical framework for the fully coupled DDC model was presented first and then validated against documented experimental and numerical results. Multiphysics simulation with unique non-isothermal and non-isosolutal hydrodynamics was conducted using the validated model to shed light on the formation and evolution of thermohaline stratifications in the large-scale mine water.

The simulation succeeded in explaining the mechanism of heat and mass transfer in the DDC process, and reproducing the key phenomenon regarding thermohaline stratifications observed from field measurements. It was found that intrusions by lateral temperature and salinity gradients can lead to thermohaline stratifications in the large-scale mine water with initially linear distributions of temperature and salinity. The layer-merging even is involved in the evolution of stratifications. Some of the small layers gradually merge to form layers with a larger thickness, leading to a decrease in the number of layers.

To successfully reproduce thermohaline stratifications in numerical simulation, the lateral salinity flux is a not required condition. In contrast, the lateral heat flux is necessary. A difference between lateral heat fluxes is also required for successfully simulating thermohaline stratifications. Thermohaline stratifications can form as long as the lateral heat flux with a difference in this heat flux is considered. The simulation results revealed that this difference significantly influences the development of thermohaline stratifications. The higher the difference, the smaller the number of layers.

No research has been reported prior to the current chapter on offering these significant apperceptions and explaining the formation and evolution of thermohaline stratifications. It is the first time, to the best of my knowledge, that thermohaline stratifications in the large-scale subterranean water bodies have been successfully reproduced. It is believed that this scientific breakthrough is significant and valuable for future recovering geothermal energy via the mine water from abandoned mines in an efficient, sustainable and economical way.

5 Understanding of Thermohaline Stratification: Factors and Mechanisms

This chapter provides insights into thermohaline stratifications for understanding the dominant heat and mass transport mechanisms underlying thermohaline stratifications and the factors influencing thermohaline stratifications by investigating six critical issues: (1-3) influences of key transport parameters, i.e., effective thermal diffusivity, effective kinematic viscosity, and diffusivity ratio, on thermohaline stratifications; (4) mechanisms behind the layer-merging; (5) effect of the buoyancy ratio; and (6) possibility of predicting the initial distributions of temperature and salinity for the purpose in predicting the future development of thermohaline stratifications from the current status.

5.1 Introduction

Double-Diffusive Convection (DDC) is believed to be a major mechanism behind the formation of thermohaline stratifications in the mine water according to (Brandt and Fernando 1995). DDC occurs when two bodies of water with different molecular diffusivities contribute in the opposite way to the vertical water density gradient (Wolkersdorfer 2008; Turner 1974). In oceans, the phenomenon regarding DDC is commonly observed and two types of DDC can occur in oceanic water if large-scale gradients of temperature and salinity exist in the same vertical direction (Kelley et al. 2003): (1) the salt-finger type, i.e., warm and salty water overlies cold and fresh water, and (2) the diffusive convection type, i.e., cold and fresh water overlies warm and salty water.

For the mine water targeted in this study, the mode for DDC is the diffusive convection type as cold and fresh water overlies warm and salty water due to geothermal (temperature) and geochemical (salinity) gradients. Under this condition, the bottom water with high salinity can suppress the thermal convection in the vertical direction. This is because the bottom water with a high temperature is lighter compared to the cold top water and thus moves up due to the natural thermal convection. Because of the existence of salinity, high salinity makes that bottom water heavier than the fresh top water. Therefore, temperature and salinity in the mine water contribute in the opposite way to the vertical water density gradient. In fact, this coupled DDC process in the mine water is critical to the efficient use of the mine water for geothermal applications because the DDC determines the distributions and variations of the water temperature.

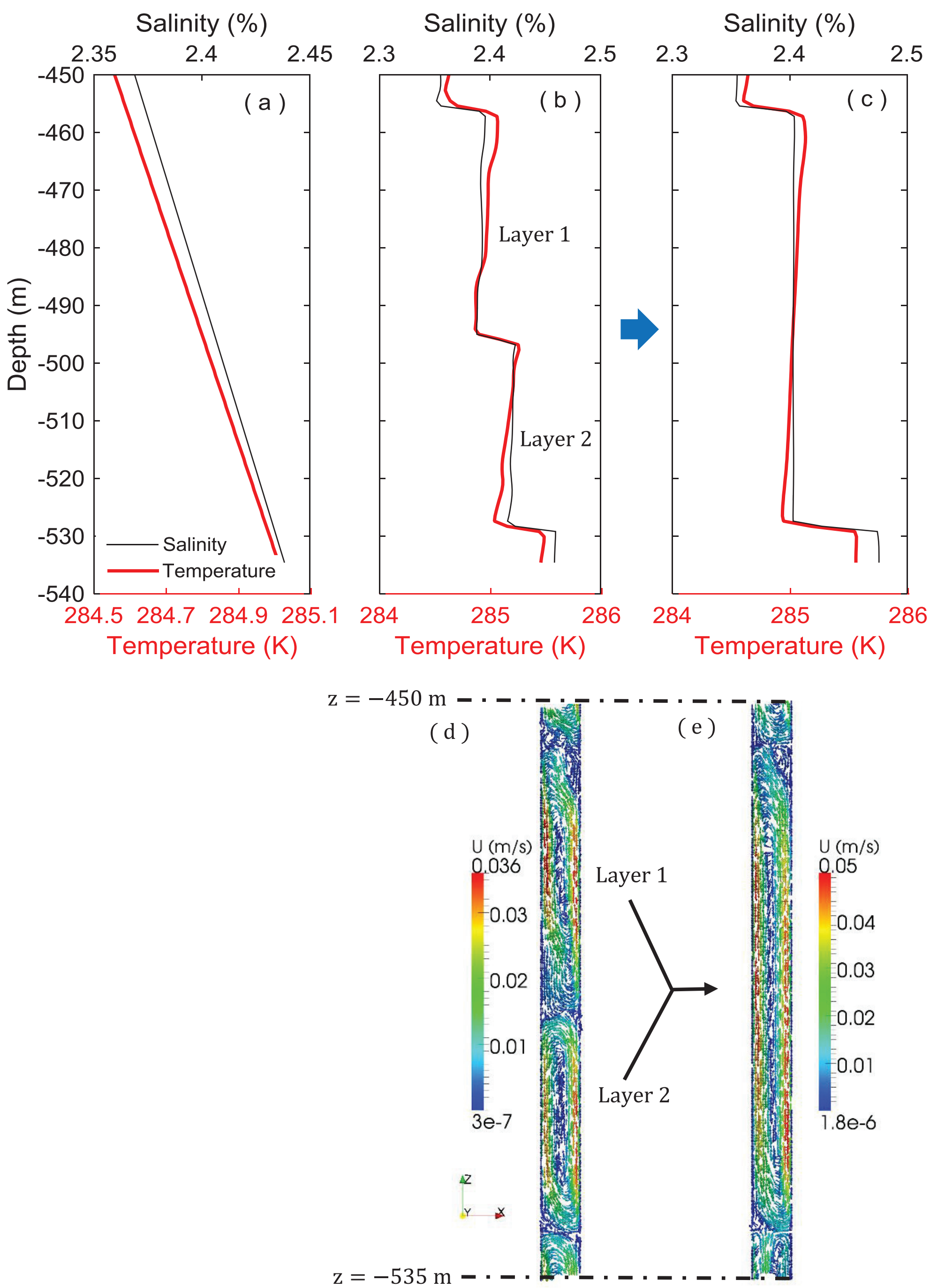

Figure 5.1. Formation and evolution of thermohaline stratifications. The presented results were obtained from the simulation of Hancock Shaft 2 in an elevation range between -450 m and -535 m (ground surface=0). The distributions of temperature and salinity

along the shaft axis were obtained at the time of (a) 0 (initial condition), (b) 6 hours, and (c) 12.5 hours. The corresponding flow patterns for (b) and (c) are presented in (d) and (e). In this example, the buoyancy ratio $N = 2$ and the diffusivity density ratio (heat/salt) $\lambda = 1/500$. A detailed description of the simulation can be found in Section 5.2.

Research attention, therefore, has been focused on understanding the coupled DDC process and exploring the thermohaline stratification in the mine water, though very few. Reichart et al. (2011) investigated the DDC process in the mine water using 2-Dimensional (2D) model to preliminary test the transient DCC flow and the transport of heat and mass in this dynamic process. However, thermohaline stratification was not successfully simulated, and the computational scale of the mine water (around 1 m) is very small in the study (Reichart et al. 2011). Therefore, that scale is not realistic for real mines. As presented in Chapter 4, thermohaline stratifications can be successfully produced in the large-scale mine water (around 1 km) using coupled non-isothermal and non-isosolutal hydrodynamics. Figure 5.1 presents an example of the formation and evolution of thermohaline stratifications in the mine water. The distributions of temperature and salinity are initially linear (Figure 5.1a) and then exhibit a “staircase” shape (Figure 5.1b) caused by the lateral double-diffusive intrusion (i.e., heat and salt fluxes). Water circulates in each layer individually (Figure 5.1d) and there are significant temperature and salinity differences between adjacent layers (Figure 5.1b). As time elapses, layers (e.g., Layer 1 and Layer 2) merge to form a layer with a larger thickness (Figure 5.1c and Figure 5.1e).

Despite the above progress, numerical investigations for understanding heat and mass transport of the dynamic DDC process in the mine water are still very rare. No research has been reported to provide in-depth insights into the formation and evolution of thermohaline stratifications. In particular, six critical issues for thermohaline stratification modeling have not been well understood: (1) the influence of the effective thermal diffusivity on the formation of thermohaline stratifications; (2) the influence of the effective kinematic viscosity on thermohaline stratifications; (3) the influence of the diffusivity ratio (heat/solute) on thermohaline stratifications; (4) the mechanisms behind the layer-merging in thermohaline stratifications; (5) the effect of the buoyancy ratio on the structure and development of thermohaline stratifications; and (6) the possibility of predicting the initial distributions of temperature and salinity for the purpose in predicting the future development of thermohaline stratifications from the current status..

To advance the topic, in this chapter, we provide critical insights into the formation and evolution of the thermohaline stratification, which is the primary physical mechanism determining the temperature distributions and variations and also a key consideration for the future optimal design of this geothermal application. A scientific framework for non-isothermal and non-isosolutal hydrodynamics presented and validated against documented results in Chapter 4 is used. Multiphysics simulation is conducted for a vertical mine shaft in the Upper Peninsula (U.P.) of Michigan using the validated model. Based on the simulation, we address the above critical issues in providing an in-depth understanding of the formation and evolution of thermohaline stratifications.

5.2 DDC Dominant Transport Analysis

In this section, the heat and solute transport (i.e., diffusion or convection) in the dynamic DDC process is evaluated. The purpose is to reveal the dominant heat and mass transport when thermohaline stratifications form. According to Section 4.3.3, the lateral salinity flux is not required for simulating thermohaline stratifications. In the following, we only consider the intrusion due to the lateral heat flux.

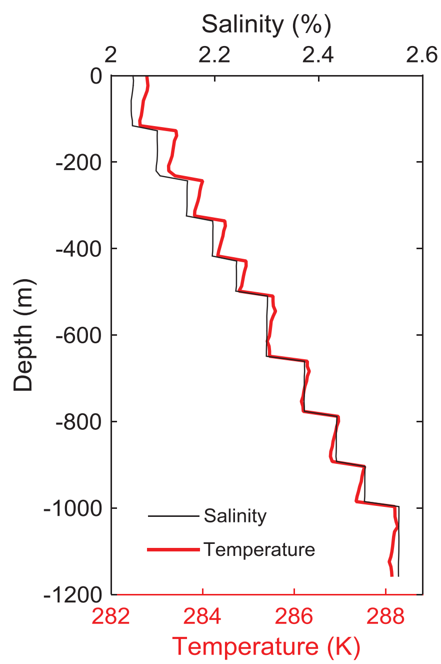

Figure 5.2. Thermohaline stratifications in the mine water along the center axis of Shaft 2 at t=13 hours when N=1.26.

Figure 5.2 presents simulated thermohaline stratifications in the mine water along the center axis of Shaft 2 at t=13 hours when N=1.26. For this N value, the range of salinity was assumed between 2% (top) and 2.6% (bottom). As can be seen in Figure 5.2, a "staircase" shape is exhibited for stratifications. Each staircase represents an individual layer that has almost the same temperature and salinity. There are significant temperature and salinity differences between two adjacent layers. The number of layers and the location to form layers are highly identical for both temperature and salinity. The above layers in Figure 5.2 arise from the dynamic DDC process with the lateral double-diffusive intrusion. To evaluate the dominant heat and solute transfer type (i.e., diffusion or convection) in this process, we can compare the Rayleigh number Ra with the critical Rayleigh number Ra_c. Because of the existence of both temperature and salinity, Ra in this process is calculated using Eq. (5.1) by the sum of thermal Ra_T and solutal Ra_S

$$Ra = Ra_T + Ra_S = \frac{g\beta_T\left(T_b - T_t\right)w^3}{\alpha_{eff}^T \nu_{eff}} + \frac{g\beta_S\left(S_b - S_t\right)w^3}{\alpha_{eff}^S \nu_{eff}} \tag{5.1}$$

where w is the shaft width. According to Love et al. (2007), the critical Rayleigh number Ra_c in DDC for the onset of convection in a vertical shaft can be estimated by

$$Ra_c = \frac{215.6}{r^4}(1 + 3.84r^2) \tag{5.2}$$

where r is the aspect ratio ($r = w / h_d$) and h_d is the mine water depth. By employing parameter values in Table 4.1, Ra is equal to 1.99×10^9, which is lower than $Ra_c = 3.44 \times 10^{11}$. Therefore, diffusion is predominant in the DDC process. This is realistic because if convection is dominant, temperature and salinity in a shaft will mix very quickly and merge into one layer with almost constant temperature and salinity, (e.g., considering temperature only in an inclined shaft (Bao and Liu 2016)). Therefore, thermohaline stratifications may disappear very quickly or even not be observed in the DDC process if convection is dominant.

Though thermohaline stratifications can be successfully reproduced (see Figure 5.2), the mechanisms for their formation and evolution are little understood. To provide more insights into thermohaline stratifications, we will discuss six critical issues in the following for better understanding the mechanisms behind the thermohaline stratification and its influential factors. The buoyancy ratio $N = 1.26$ was thoroughly used in the following simulation except for Section 5.3.4. Since the structures of temperature and salinity layers are identical (see Figure 5.2), we will primarily present simulation results for temperature. The results for salinity are shown if necessary. Also, no lateral salinity flux is applied to the lateral boundaries, i.e., we only consider the lateral heat flux (see boundary conditions in Section 4.2.3).

5.3 Influence of Effective Thermal Diffusivity

The simulated thermohaline stratifications in Figure 5.2 were obtained when Ra_T is equal to 3.19×10^6 and the corresponding effective thermal diffusivity α_{eff}^T is equal to 4.93e-4 m^2/s. It is also known in Section 4.1 that diffusion is predominant in the dynamic DDC process to reproduce thermohaline stratifications. The effective thermal diffusivity α_{eff}^T is a key transport parameter in heat diffusion. The influence of α_{eff}^T on thermohaline stratifications is thus investigated in this section. For the purpose, α_{eff}^T varies only and all other conditions remain unchanged.

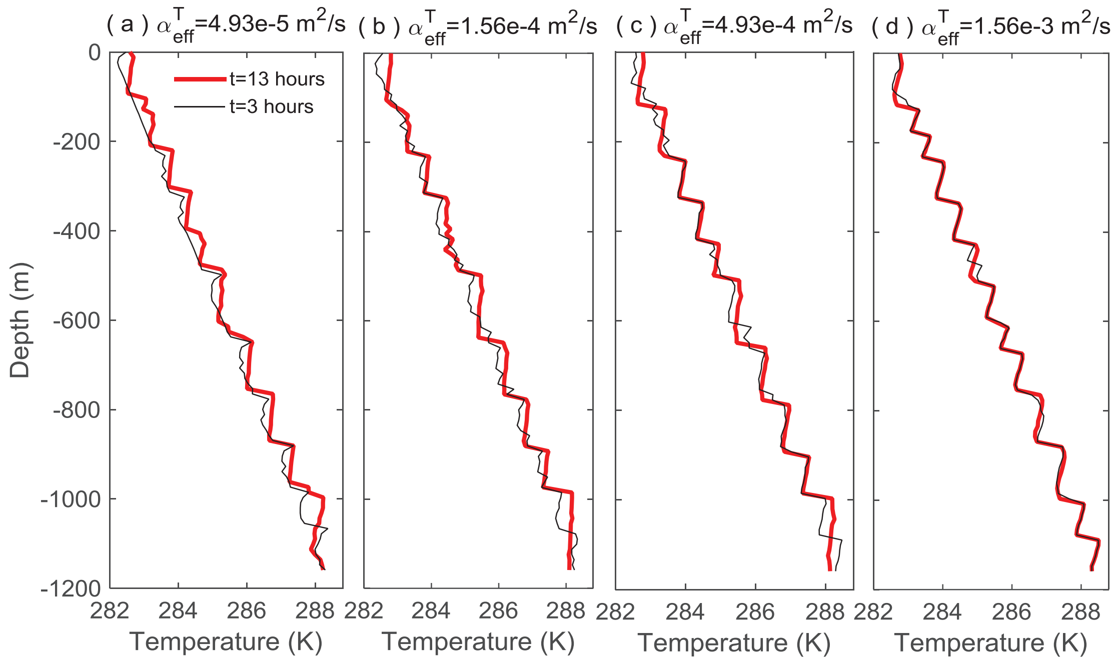

Figure 5.3. Formation of temperature layers under different α^T_{eff} at different times. Corresponding thermal Rayleigh number Ra_T is equal to (a) 3.19×10^7, (b) 1.01×10^7, (c) 3.19×10^6, and (d) 1.01×10^6.

The formation of thermohaline stratifications differs under different values of α^T_{eff}, as shown in Figure 5.3. At *t*=3 hours, no layers can be observed when α^T_{eff} is equal to 4.93e-5 m^2/s (Figure 5.3a). At the same calculation time, almost no layers form when $\alpha^T_{eff}=1.56\text{e-}4$ m^2/s (Figure 5.3b). However, it can be clearly seen that about six layers form when $\alpha^T_{eff}=4.93\text{e-}4$ (Figure 5.3c) and more layers (about thirteen) can be clearly observed when α^T_{eff} further increases to 1.56e-3 m^2/s. At *t*=13 hours, layers can be clearly seen in all considered cases with different values of α^T_{eff}. Therefore, the effective thermal diffusivity influences the formation of layers in determining the speed to form layers. The higher the effective thermal diffusivity, the faster the formation of layers.

5.4 Influence of Effective Kinematic Viscosity

The effective kinematic viscosity ν_{eff} is another key transport parameter to influence both heat and salt convections in the dynamic DDC process by determining the speed of fluid movement. In this section, we investigate the influence of ν_{eff} on thermohaline stratifications by only modifying the value of ν_{eff}.

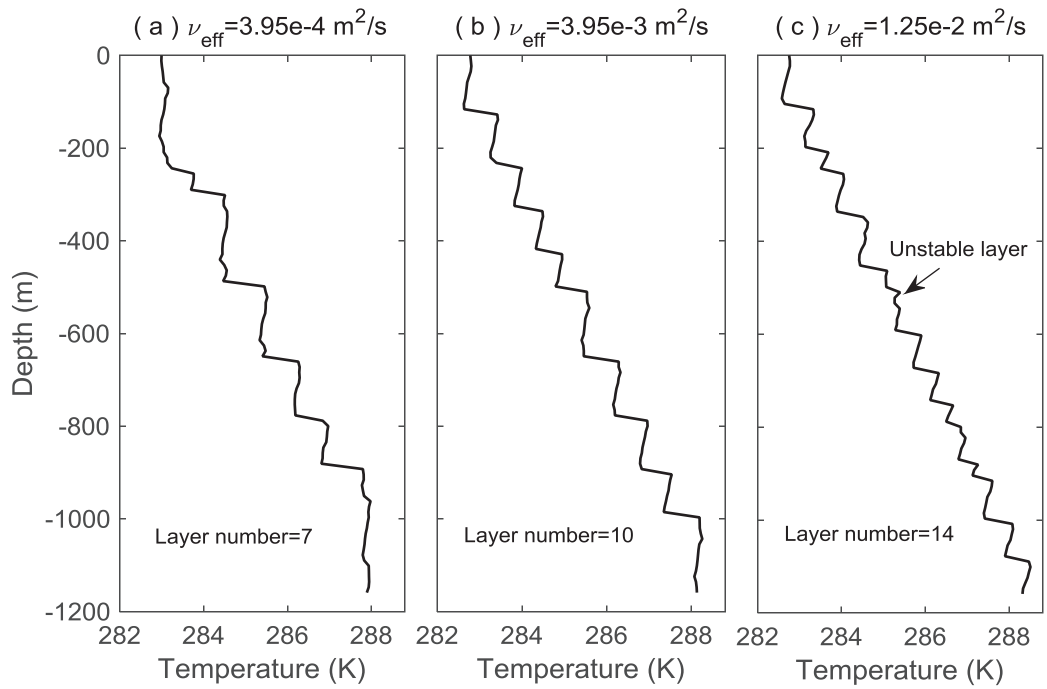

Figure 5.4. Temperature layers under different values of ν_{eff} at t=13 hours.

Simulated thermohaline stratifications are significantly different under different values of ν_{eff}, as shown in Figure 5.4,. At the same calculation time, there are seven layers when $\nu_{eff} = 3.95\text{e-}4$ m^2/s (Figure 5.4a), while ten and fourteen layers can be observed when ν_{eff} is equal to 3.95e-3 m^2/s (Figure 5.4b) and 1.25e-2 m^2/s (Figure 5.4c), respectively. There is an unstable layer in Figure 5.4c, because the layer-merging happens at that location, which will be discussed in Section 4.2.3. Therefore, the layer number decreases with the increase of ν_{eff}. The reason is that a higher ν_{eff} provides a large resistance of moving fluids, therefore, convection becomes less significant. Due to this reason, the speed to mix temperature and salinity in the layer-merging process becomes slower, leading to a larger layer number.

The observations in Figure 5.4 imply that ν_{eff} significantly influences the speed of the layer-merging. According to Wolkersdorfer (2008), layers observed from flooded mines can relatively remain for a long time. In fact, the observations in Figure 5.4 can provide a possible reason for the above observed phenomenon. Because ν_{eff} may not a constant and can increase to a very high value, layers merge very slowly and thus can remain for a long time. This can be confirmed by the simulation results of a simple example via increasing the value of ν_{eff}. Figure 5.5a shows the comparison of layers obtained at different times under the same $\nu_{eff} = 3.95\text{e-}3$ m^2/s. The number layer decreases from nine to six during the calculation period from 1 day to 2.5 days. However, the layer number remains unchanged when ν_{eff} increases from 3.95e-3 m^2/s to 1.25e-2 m^2/s, as shown in Figure 5.5b. The slim black line (i.e., t=1 day) was obtained when m^2/s $\nu_{eff} = 3.95\text{e-}3$ m^2/s, which serves as the initial condition for the situation when $\nu_{eff} = 1.25\text{e-}2$ m^2/s. Therefore, increasing the value of ν_{eff} can significantly slow down the layer-merging process and make the layers remain for a long time.

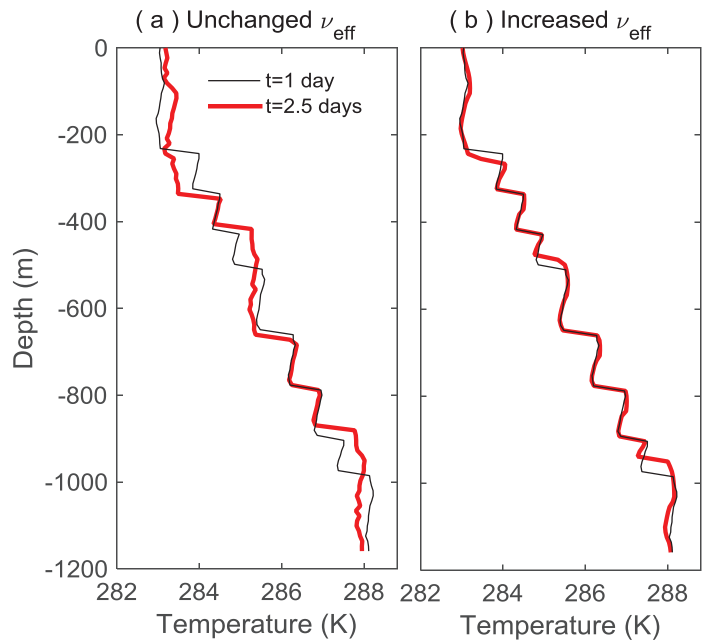

Figure 5.5. Comparisons of temperature layers: (a) unchanged $\nu_{eff} = 3.95\text{e-}3$ m^2/s and (b) increased ν_{eff} from $3.95\text{e-}3$ m^2/s to $1.25\text{e-}2$ m^2/s. The slim black line at t=1 day was obtained in this figure when $\nu_{eff} = 3.95\text{e-}3$ m^2/s, which serves as the initial condition for the situation in (b) when ν_{eff} increases to $1.25\text{e-}2$ m^2/s.

5.5 Influence of Diffusivity Ratio

In addition to the effective thermal diffusivity and the effective kinematic viscosity, the effective solutal diffusivity α_{eff}^{S} is also important transport parameter, which determines the strength of salinity diffusion. Therefore, the influence of α_{eff}^{S} on thermohaline stratifications deserves to understand. Due to the existence of both heat and salt diffusions in the system, it is more helpful to indirectly investigate the influence of α_{eff}^{S} by discussing the influence of the diffusivity ratio (heat/solute) $\lambda = \alpha_{eff}^{T} / \alpha_{eff}^{S}$ on thermohaline stratifications. According to the literature for DDC modeling in oceans (Carpenter et al. 2012; Radko et al. 2014), the value of λ should be lower than 1.0 (i.e., heat diffuses faster than salt). Therefore, in this section, we investigate the influence of λ whose value is lower than 1.0. For the purpose, α_{eff}^{T} remains unchanged while λ varies.

Though not significant, the diffusivity ratio λ influences thermohaline stratifications. Figure 5.6 demonstrates the comparisons of temperature layers obtained at the same calculation time using four different values of λ, i.e., 1/6, 1/50, 1/250, and 1/1000. As can be seen that the layer number increases from eight to nine when λ decreases from 1/6 to 1/50. The layer number remains unchanged (i.e., nine) when $\lambda = 1/250$. There is an unstable layer in Figure 5.6b and Figure 5.6c because of the layer-merging. The layer number further increases to ten when $\lambda = 1/1000$. This implies that the diffusivity density ratio influences the development of layers in controlling the speed of the layer-merging process for determining the layer number.

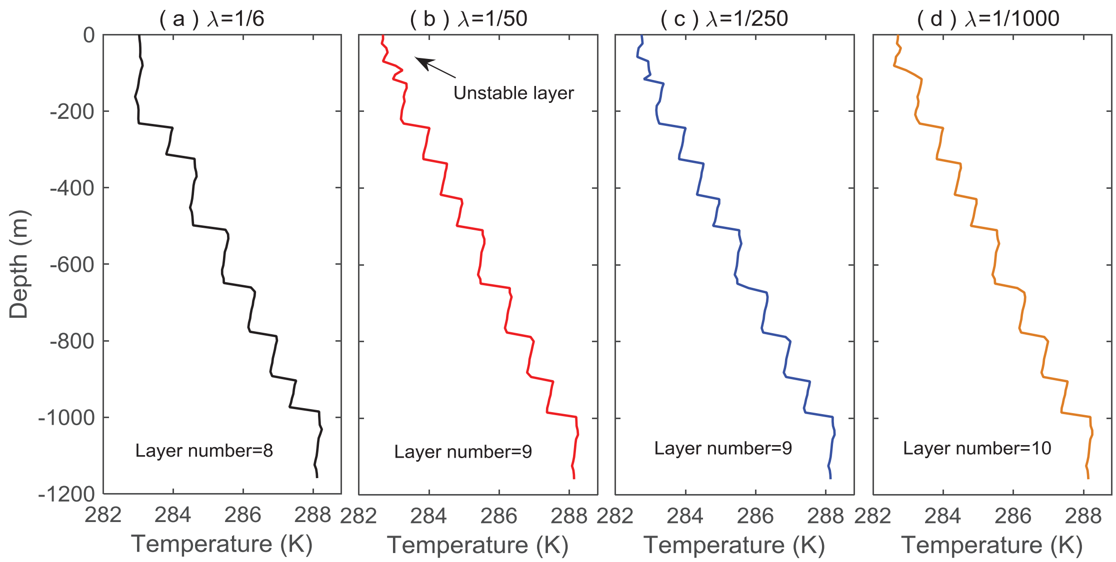

Figure 5.6. Comparisons of temperature layers without considering the lateral salinity flux under different diffusivity ratios at *t*=16 hours.

5.6 Mechanisms for the Layer-Merging

The layer-merging is a special feature in the evolution of thermohaline staircases in oceans (Radko et al. 2014). Such a feature is also distinct and can be observed in the evolution of thermohaline stratifications in the mine water (see Figure 5.1). However, the mechanisms behind the layer-merging in the mine water are rarely understood. The purpose of this section is to provide insights into the mechanisms behind the layer-merging in large bodies of mine water.

For this purpose, since the scale of the mine water is very large, it is helpful to focus on the evolution of thermohaline stratifications and their corresponding flow patterns simultaneously in a small elevation range. Figure 5.7 presents the layer-merging development at different times in the elevation range between -875 m and -1159.2 m. It is seen in Figure 5.7a that there are three clear layers in this range at t=300 min. Water circulates in each layer and the water velocity is very small (around 7e-9 m/s) at the interface between adjacent layers. When the layer-merging tends to start at t=306 min, water movement breaks the interface of Layer 1 and Layer 2, as shown in Figure 5.7b. The warm and salty water in Layer 1 moves up to Layer 2 that has the relatively cold and fresh water. Since the water velocity at this interface is still small (below 0.02 m/s), there are no significant changes for the temperature and salinity distributions at t=306 min. However, this interface is already broken up, temperature and salinity within Layer 1 and Layer 2 will mix gradually due to convection. Therefore, this interface is eroded (Figure 5.7c) and gradually disappear to form a new layer with a larger thickness (Figure 5.7d). It is also seen in Figure 5.7c that Layers 1 and 2 are eroded along the horizontal direction, which matches the way of the "B-mode" for merging layers according to the classification of the layer-merging mode (Radko et al. 2014; Radko 2007). Therefore, the "B-mode" is the dominant layer-merging type in the mine water. It also can be seen that the merging process of Layers 1 and 2 does not hurt the interface of Layers 2 and 3 because its location and the thickness of Layer 3 almost remain unchanged, as shown in Figure 5.7c and Figure 5.7d.

(a) t = 300 min

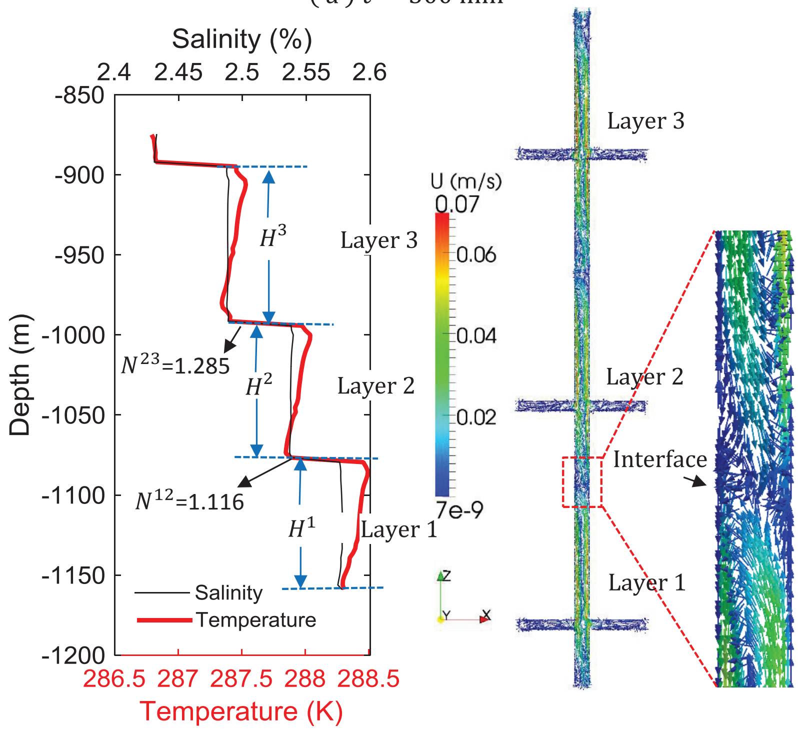

(b) t = 306 min

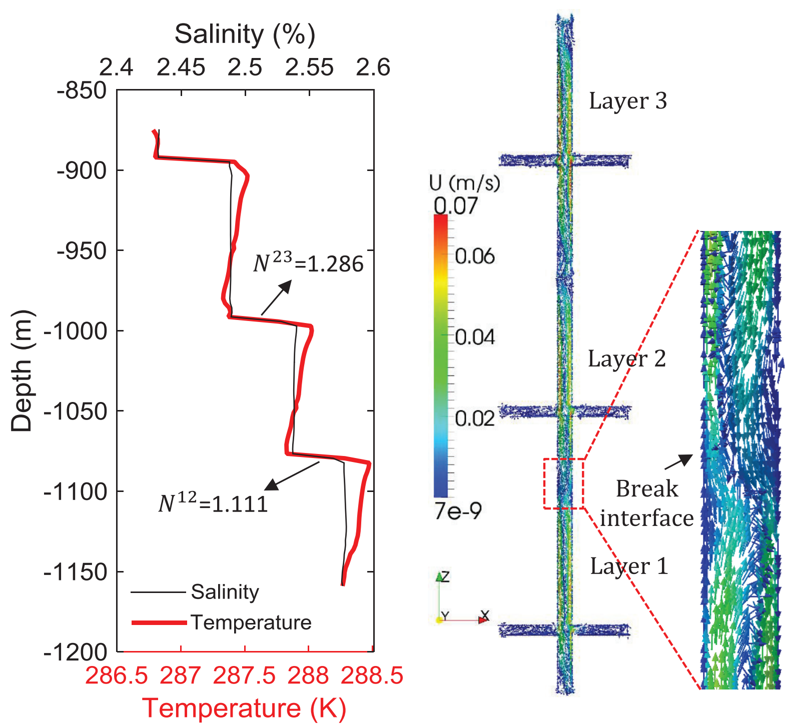

(c) t = 360 min

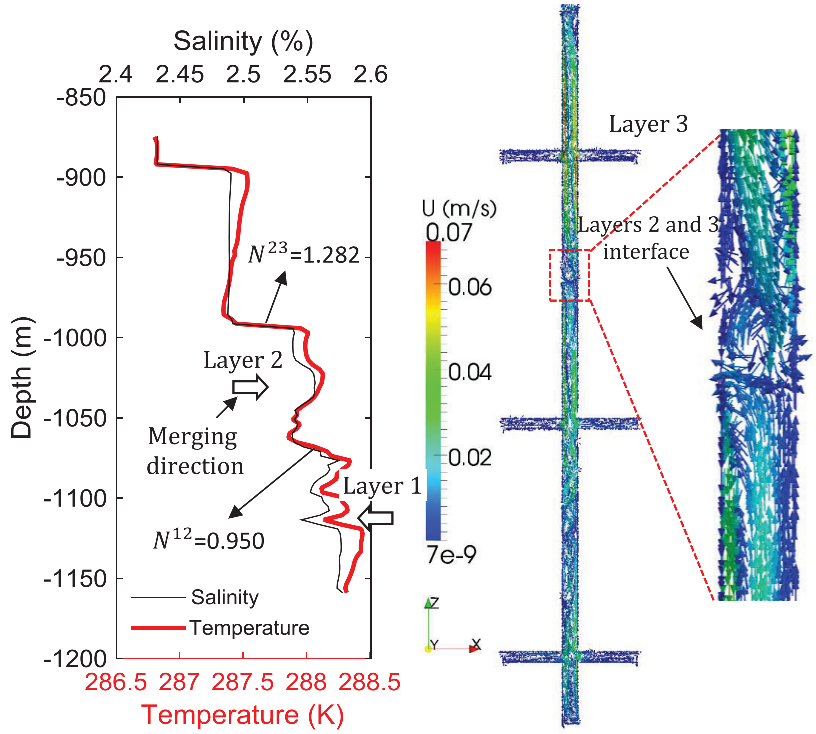

(d) t = 615 min

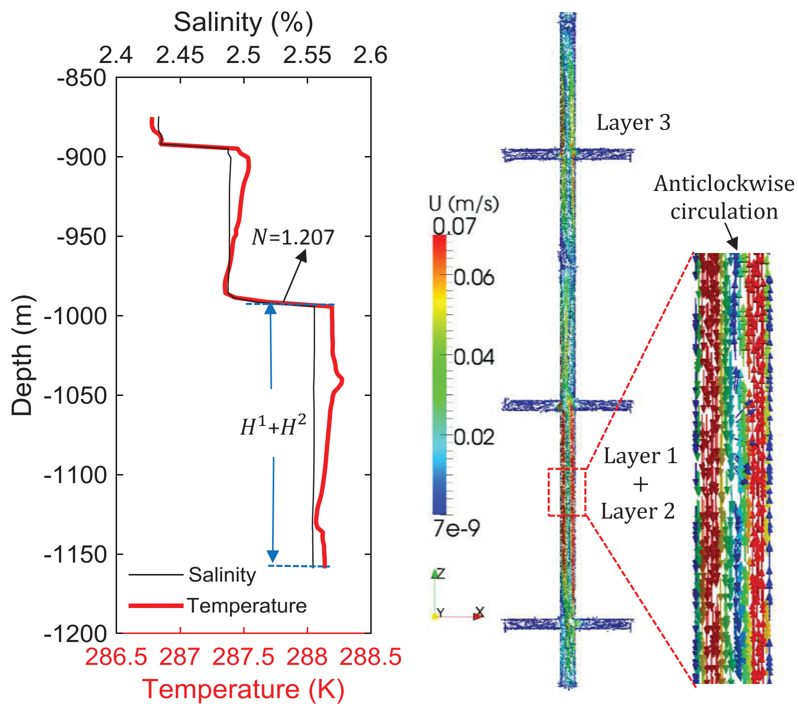

Figure 5.7. Layer-merging process in the evolution of thermohaline stratifications and their corresponding flow patterns when the time is equal to (a) 300 min, (b) 306 min (c) 360 min, and (d) 615 min. The thermohaline stratifications and their corresponding flow patterns were obtained in the elevation range between -875 m and -1159.2 m.

The mechanisms of the layer-merging in mine water in Figure 5.7 are suspected to be similar to the layer-merging theory for thermohaline staircases in oceans. According to the layer-merging theory in oceans (Radko 2007), the layer-merging by erosion of "weak interfaces" occurs when the vertical buoyancy flux decreases with the buoyancy variation across those "weak interfaces". This theory indicates that the variation of the difference in the buoyancy force across an interface between adjacent layers determines if such an interface will be eroded or not. In the dynamic DDC process of the mine water, the difference in the buoyancy force across an interface is determined by the buoyancy ratio that controls the process of convection to mix temperature and salinity. For each two adjacent layers, there are a difference in the buoyancy force between them and a buoyancy ratio across an interface between them. If that buoyancy ratio decreases, the salinity difference between these two layers decreases, which reduces the suppression caused by the salinity difference for the thermal convection. As a result, the buoyancy force difference between these two layers decreases. Therefore, the variation of the buoyancy ratio N across an interface of Layers 1 and 2 triggers the layer-merging in the mine water.

To further illustrate the variation of the buoyancy ratio during the layer-merging process, we calculate the buoyancy ratios across interfaces of Layers 1 and 2 (i.e., N^{12})

and Layers 2 and 3 (i.e., N^{23}) using Eq. (4.7) based on the average values of temperature and salinity within the thickness of each layer, i.e., H^1, H^2 and H^3 for Layers 1, 2 and 3 respectively, as shown in Figure 5.7a. The thickness of Layer 1 and Layer 2 will change (see Figure 5.7c) during the layer-merging. In the calculation, the average values of temperature and salinity in Layers 1 and 2 were still calculated based on their original H^1 and H^2. The buoyancy ratios across the interfaces of adjacent layers in Figure 5.7a are $N^{12} = 1.116$ and $N^{23} = 1.285$, respectively. Because of $N^{23} > N^{12}$, the interface of Layers 1 and 2 is the "weak interface" that will be eroded first. This explains why the layer-merging process does not hurt the interface of Layers 2 and 3 in Figure 5.7. At t=360 min, $N^{12} = 0.950$ and its decreasing percentage is about 14.9%. N^{12} further decreases during the layer-merging process, which can be clearly seen in Figure 5.8. N^{12} significantly decreases with time. It is also seen that N^{23} slightly decreases. This is because the temperature and salinity in Layer 2 will increase during the layer-merging of Layers 1 and 2, while the temperature and salinity in Layer 3 almost remain unchanged. However, the decrease in N^{12} is more significant than that in N^{23} because the interface of Layers 1 and 2 is more "weak". Therefore, this "weak interface" is eroded and disappear first. The results in Figure 5.7 and Figure 5.8 infer that the buoyancy ratio N dominates the layer-merging. The smallest N corresponds to the most "weak interface". Such an interface will be eroded first because its corresponding N decreases significantly.

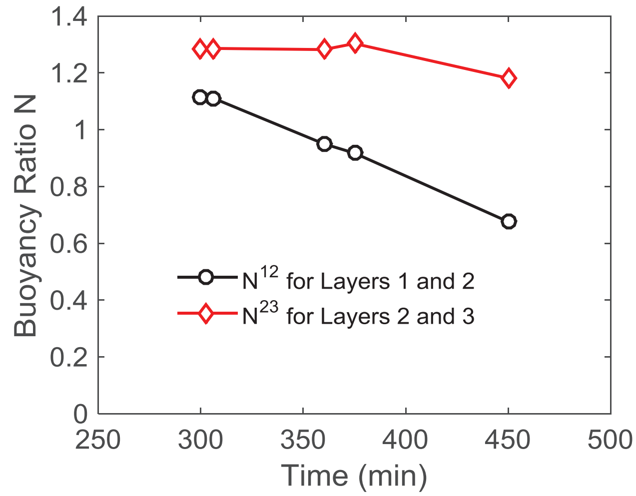

Figure 5.8. Variations of the buoyancy ratio with time across the interfaces during the layer-merging process.

5.7 Effect of Buoyancy Ratio

The buoyancy ratio determines the layer-merging as introduced in Section 5.6 and also controls the heat and mass transport in the vertical direction. The effect of the buoyancy ratio on thermohaline stratifications is significant and investigated in this section. To consider such an effect, ΔT (i.e., 6.2 K) and S_t (i.e., 2%) remain unchanged while S_t varies to obtain three different values of *N*, i.e., 1.26, 2, and 4.

Different observations are obtained in the structure of layers when the buoyancy ratio is different, as shown in Figure 5.9. At the same calculation time, the number of layers increases with the increase of the buoyancy ratio. However, the smaller the buoyancy ratio, the larger the thickness of layers. This is because the process of the layer-merging with a high buoyancy ratio is much slower than that with a low buoyancy ratio, leading to a larger number of layers with a smaller thickness. Therefore, the process of the layer-merging event is very slow with a high buoyancy ratio. This fact gives another possible explanation, in addition to the effective kinematic viscosity in Section 5.4, for the field observation that layers remain relatively stable for years. That is, because of a high buoyancy ratio, the layer-merging process in large bodies of mine water is very slow. Observations presented in Figure 5.9 reveal the key mechanism underlying the occurrence of thermohaline stratifications with different thicknesses: the buoyancy ratio effect.

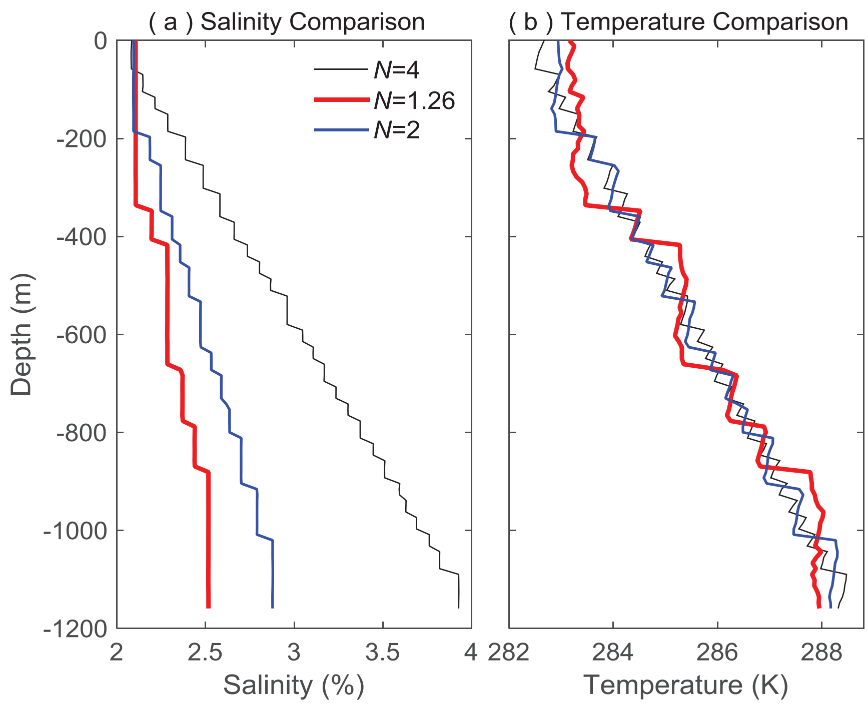

Figure 5.9. Effect of the buoyancy ratio on the evolution of stratifications at t=2.5 days: (a) salinity comparison and (b) temperature comparison.

5.8 Possibility of Predicting Initial Temperature and Salinity Conditions

Field observations from flooded mines showed that temperature and salinity of the mine water in those mines are already stratified into different layers (Wolkersdorfer 2008). However, it is still uncertain how can we exactly reproduce the field observed thermohaline stratifications (e.g., temperature value and temperature difference location), so that we can predict their future development. It is incorrect to directly define the stratified temperature and salinity as the initial conditions for reproducing the observed layers. This is because the true boundary conditions are unknown, therefore, the reproduced layers based on the initially stratified temperature and salinity will not develop in a realistic way. The most feasible way for solving the above uncertainty is first to analyze observed layers (i.e., temperature and salinity) and then obtain the initial distributions of temperature and salinity based on the observed data. With the initial distributions, we can identically reproduce the observed layers to its current status and predict their future development. Therefore, the accurate prediction of the initial distributions of temperature and salinity is a key step. Therefore, in this section, we propose a method to predict the initial linear distributions of temperature and salinity.

The method is that we predict the initial distributions by back-calculating the values of temperature and salinity picked from the existing layers in the measurements. Figure 5.10 presents the detail of the method regarding data pick-up and calculation of temperature and salinity from observed layers. For each layer and interface, the coordinates of their centers are calculated using the equation presented Figure 5.10. The center coordinates of layers and interfaces correlate the depth and temperature or salinity. Therefore, the information is involved in the later accurate prediction of the initial distributions. The number of the centers is a sum of the layers and interfaces. This number, i.e., all the centers from layers and interfaces, then will be utilized to predict the initial distributions based on the linear regression.

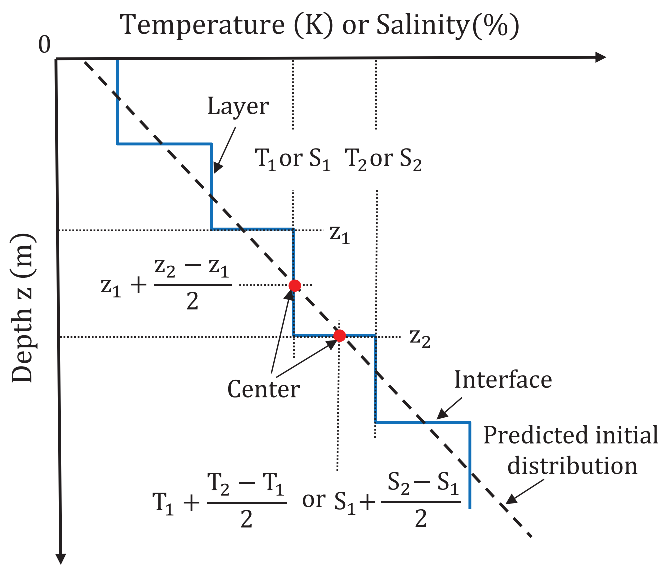

Figure 5.10. Schematic of illustrating data pick-up and calculation of temperature and salinity from the existing layers.

To evaluate the proposed method, we consider three cases shown in Figure 5.11 with different layer numbers. The cases correspond to *t*=25 hours (Case 1), 2.5 days (Case 2), and 4.5 days (Case 3) and their layer numbers are nine, six, and three, respectively. This consideration was due to the fact that the existing layers are still in the dynamic process and thus could have different numbers. The coordinates of the centers of each layer and interface in each case were calculated based on the equation in Figure 5.11. The initial distributions of temperature and salinity that were used to obtain the cases in Figure 5.11

were treated as the true distributions, which will be compared with the predicted distributions using the proposed method. The linear least squares approach was used for the linear regression.

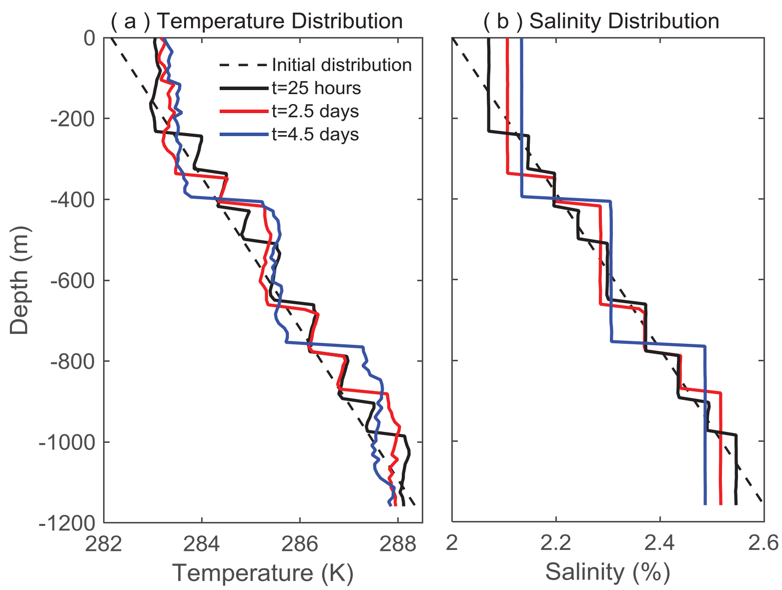

Figure 5.11. Three cases with different layer numbers for the prediction of the initial distributions.

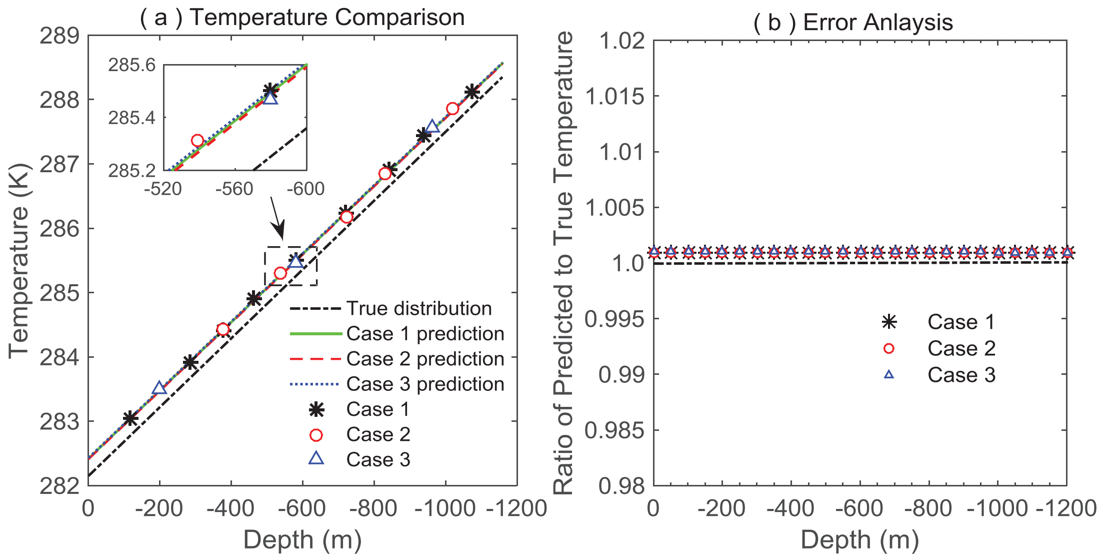

Figure 5.12. Predictions of the initial temperature distribution: (a) temperature comparison and (b) error analysis.

The predicted initial temperature distributions are in good agreement with the true distributions, as shown in Figure 5.12a. The predictions for Cases 1, 2 and 3 highly coincide. The difference between the predicted and true temperature is about 0.2 K at a certain depth. The error analysis presented in Figure 5.12b further proves that the error of the predictions is very small. The ratios of the predicted to true temperatures are almost equal to 1.0 for all cases. The initial salinity distributions can also be accurately predicted with the proposed method. As can be seen in Figure 5.13a, the predictions for the three cases almost overlap the true distribution, especially those of Case 1 and Case 2. The error analysis shown in Figure 5.13b also indicates that the salinity predictions are highly accurate for Cases 1 and 2, in which their ratios of the predicted to true salinity are very close to 1.0. Though there is a difference in the salinity prediction of Case 3, this difference is negligible because the ratio difference is less than 0.025, as shown in Figure 5.13b. The results in Figure 5.12 and Figure 5.13 confirmed the feasibility of predicting the initial distributions of temperature and salinity and also proved the high reliability and accuracy of utilizing the proposed method for their predictions. Based on the predictions, the current status of the observed layers can be reproduced with a high accuracy to predict the future development of the layers.

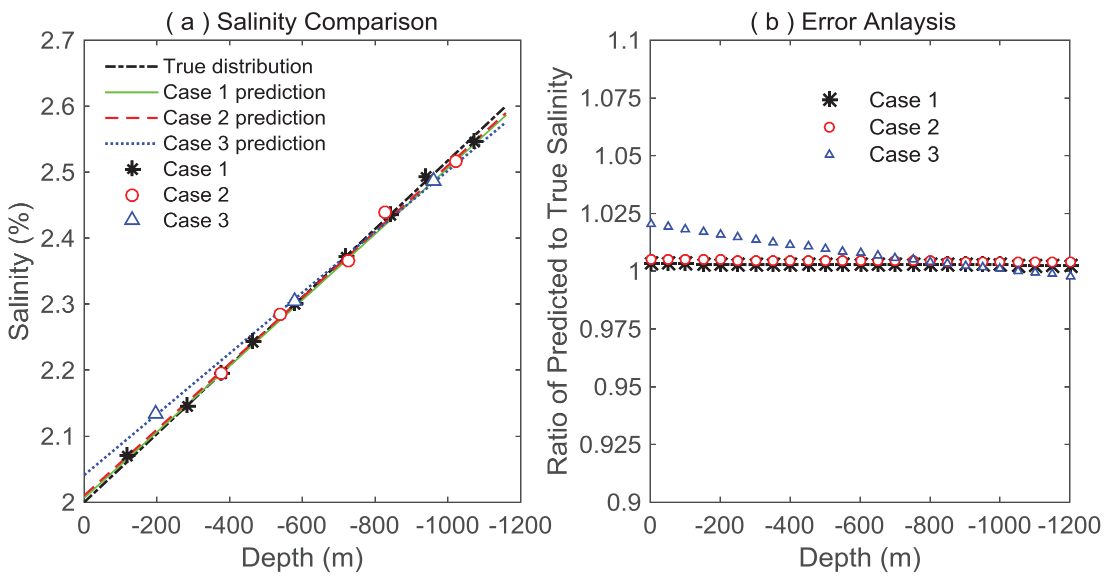

Figure 5.13. Predictions of the initial salinity distribution: (a) salinity comparison and (b) error analysis.

5.9 Conclusions

Thermohaline stratifications observed in the natural large-scale mine water reservoir system have been little understood. The thermohaline stratification is the primary physical mechanism to determine the temperature distributions and variations, which is thus critical to the mine water-based geothermal application. However, no research has been reported on providing the in-depth understanding of the formation and development of thermohaline stratifications. This chapter presents such a study based on non-isothermal and non-isosolutal hydrodynamics for a real vertical shaft filled with water to provide critical insights into thermohaline stratifications.

The evaluation of the heat and solute transport (i.e., diffusion or convection) demonstrated that diffusion is predominant in the dynamic DDC process when thermohaline stratifications form. The occurrence and evolution of thermohaline stratifications are significantly influenced by transport parameters. The effective thermal diffusivity influences the formation of layers via affecting the speed to form layers. The higher the effective thermal diffusivity, the faster the formation of layers. After layers form, the layer-merging is a distinct feature that can be observed in the dynamic DDC process. The speed of the layer-merging is affected by both the effective kinematic viscosity and the diffusivity ratio via influencing the speed of the layer-merging.

In the layer-merging process, not all the layers merge simultaneously by the erosion of their interfaces. In fact, "weak interfaces" are eroded and disappear first. These interfaces are "weak" as the buoyancy ratios across them are smaller than those of not "weak" ones. The major reason for the layer-merging was found that the buoyancy ratios across those "weak interfaces" significantly decrease. Though the buoyancy ratios across those not "weak interfaces" also decrease, the reduction in the buoyancy ratios of those "weak interfaces" is more significant. Therefore, "weak interfaces" are eroded and disappear first.

The simulation results also revealed that the buoyancy ratio has a significant effect on the evolution of stratifications. The number of layers increases with the increase of the buoyancy ratio. However, the smaller the buoyancy ratio, the larger the thickness of layers. Therefore, the buoyancy ratio effect is the key mechanism for the formation of stratifications with different thicknesses. This effect also helps explain why stratifications from field measurements remain relatively stable for years.

The prediction of the initial distributions of temperature and salinity is a key step to answer “how can we exactly reproduce the observed thermohaline stratifications?” We addressed this key step by proposing a method to accurately predict the initial distributions. The evaluation results confirmed the feasibility of the predictions and also proved the high reliability and accuracy of utilizing the proposed method for the predictions.

The insights discussed in this chapter provide critical scientific bases for understanding this natural large-scale mine water reservoir system, which is of practical significance to the mine water-based geothermal applications. Further work on th evaluation of heat extraction from the mine water involving realistic thermohaline stratifications for the optimal design of this geothermal application can be carried out based on the knowledge gained in this chapter.

6 Summary and Future Work

6.1 Summary and Conclusion

In this dissertation, an investigation with multiphysics numerical analysis was conducted on the basis of geology, field study, energy reserve estimate and a demonstration project to understand the heat and mass transport in the large-scale natural mine water-geologic formation system for guiding and optimizing the large-scale application of geothermal energy recovery from flooded mines. For the purpose, four specific investigations were presented: (1) reporting an site exploration, the geologic and field conditions, energy reserve estimations, a demonstration project, and lessons learned from the demonstration project of a study on the large-scale geothermal application from deep abandoned copper mines; (2) providing the scientific understanding of the natural mine water-geologic formation system, especially the transport of heat and mass in this large-scale natural system; (3) addressing a key scientific myth that remains little understood in the past three decades: the layering phenomenon observed in flooded mines; and (4) providing insights into thermohaline stratifications by investigating six critical issues.

The main contributions and findings for the key chapters (Chapters 2 to 5) are summarized as follows:

Chapter 2. Site Geology, Site Exploration, and Demonstration Project

Three major components, relevant geologic information, i.e., properties of representative rocks, faults and fissures and underground hydrology, the site exploration and its energy reserve estimation, and a real project demonstration, were presented to provide a complete background and preliminary results for understanding the recovery of the geothermal energy from the deep abandoned mines in the site. The results indicated that there is a great amount of thermal energy potential stored in the Quincy mine in the U.P., which can be used for geothermal applications.

Data from the demonstration project indicated that house heating with this renewable energy could be the second most economical heating option in very economically favorable conditions. As for the large-scale mine water-geologic formation system, the analysis for the renewability of the energy revealed that the thermal energy recharge to the mine water is very significant, and thus, cannot be neglected. Energy reserve and economic analyses considering the renewability of the energy concluded that a typical deep mine has the potential to provide energy comparable to a small-scale power station.

The effort of this chapter is of great significance because it not only proved the feasibility of recovering geothermal energy from deep abandoned mines in the U.P., but set up a paradigm in the U.S. for recovering geothermal energy from abandoned mines in other mining areas. It is the first time that the economic value of this energy renovation is validated by comparing to other heating options based on a large-scale demonstration project and that the high power of this type of low-enthalpy geothermal energy reservoir is investigated and reported for deep mines.

Chapter 3. Heat Potential Evaluation and Understanding of Heat Transfer Mechanisms

Three essential components for understanding the physical processes involved in the geothermal application of the mine water were introduced: a field study, a theoretical framework, and numerical simulations. The field study yielded measurements of temperatures, electrical conductivity, and chemical concentrations in a local mine shaft in the U.P. The main purpose is to understand the key scientific issue in the use of the mine water as a geothermal resource, i.e., the temperature distribution in the mine water. The theoretical framework development provided a mathematical description for the thermo-hydrodynamic process in the mine water coupled with the heat transfer in the surrounding geologic formations for studying the scientific issue. Simulations were conducted to preliminarily investigate the quasi-equilibrium water movement in the mine shaft due to geothermal gradients to shed light on the phenomena observed in the field study.

The simulation based on the proposed framework provided explanations to the data obtained in the field from a scientific perspective, which is of practical meaning to the success of this energy renovation with water in deep mines. No research is reported prior to the current study to include the comprehensive information as detailed in this study. This study fills this gap with simulations accompanied by field studies on the same deep flooded mine shaft, a pioneering one in the United States. Also, a theoretical framework for the mine water-surrounding geologic formation system has been successfully implemented to test a realistic case. Serving as a solid cornerstone, this study will be further continued for a scientific understanding to help predict the efficiency and sustainability of the energy exploration from abandoned underground mines using the mine water as a safe, green, relatively renewable and adaptable geothermal resource.

Chapter 4. Double-Diffusive Convection Simulating of Thermohaline Stratification

The multiphysics simulation with unique non-isothermal and non-isosolutal hydrodynamics succeeded in explaining the mechanism of heat and mass transfer in the DDC process and reproducing the key phenomenon regarding thermohaline stratifications observed from field measurements. It was found that intrusions by lateral temperature and salinity gradients can lead to thermohaline stratifications in the large-scale mine water with initially linear distributions of temperature and salinity. The layer-merging even is involved in the evolution of stratifications. Some of the small layers gradually merge to form layers with a larger thickness, leading to a decrease in the number of layers.

To successfully reproduce thermohaline stratifications, the lateral salinity flux is a not required condition. In contrast, the lateral heat flux is necessary. A difference in lateral heat fluxes is also required for successfully simulating thermohaline stratifications. Thermohaline stratifications can form as long as the lateral heat flux with a difference is considered. The simulation results revealed that this difference significantly influences the development of thermohaline stratifications. A higher difference, a smaller the number of layers.

No research has been reported prior to the current chapter on presenting these significant insights and explaining the formation and evolution of thermohaline stratifications. It is the first time, to the best of our knowledge, that thermohaline stratifications in the large-scale subterranean water bodies have been successfully reproduced. It is believed that this scientific breakthrough is significant and valuable for future recovering geothermal energy via the mine water from abandoned mines in an efficient, sustainable and economical way.

Chapter 5. Critical Insights into Thermohaline Stratifications

Critical insights into the heat and mass transport mechanism of thermohaline stratifications were provided. The evaluation of the heat and solute transfer type demonstrated that diffusion is predominant in the dynamic DDC process when thermohaline stratifications form. The formation and evolution of thermohaline stratifications are significantly influenced by transport parameters. The effective thermal diffusivity influences the formation of layers via affecting the speed to form layers. The higher the effective thermal diffusivity, the faster the formation of layers. After layers form, the layer-merging is a distinct feature that can be observed in the dynamic DDC process. The speed of the layer-merging is affected by both the effective kinematic viscosity and the diffusivity ratio via influencing the speed of the layer-merging.

In the layer-merging process, not all the layers merge simultaneously by the erosion of their interfaces. In fact, "weak interfaces" are eroded and disappear first. These interfaces are "weak" as the buoyancy ratios across them are smaller than those of not "weak" ones. The major reason for the layer-merging was found that the buoyancy ratios across those "weak interfaces" significantly decrease. Though the buoyancy ratios across those not "weak interfaces" also decrease, the reduction in the buoyancy ratios of those "weak interfaces" is more significant. Therefore, "weak interfaces" are eroded and disappear first.

The simulation results also revealed that the buoyancy ratio has a significant effect on the evolution of stratifications. The number of layers increases with the increase of the buoyancy ratio. However, the smaller the buoyancy ratio, the larger the thickness of layers. Therefore, the buoyancy ratio effect is the key mechanism for the formation of stratifications with different thicknesses. This effect also helps explain why stratifications from field measurements remain relatively stable for years.

The prediction of the initial distributions of temperature and salinity is a key step to answer "how can we exactly reproduce the observed thermohaline stratifications?" We addressed this key step by proposing a method to accurately predict the initial distributions. The evaluation results confirmed the feasibility of the predictions and also proved the high reliability and accuracy of utilizing the proposed method for the predictions.

The insights discussed in this chapter provide critical scientific bases for understanding this natural large-scale mine water reservoir system, which is of practical significance to the mine water-based geothermal applications.

6.2 Future Work

This dissertation has provided in-depth understanding for the large-scale natural mine water-geologic formation system, especially the heat coupling in the natural mine water-geologic formation system and the heat and mass transport mechanisms of the layering phenomenon (i.e., thermohaline stratifications). Despite the progress made in this dissertation, the state of the art of the current study can still be further advanced in the following aspects.

First, for the thermal coupling between the mine water and the surrounding geologic formation system, the influences of the ongoing flooding process from groundwater and the intrusion through the connected drifts from adjacent mines on mine water movement are not considered. Therefore, further research can be carried out to assess such influences.

Second, complicated underground mine geometries (such as drifts and fissures) are not included in the natural mine water-geologic formation system, which may affect thermohaline stratifications by influencing mine water flow directions. Therefore, further work is needed to discuss the above influence by considering complicated underground mine geometries.

Third, strategies of heat extraction, e.g., target temperature layer and location of pump pipes, are not investigated. Therefore, further work should be placed on the evaluation of heat extraction from the mine water involving realistic thermohaline stratifications for the optimal design of this large-scale geothermal application in a sustainable and efficient way.

Fourth, 2D multiphysics simulations are conducted for modeling thermocline stratifications in this dissertation. As a result, effects of 3D multiphysics simulations are not little understood. Therefore, it is recommended to conduct 3D simulations of thermohaline stratification via double-diffusive convection for understanding the 3D effects.

7 Reference List

Williamson, K. H., Gunderson, R. P., Hamblin, G. M., Gallup, D. L., and Kitz, K. (2001). "Geothermal power technology." *Proceedings of the IEEE*, 89(12), 1783-1792.

Gallup, D. L. (2009). "Production engineering in geothermal technology: a review." *Geothermics*, 38(3), 326-334.

Kagel, A., Bates, D., and Gawell, K. (2005). *A guide to geothermal energy and the environment*, Geothermal Energy Association Washington, D.C.

Rybach, L. (2003). "Geothermal energy: sustainability and the environment." *Geothermics*, 32(4), 463-470.

Rybach, L., and Mongillo, M. (2006). "Geothermal sustainability-a review with identified research needs." *GRC Transactions*, 30, 1083-1090.

Mock, J. E., Tester, J. W., and Wright, P. M. (1997). "Geothermal energy from the earth: its potential impact as an environmentally sustainable resource." *Annual review of Energy and the Environment*, 22(1), 305-356.

Handbook, A. F. (2009). *American society of heating, refrigerating and air-conditioning engineers*, ASHRAE Research, Atlanta, GA, USA.

Lund, J. W. (1990). "Geothermal heat pump utilization in the United States." Geo-Heat Center, U.S. Department of Energy.

Lienau, P. J. (1997). "Geothermal heat pump performance and utility programs in the United States." *Energy Sources*, 19(1), 1-8.

Hepbasli, A., and Akdemir, O. (2004). "Energy and exergy analysis of a ground source (geothermal) heat pump system." *Energy Conversion and Management*, 45(5), 737-753.

Lund, J., Sanner, B., Rybach, L., Curtis, R., and Hellström, G. (2004). "Geothermal (ground-source) heat pumps-a world overview." *GHC Bulletin*, 25(3), 1-10.

Chiasson, A. D. (1999). "Advances in modeling of ground-source heat pump systems." MS, Oklahoma State University, Stillwater, OK, USA.

Jessop, A. M., MacDonald, J. K., and Spence, H. (1995). "Clean energy from abandoned mines at Springhill, Nova Scotia." *Energy sources*, 17(1), 93-106.

Rottluff, F. (1998). "Neue Warmepumpenanlage im Besucherbergwerk Zinngrube Ehrenfriedersdorf." *Geotermische Energie*, 21, 811.

Raymond, J., Therrien, R., and Hassani, F. (2008). "Overview of geothermal energy resources in Québec (Canada) mining environments." *Proc., 10th International Mine Water Association Congress: mine water and the environment. Technical University of Ostrava, Ostrava, Czech Republic*, IMWAC.

Behrooz, B. S., Elianne, D., and Jan-Jaap, V. B. (2008). "Geothermal use of deep flooded mines." *Proc., International Symposium on Post-Mining*, ISPM, 1-10.

Jessop, A. (1995). "Geothermal energy from old mines at Springhill, Nova Scotia, Canada."Nova Scotia, Canada, 463-468.

Watzlaf, G. R., and Ackman, T. E. (2006). "Underground mine water for heating and cooling using geothermal heat pump systems." *Mine Water and the Environment*, 25(1), 1-14.

Ghomshei, M., and Eng, P. (2007). "Geothermal energy from Con Mine for Heating the City of Yellowknife, NWT: A concept study." The University of British Columbia, Vancouver, Canada, 1-18.

Renz, A., Rühaak, W., Schätzl, P., and Diersch, H. (2009). "Numerical modeling of geothermal use of mine water: challenges and examples." *Mine Water and the Environment*, 28(1), 2-14.

Ramos, E. P., and Falcone, G. (2013). "Recovery of the geothermal energy stored in abandoned mines." *Clean Energy Systems in the Subsurface: Production, Storage and Conversion*, Springer, Goslar, Germany, 143-155.

Gammons, C. H., Snyder, D. M., Poulson, S. R., and Petritz, K. (2009). "Geochemistry and stable isotopes of the flooded underground mine workings of Butte, Montana." *Economic Geology*, 104(8), 1213-1234.

Malolepszy, Z. (2003). "Low temperature, man-made geothermal reservoirs in abandoned workings of underground mines." *Proc., Proceedings of the 28th workshop on geothermal reservoir engineering*, Stanford University, 259-265.

Barsuglia, F., and Garzonio, C. (2005). "The post-closure mine hydrogeological problems of Gavorrano (Italy)." *Proc., 9th International Mine Water Congress(IMWA 2005)*, International Mine Water Association, 147-155.

Burke, T. (2002). "The use in Scotland of flooded mine workings as a source of geothermal energy." *Geothermal Energy in Underground Mines*, 191-200.

Hall, A., Scott, J. A., and Shang, H. (2011). "Geothermal energy recovery from underground mines." *Renewable and Sustainable Energy Reviews*, 15(2), 916-924.

Wolkersdorfer, C. (2008). *Water management at abandoned flooded underground mines: fundamentals, tracer tests, modelling, water treatment*, Springer Science & Business Media, München, Germany.

Banks, D., Skarphagen, H., Wiltshire, R., and Jessop, C. (2003). "Mine water as a resource: space heating and cooling via use of heat pumps." *Land Contamination & Reclamation*, 11(2), 191-198.

Kotyrba, A., and Michalak, J. (1987). "Geothermal energy of the Upper Silesian Coal Basin and perspectives of its usage, in Polish." *Prace Komisji Nauk PAN, Branch in Katowicach*, 12, 193-195.

Malolepszy, Z., and Ostaficzuk, S. (1999). "Geothermal potential of the Upper Silesian Coal Basin, Poland." *Bulletin d'Hydroge'ologie, Editions Peter Lang, Université de Neuchatel*, 17, 67-76.

Wieber, G., and Pohl, S. (2008). "Mine water: a source of geothermal energy-examples from the Rhenish Massif." *Proc., 10th International Mine Water Association Congress: Mine Water and the Environment*, Citeseer, 1-4.

Malolepszy, Z., Demollin-Schneiders, E., and Bowers, D. (2005). "Potential use of geothermal mine waters in Europe." *Proc., Proceedings of the World Geothermal Congress*, World Geothermal Congress, 1-3.

Ordóñez, A., Jardón, S., Álvarez, R., Andrés, C., and Pendás, F. (2012). "Hydrogeological definition and applicability of abandoned coal mines as water reservoirs." *Journal of Environmental Monitoring*, 14(8), 2127-2136.

Tóth, A., and Bobok, E. (2007). "A prospect geothermal potential of an abandoned copper mine." *Proc., Proceedings of the 32nd Workshop on Geothermal Reservoir Engineering*, 13.

Ghomshei, M., and Meech, J. (2005). "Usable heat from mine waters: Coproduction of energy and minerals from" mother earth." *Intelligence in a Small Materials World*, 401-411.

Hamm, V., and Sabet, B. B. (2010). "Modelling of fluid flow and heat transfer to assess the geothermal potential of a flooded coal mine in Lorraine, France." *Geothermics*, 39(2), 177-186.

Hamm, V., Collon-Drouaillet, P., and Fabriol, R. (2008). "Two modelling approaches to water-quality simulation in a flooded iron-ore mine (Saizerais, Lorraine, France): a semi-distributed chemical reactor model and a physically based distributed reactive transport pipe network model." *Journal of contaminant hydrology*, 96(1), 97-112.

Reichart, G., Vaute, L., Collon-Drouaillet, P., and Buès, M. A. (2011). "Modelling heat and salinity related convective processes in deep mining flooded wells." *Proc., 11th International Mine Water Association Congress*, IMWA, 183-187.

Kories, H., Rüterkamp, P., and Sippel, M. (2004). "Field and numerical studies of water stratification in flooded shafts." *Proc., Proceedings International Mine Water Association Symposium*, IMWA, 149-159.

White, W. S. (1968). "The native-copper deposits of northern Michigan." *Ore deposits of the United States, 1933-1967*, American Institute of Mining, Metallurgy and Petroleum Engineers, New York, 303-325.

Bornhorst, T. J., and Barron, R. J. (2011). "Copper deposits of the western Upper Peninsula of Michigan." *Geological Society of America Field Guide 24*, 83-99.

Cannon, W. F. (1994). "Closing of the Midcontinent rift-A far-field effect of Grenvillian compression." *Geology*, 22(2), 155-158.

Bornhorst, T. J., and Williams, W. C. (2013). "The Mesoproterozoic Copperwood sedimentary rock-hosted stratiform copper deposit, Upper Peninsula, Michigan." *Economic Geology*, 108(6), 1325-1346.

Tardy, S. W. (2006). *Soil survey of Keweenaw County area, Michigan*, Natural Resources Conservation Service.

MNA (2010). "The secret behind the Copper Country's native deposits." <https://michigannature.wordpress.com/2010/07/15/the-secret-behind-the-copper-country%E2%80%99s-native-deposits/>. (2015.05.22).

Apple, B. A., and Reeves, H. W. (2007). "Summary of hydrogeologic conditions by county for the state of Michigan." Geological Survey (US), Reston, Virginia, USA.

GWMAP (2005). "Groundwater inventory and mapping project (GWMAP) & well viewer." Department of Environmental Quality (DEQ), U.S. Geological Survey (USGS) and Michigan State University (MSU), East Lansing, Michigan, USA.

Butler, B. S., and Burbank, W. S. (1929). *The copper deposits of Michigan*, US Government Printing Office.

Raymond, J., and Therrien, R. (2008). "Low-temperature geothermal potential of the flooded Gaspé Mines, Québec, Canada." *Geothermics*, 37(2), 189-210.

Van Orstrand, C. (1920). "Geothermal data of the United States." Department of the Interior, US Geol. Survey, Washington D.C., USA.

Muffler, P., and Cataldi, R. (1978). "Methods for regional assessment of geothermal resources." *Geothermics*, 7(2-4), 53-89.

Zhang, G., Zhu, J., Li, J., and Wang, Q. (2015). "The analytical solution of the water-rock heat transfer coefficient and sensitivity analyses of parameters." *Proc., Proceedings of the World Geothermal Congress*, World Geothermal Congress, 1-8.

Zheng, W., Ye, T., You, S., and Zhang, H. (2015). "The thermal performance of seawater-source heat pump systems in areas of severe cold during winter." *Energy conversion and management*, 90, 166-174.

ASHRAE (2009). *Fundamentals handbook-American society of heating, refrigerating and air-conditioning engineers*, ASHRAE, Atlanta, GA, USA.

Raymond, J., Therrien, R., and Hassani, F. (2008). "Overview of geothermal energy resources in Québec (Canada) mining environments." *Proc., 10th International Mine Water Association Congress: mine water and the environment*, 1-12.

Limanskiy, A., and Vasilyeva, M. (2016). "Using of low-grade heat mine water as a renewable source of energy in coal-mining regions." *Ecological Engineering*, 91, 41-43.

Burnside, N., Banks, D., and Boyce, A. (2016). "Sustainability of thermal energy production at the flooded mine workings of the former Caphouse Colliery, Yorkshire, United Kingdom." *International Journal of Coal Geology*, 164, 85-91.

Burnside, N., Banks, D., Boyce, A., and Athresh, A. (2016). "Hydrochemistry and stable isotopes as tools for understanding the sustainability of minewater geothermal energy production from a 'standing column' heat pump system: Markham Colliery, Bolsover, Derbyshire, UK." *International Journal of Coal Geology*, 165, 223-230.

Streb, C., and Wieber, G. (2011). "Geothermal energy from a flooded mine: a hydraulic model." *Rüde RT, Freund A, Wolkersdorfer Ch (Eds), Mine Water-Managing the Challenges, IMWA*, 189-193.

Arias, C. A., Alonso, A. O., and García, R. Á. (2014). "Hydrogeological and thermal modelling of an underground mining reservoir." *Mathematics of Planet Earth*, Springer, 419-423.

Clark, R. R. (1988). "A new continuous-sampling wireline system for acquisition of uncontaminated, minimally disturbed soil samples." *Groundwater Monitoring & Remediation*, 8(4), 66-72.

Dines, C., Cowan, P., and Headworth, C. (1988). "An operational subsea wireline system." *Proc., SPE offshore South East Asia conference and exhibition*, Society of Petroleum Engineers.

Piatak, N. M., Seal, R. R., Hammarstrom, J. M., Kiah, R. G., Deacon, J. R., Adams, M., Anthony, M. W., Briggs, P. H., and Jackson, J. C. (2006). "Geochemical characterization of mine waste, mine drainage, and stream sediments at the Pike Hill copper mine superfund site, Orange County, Vermont." U.S. Environmental Protection Agency U.S. Geological Survey, Reston, Virginia, 1-131.

Kubitz, J., Lewek, E., Besser, J., Drake, J., and Giesy, J. P. (1995). "Effects of copper-contaminated sediments on Hyalella azteca, Daphnia magna, and Ceriodaphnia dubia: survival, growth, and enzyme inhibition." *Archives of environmental contamination and toxicology*, 29(1), 97-103.

Liu, Z., and Yu, X. (2011). "Coupled thermo-hydro-mechanical model for porous materials under frost action: theory and implementation." *Acta Geotechnica*, 6(2), 51-65.

Liu, Z., Yu, X. B., Tao, J., and Sun, Y. (2012). "Multiphysics extension to physically based analyses of pipes with emphasis on frost actions." *Journal of Zhejiang University Science A*, 13(11), 877-887.

Braga, S., and Viskanta, R. (1992). "Transient natural convection of water near its density extremum in a rectangular cavity." *International journal of heat and mass transfer*, 35(4), 861-875.

McDonough, M., and Faghri, A. (1994). "Experimental and numerical analyses of the natural convection of water through its density maximum in a rectangular enclosure." *International journal of heat and mass transfer*, 37(5), 783-801.

Oliveira, P. J., and Issa, R. I. (2001). "An improved PISO algorithm for the computation of buoyancy-driven flows." *Numerical Heat Transfer: Part B: Fundamentals*, 40(6), 473-493.

Ferziger, J. H., and Peric, M. (2012). *Computational methods for fluid dynamics*, Springer Science & Business Media.

Bao, T., and Liu, Z. (2016). "Large-scale thermo-hydrodynamic modeling of a flooded underground mine for geothermal applications." *Geo-Chicago 2016*, ASCE, 72-83.

Schön, J. H. (2015). *Physical properties of rocks: Fundamentals and principles of petrophysics*, Elsevier.

Manger, G. E. (1963). "Porosity and bulk density of sedimentary rocks." Geological Survey Bulletin, Washington, 1-60.

Robertson, E. C. (1988). "Thermal properties of rocks." US Geological Survey, Reston, Virginia, 1-110.

Lund, J. W., Freeston, D. H., and Boyd, T. L. (2005). "Direct application of geothermal energy: 2005 worldwide review." *Geothermics*, 34(6), 691-727.

Milora, S. L., and Tester, J. W. (1977). "Geothermal energy as a source of electric power." *Geological Magazine*, 114(5), 1-3.

Bertani, R. (2012). "Geothermal power generation in the world 2005–2010 update report." *Geothermics*, 41, 1-29.

Self, S. J., Reddy, B. V., and Rosen, M. A. (2013). "Geothermal heat pump systems: status review and comparison with other heating options." *Applied Energy*, 101, 341-348.

Ochsner, K. (2012). *Geothermal heat pumps: a guide for planning and installing*, Routledge, New York, NY, USA.

Chua, K. J., Chou, S. K., and Yang, W. (2010). "Advances in heat pump systems: a review." *Applied energy*, 87(12), 3611-3624.

Ramos, E. P., Breede, K., and Falcone, G. (2015). "Geothermal heat recovery from abandoned mines: a systematic review of projects implemented worldwide and a methodology for screening new projects." *Environmental Earth Sciences*, 73(11), 6783-6795.

Allen, D., Ghomshei, M., Sadler-Brown, T., Dakin, A., and Holtz, D. (2000). "The current status of geothermal exploration and development in Canada." *Proc., Proceedings from World Geothermal Congress*, 55-58.

Malolepszy, Z. (2003). "Low temperature, man-made geothermal reservoirs in abandoned workings of underground mines." *Proc., Proceedings of the 28th workshop on geothermal reservoir engineering, Stanford University, USA*, 259-265.

Bazargan, B., Demollin, E., and Van Bergermeer, J.-J. (2008). "Geothermal use of deep flooded mines." *Proc., Proc. of the Post Mining Symposium*, 1-10.

Loredo, J., Ordóñez, A., Jardón, S., and Álvarez, R. (2011). "Mine water as geothermal resource in Asturian coal mining basins (NW Spain)." *Proc., Proceedings of 11th International Mine Water Association Congress*, Rüde TR, Freund A, Wolkesdorfer C (eds) Mine water: managing the challenges, 177-182.

Hasche-Berger, A. (2013). "Hydrodynamics in a flooded underground limestone mine." *Proc., Reliable Mine Water Technology*, IMWA, 1165-1172.

Preene, M., and Younger, P. (2014). "Can you take the heat? -Geothermal energy in mining." *Mining Technology*, 123(2), 107-118.

Raymond, J., and Therrien, R. (2014). "Optimizing the design of a geothermal district heating and cooling system located at a flooded mine in Canada." *Hydrogeology Journal*, 22(1), 217-231.

Radko, T., Bulters, A., Flanagan, J., and Campin, J.-M. (2014). "Double-diffusive recipes. Part I: Large-scale dynamics of thermohaline staircases." *Journal of Physical Oceanography*, 44(5), 1269-1284.

Turner, J. (1974). "Double-diffusive phenomena." *Annual Review of Fluid Mechanics*, 6(1), 37-54.

Sezai, I., and Mohamad, A. (2000). "Double diffusive convection in a cubic enclosure with opposing temperature and concentration gradients." *Physics of Fluids*, 12(9), 2210-2223.

Lee, J., Hyun, M., and Kang, Y. (1990). "Confined natural convection due to lateral heating in a stably stratified solution." *International journal of heat and mass transfer*, 33(5), 869-875.

Lee, J. W., and Hyun, J. M. (1991). "Double diffusive convection in a cavity under a vertical solutal gradient and a horizontal temperature gradient." *International journal of heat and mass transfer*, 34(9), 2423-2427.

Merryfield, W. J. (2000). "Origin of thermohaline staircases." *Journal of Physical Oceanography*, 30(5), 1046-1068.

Kelley, D., Fernando, H., Gargett, A., Tanny, J., and Özsoy, E. (2003). "The diffusive regime of double-diffusive convection." *Progress in Oceanography*, 56(3), 461-481.

Radko, T. (2003). "A mechanism for layer formation in a double-diffusive fluid." *Journal of Fluid Mechanics*, 497, 365-380.

Gandy, C., and Younger, P. (2007). "Predicting groundwater rebound in the South Yorkshire Coalfield, UK." *Mine Water and the Environment*, 26(2), 70-78.

Banks, D., Frolik, A., Gzyl, G., and Rogoż, M. (2010). "Modeling and monitoring of mine water rebound in an abandoned coal mine complex: Siersza Mine, Upper Silesian Coal Basin, Poland." *Hydrogeology Journal*, 18(2), 519-534.

Zhao, Z. (2014). "On the heat transfer coefficient between rock fracture walls and flowing fluid." *Computers and Geotechnics*, 59, 105-111.

Hull, J. R., Nielsen, J., and Golding, P. (1988). *Salinity gradient solar ponds*, CRC Press Inc, Boca Raton, FL (USA).

Vallis, G. K. (2017). *Atmospheric and oceanic fluid dynamics*, Cambridge University Press.

Bayless, E. R., and Olyphant, G. A. (1993). "Acid-generating salts and their relationship to the chemistry of groundwater and storm runoff at an abandoned mine site in southwestern Indiana, USA." *Journal of Contaminant Hydrology*, 12(4), 313-328.

Brandt, A., and Fernando, H. (1995). *Double-diffusive convection*, American Geophysical Union Washington DC.

Carpenter, J., Sommer, T., and Wüest, A. (2012). "Simulations of a double-diffusive interface in the diffusive convection regime." *Journal of Fluid Mechanics*, 711, 411-436.

Radko, T., Flanagan, J., Stellmach, S., and Timmermans, M.-L. (2014). "Double-diffusive recipes. Part II: Layer-merging events." *Journal of Physical Oceanography*, 44(5), 1285-1305.

Radko, T. (2007). "Mechanics of merging events for a series of layers in a stratified turbulent fluid." *Journal of Fluid Mechanics*, 577, 251-273.

Appendix A. Copyright Documentation

Copyright Clearance Center RightsLink®

Home | Create Account | Help

ASCE AMERICAN SOCIETY OF CIVIL ENGINEERS

Conference Proceeding: Geo-Chicago 2016: Geotechnics for Sustainable Energy

Conference Proceeding Paper: Large-Scale Thermo-Hydrodynamic Modeling of a Flooded Underground Mine for Geothermal Applications

Author: Ting Bao, Zhen (Leo) Liu

Publisher: American Society of Civil Engineers

Date: 08/11/2016

LOGIN

If you're a copyright.com user, you can login to RightsLink using your copyright.com credentials.

Already **a RightsLink user** or want to learn more?

Permissions Request

As an ASCE author, you are permitted to reuse you own content for another ASCE or non-ASCE publication.

Please add the full credit line "With permission from ASCE" to your source citation. Please print this page for your records.

Type of use: Dissertation/Thesis

Portion: excerpt

Format: electronic

Use of this content will make up more than 25% of the new work: no

Author of this ASCE work or ASCE will publish the new work: yes

BACK | CLOSE WINDOW